Time Dependent Flexural Analysis of Reinforced Concrete Members

Prepared by

Noor Md. Sadiqul Hasan

B.Sc (Civil Engineering) and M.Sc (Structural Engineering)

A dissertation submitted for the degree of

Doctor of Philosophy (Structural Engineering)

School of Civil, Environment and Mining Engineering

The University of Adelaide

Australia

-August 2016-

ABSTRACT

Concrete is one of the most widely used building materials in the construction industry in the world. Time dependent behaviour of concrete is the major concern for the structural engineers due to its significant effect in the long term serviceability and durability. Reinforced concrete (RC) members are prone to the effect of time dependent deformations that are known as shrinkage and creep, can produce substantial deformations and deflections to the structure.

The mechanics of quantifying the serviceability deflection of RC beams is complex due to flexural cracking and the associated partial interaction (PI) behaviour of slip between the reinforcement and adjacent concrete. Add the additional complexity of time dependent concrete shrinkage to this partial-interaction (PI) behaviour and the problem becomes very complex.

Current design and analysis techniques to quantify serviceability deflection of reinforced concrete (RC) members are generally built on two major principles which are full interaction (FI) through the use of moment curvature approaches; and a uniform longitudinal shrinkage strain ε_{sh} within the member to simplify the analysis technique. Both of the premises are gross approximations and with regard to the first premise, RC beams are subject to flexural cracking and the associated partial interaction (PI) behaviour of slip between the reinforcement and adjacent concrete. Furthermore with regard to the second premise, numerous tests have shown that ε_{sh} varies along both the depth and width of the beam and which is far from uniform. Hence there are two major sources of error in the quantification of serviceability deflections of RC beams for design and which are due to the PI mechanisms that occur in practice; and that due to the time dependent material properties of creep and shrinkage.

This thesis deals with the development of PI numerical mechanics models with non-linear shrinkage strain variations achieved from a moisture diffusion model developed in this study and that is required to simulate the PI behaviour of RC beams in order to considerably reduce the source of error occurred due to the application of numerical mechanics model. Hence this new mechanics model will allow: the development of better design mechanics rules for serviceability deflection; and also assist in the better quantification of non-linear shrinkage and creep by removing or considerably reducing

the existing mechanics source of error. Importantly, this research provides mechanics solutions for all the facets that control the serviceability time dependent behaviour of RC beams and it is envisaged that these numerical mechanics solutions can provide researchers with the tools to develop simple design procedures as they simulate the major mechanisms influencing cracking and tension stiffening in reinforced concrete beams.

Current shrinkage test methodology is having some limitations that are all surfaces are exposed to the environment and they are small scaled which leads to a uniformity of shrinkage strain and which are not present in real size RC beams. Therefore in this thesis, a new form of experimental setup for shrinkage have been proposed to better quantify the shrinkage variations along both the width and depth of RC members with varying the sizes and surface boundary conditions.

STATEMENT OF ORIGINALITY

I certify that this work contains no material which has been accepted for the award of any other degree or diploma in my name, in any university or other tertiary institution and, to the best of my knowledge and belief, contains no material previously published or written by another person, except where due reference has been made in the text. In addition, I certify that no part of this work will, in the future, be used in a submission in my name, for any other degree or diploma in any university or other tertiary institution without the prior approval of the University of Adelaide and where applicable, any partner institution responsible for the joint-award of this degree.

I give consequent to this copy of my thesis when deposited in the University Library, being made available for loan and photocopying, subject to the provisions of the Copyright Act 1968.

The author acknowledges that copyright of published works contained within this thesis resides with the copyright holder(s) of those works.

I also give permission for the digital version of my thesis to be made available on the web, via the University's digital research repository, the Library Search and also through web search engines, unless permission has been granted by the University to restrict access for a period of time.

_____ _____

Noor Md. Sadiqul Hasan Date

ACKNOWLEDGEMENT

At first I would like to express my deepest gratitude and sincere appreciation to my principal supervisor Emeritus Professor Deric John Oehlers for his excellent supervision during my PhD study. I also would like to express my sincere appreciation to my co-supervisor Dr. Phillip Visintin for his wonderful supervision throughout the PhD research were an enormous help to me in the completion of this work. Their invaluable advice, continuing support, encouragement, patience and weekly regular meetings were generous help throughout the PhD work reached me to the final level.

I would also like to thank Dr. Terry Bennett for his good collaboration in solving my issues, providing guidance and his valuable advices throughout my PhD research.

The financial support from the Adelaide Scholarship International (ASI) through the University of Adelaide (UoA) are highly appreciated.

Finally, I am very much grateful to my parents, family members and relatives for their love, continuing support, motivation, understanding and encouragement during my PhD start to the final day. A special thanks goes to my beloved Wife for her continuous support when it was needed, distraction when it was required and motivation when I lost mine. Last but not the least, I would like to dedicate my PhD thesis to my beloved parents.

List of Publication

Based on the research work one journal paper has been submitted for publication in Proceedings of the Institution of Civil Engineers – Structures and Buildings.

Hasan, N. M. S., Bennett, T., Visintin, P., Oehlers, D. J. (2016). "Mechanics of simulating the serviceability deflection of RC beams allowing for partial interaction and non-linear shrinkage" (Submitted to Proceedings of the Institution of Civil Engineers – Structures and Buildings).

Table of Contents

List of Figures

List of Tables

Chapter 1 Introduction

1.1 Introduction

The versatility of concrete in terms of both application and material properties make it one of the most widely used building materials in the world. When concrete is subjected to a load, its deformation response, shown in Figure 1.1 is both immediate and time dependent. The time dependent behaviour of concrete due to shrinkage and creep can produce substantial time dependent deflections and increases crack widths. Significantly, the increase in member deflection and crack width may lead to serviceability failures and adversely affect the durability of RC structures.

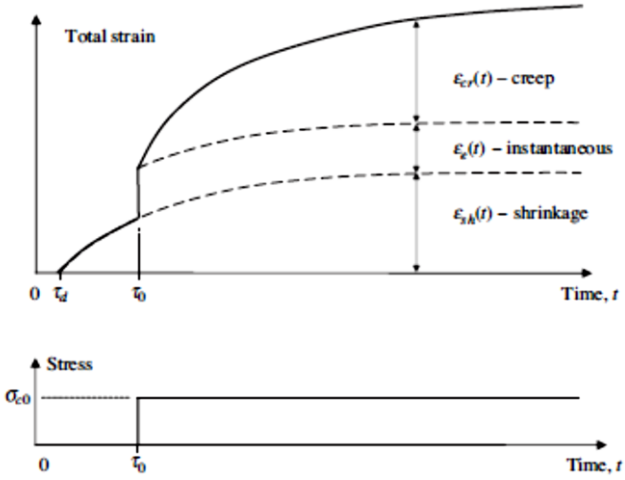

Figure 1.1: Concrete strain component under sustained compressive stress (Gilbert and Ranzi 2011)

Concrete shrinkage can be divided into four distinct phases: (i) Plastic shrinkage; (ii) chemical shrinkage; (iii) thermal shrinkage; and (iv) drying shrinkage, which is the major concern of this thesis. The major cause of each form of shrinkage is as follows:

- Plastic shrinkage occurs in wet concrete and is the result of capillary tension in the water contained within the porous structure of concrete.
- Chemical shrinkage, which is also known as autogenous shrinkage occurs due to chemical reactions during the cement hydration process. Chemical shrinkage is independent on the size of specimen and the surrounding environment and it occurs increasingly during the days and weeks after casting.
- Thermal shrinkage occurs due to the heat of hydration and thus gradually dissipates in the first few hours or days after setting. Thermal shrinkage is particularly important in the placement of mass concrete such as dams in which significant heat is generated during hydration.
- Drying shrinkage occurs due to the loss of pore water throughout the lifespan of a concrete structure, this form of shrinkage is caused by moisture movement throughout the concrete and results in a reduction in the volume in concrete. Drying shrinkage depends upon all the factors which affect the drying of concrete, these include: the size and shape of members, the relative humidity of the ambient environment and the mix characteristics of concrete. For example, high strength concrete undergoes less drying shrinkage than normal strength concrete as these concretes have a smaller quantity of free water after the hydration process is complete. In contrast, chemical and thermal shrinkage can be significantly higher in high strength concretes where increased hydration occurs. (Gilbert 1988, Gilbert and Ranzi 2011).

Figure 1.1 shown above is a breakdown of the total concrete strain into its individual components over time. In Figure 1.1 it can be seen that shrinkage strains begin to develop

during the drying process which begins at a time $t = \tau_d$ and that the magnitude of the shrinkage strain is independent of the applied stress σ_{c0} which is applied at time τ_0.

Following loading at time t_0 an instantaneous or elastic strain is developed due to the application of stress σ_{c0} and significantly this strain increases over time due to a variation in the stiffness of the concrete. This variation is due to concrete creep the magnitude of which depends on the applied load σ_{c0}. Concrete creep strains increases rapidly in the period initially after application of load then the rate of increment slowed down dramatically with time. After 2 -3 months of initial application of load produces about 50 percent of final creep strain whereas it reaches to about 90 percent in between 2-3 years (Gilbert and Ranzi 2011).

However, for the serviceability analysis of an RC member it is only necessary to consider drying shrinkage as the magnitude of autogenous, thermal and plastic shrinkage strains are negligible in comparison (Holt and Leivo 2004, Gribniak, Kaklauskas et al. 2008).

Concrete time dependency is incredibly important in that it can lead to serviceability and durability failures. Two major problems exist in the modelling of shrinkage: (i) how to accurately defining the shrinkage strain (ii) how to incorporate shrinkage into the analysis of a member. Issues surrounding (i) are the huge scatter of test results and which may be due to the measurement methods and the prescription of a single shrinkage constant strain to a block of concrete regardless of size. Issues surrounding (ii) arise because methods of analysis commonly assume full interaction which does not occur in practice and hence fill the gap between assumptions of analysis and experimental observations with empiricisms. This means that the approaches do not simulate what is seen in practice and cannot directly incorporate residual strains such as shrinkage. Moreover, they will have incredible difficulty incorporating real material behaviours such as non-linear shrinkage.

In this thesis, the above mentioned issues are addressed by firstly simulating the mechanics of drying shrinkage through a diffusion process and secondly simulating the mechanics of concrete cracking using partial interaction (PI) mechanics allowing for the real non-linear variation in shrinkage. The benefit of this approach is the only empiricisms are the definition of material properties and the allowance for the real distribution of shrinkage which is shown to be shape and size dependent.

Moisture diffusion in concrete greatly depends on pore relative humidity, member sizes and concrete material properties. A moisture diffusion model to quantify the shrinkage strain in concrete specimens been proposed by (Kim and Lee 1998, Kim and Lee 1999, Mu and Forth 2009, Kang, Kim et al. 2011) who consider moisture diffusion as a nonlinear diffusion problem. By using the nonlinear moisture diffusion theory it also requires a moisture diffusion coefficient expressed as a function of moisture content can be determined through the CEB FIP model code 1990 (CEB-FIP 1990) using concrete material properties and also can be obtained from experiments (Akita, Fujiwara et al. 1997, Zhang, Hou et al. 2011).

Having addressed the issues surrounding the definition and quantification of non-linear shrinkage variations in concrete member, this research aims to develop a moisture diffusion model to predict the non-linear shrinkage variations along the concrete member. Moisture diffusion from concrete emerges the shrinkage strain which shows non-linear variations in practical experiments (Terrill, Richardson et al. 1986, Mu and Forth 2009, Gilbert, Bradford et al. 2012) and it decreases with increasing of volume/exposed surface area ratios (V/S) (Hansen and Mattock 1966, Almudaiheem and Hansen 1987). Current design techniques suggest a uniform shrinkage profile throughout the member achieved from an experimental test with smaller sizes of prism specimens compared to the real sizes

of RC members. Hence an experimental set up having different V/S ratios have been proposed in Chapter 5 to show the influence of member sizes in shrinkage strain variation in concrete member.

Having now modelled the mechanisms of drying shrinkage of concrete, this study also aims to develop a member model for simulating the member deflection. Prior to flexural cracking, the deflection of an RC beam can be derived from strain based approaches, such as the use of flexural rigidities or moment-curvature, and it is fairly straightforward to incorporate constant values of shrinkage (Visintin, Oehlers et al. 2013). This can be used to predict the initial flexural crack and however once the initial flexural crack occurs then the behaviour is governed by tension-stiffening as this partial-interaction behaviour controls the crack spacing and crack widths that have a major effect on the deflection (Oehlers, Mohamed Ali et al. 2011, Visintin, Oehlers et al. 2012, Visintin, Oehlers et al. 2013). A constant shrinkage strain, that is a longitudinal shrinkage strain that is constant along both the depth and width of the member, can be added to these partial interaction analyses (Visintin, Oehlers et al. 2013) to determine the effect of shrinkage. However, numerical analyses and tests have shown that the shrinkage strain does vary along the depth and width of the member (Terrill, Richardson et al. 1986, Mu and Forth 2009, Gilbert, Bradford et al. 2012). The main aim of this study is to develop a numerical procedure that allows for non-linear shrinkage strains as happens in practice and also to determine whether a constant shrinkage strain is an adequate design simplification for the non-constant shrinkage strains that can occur in practice.

1.2 Scope of the Research

The goal of the present study is to improve the accuracy of prediction in long term deflection of RC members with incorporating the effect of creep and non-linear shrinkage variations along both the depth and width of the member. In order to achieve this goal, a numerical moisture diffusion model has developed to quantify the non-linear shrinkage variations along the RC member for any sizes of member having any concrete material properties with a variety of surface boundary conditions with any environmental conditions. Hence a segmental approach has also been developed allowing for partial interaction and non-linear shrinkage to quantify the long term deflection of RC members. Hence a new form of complete experimental setup has proposed to quantify more accurately the shrinkage variations through the depth and width of the member with varying from one up to four different exposed surface conditions and also taking into account the size effect according to the volume over exposed surface (V/S) area ratios.

1.3 Aims and Objectives of the Research

The main objectives of this research are outlined below:

- Develop a numerical diffusion model using the finite difference method to quantify the non-linear variations in shrinkage strains throughout a RC member for any environmental conditions with a variety of surface boundary conditions and for any sizes of member and with any concrete material properties.
- Develop a mechanics based model for quantifying the long term behaviour of a flexural member subjected to a sustained load. This approach is to be based on the segmental approach previously developed at the University of Adelaide and in this

thesis the model is to be extended to allow for the non-linear shrinkage variations along both the width and depth of the member.

- Proposing a new form of experiment to better quantify the shrinkage variations within a member with varying from one up to four different exposed surfaces and also considering the size variations with respect to the volume over exposed surface area ratios (V/S) of the member.

1.4 Structure of the Thesis

This thesis comprises of seven chapters as also outlined below:

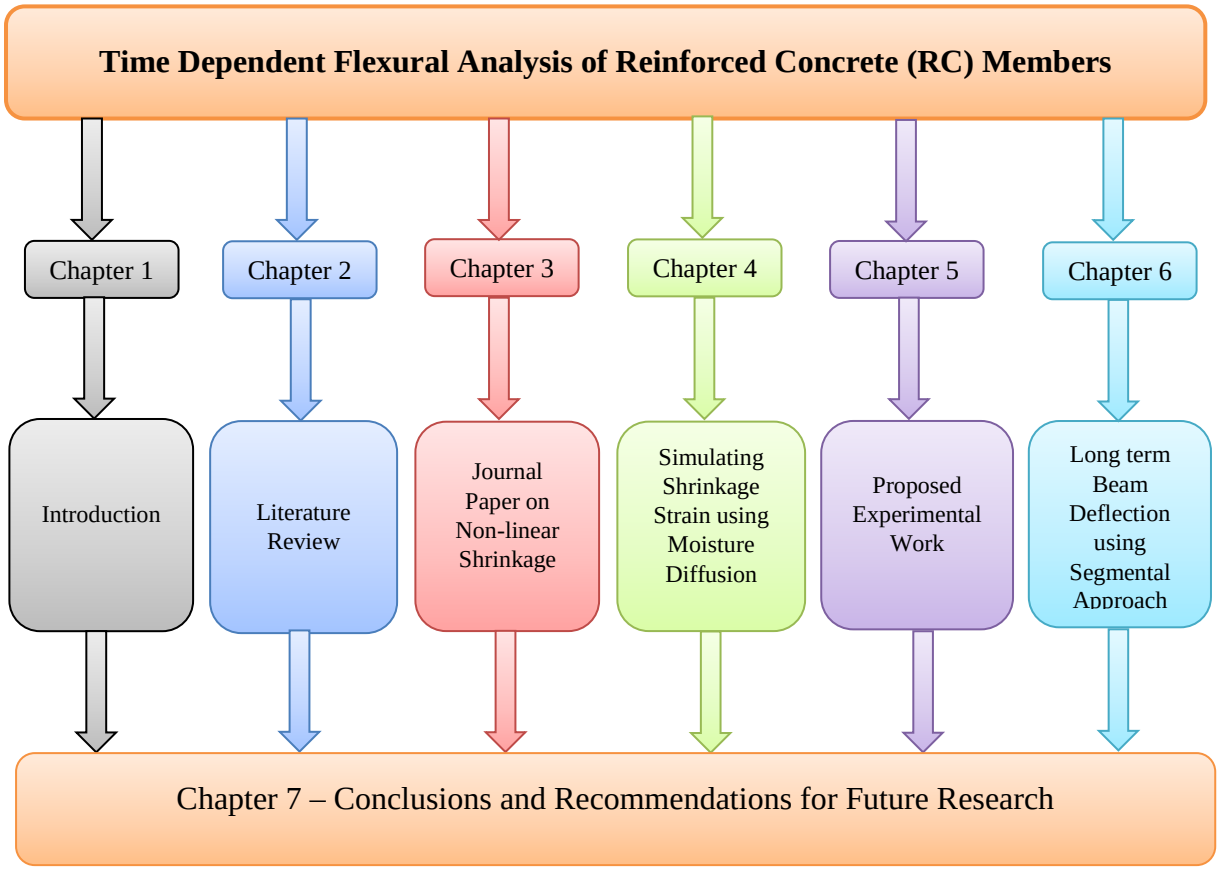

Figure 1.2: Thesis layout of this research

Chapter 1 provides the brief research background, significance of this research, aims and objectives of this study.

Chapter 2 gives the detailed literature review on shrinkage and creep and its influence on structures. Code and research based shrinkage strain prediction techniques of varying complexity are critically reviewed.

Chapter 3 contains the journal paper on 'Mechanics of Simulating the Serviceability Deflection of RC Beams allowing for Partial-interaction and Non-linear Shrinkage' where a novel technique has been developed to quantify the long term deflection of RC beams allowing for the inclusion of non-linear shrinkage variations in concrete.

Chapter 4 describes the development and application of a moisture diffusion modelling to simulate drying shrinkage of concrete subjected to any environmental conditions. This chapter also includes a validation of the diffusion model with existing experimental test results.

Chapter 5 provides recommended changes to shrinkage strain experimental tests for concrete specimens which will allow for the determination of non-linear shrinkage strain distributions.

Chapter 6 deals with the development of a new segmental approach to quantify the long-term deflection of RC members associated with the effect of creep and non-linear shrinkage strain variations of concrete members along both the depth and width of the member. It also illustrates the parametric study on variation of long-term deflection of RC beams with the effect of different exposed surfaces and also the validation of numerical segmental model with available experimental test results of six RC beams.

Chapter 7 summarises the major findings of this study and recommends the scope and opportunities for further research.

Chapter 2 Literature Review

Introduction

This chapter reviews literature surrounding the mechanisms for concrete shrinkage and creep as well as existing prediction methods applied in practice. Prediction of shrinkage strain in concrete using ten different codes and models including the most up to date prediction techniques to predict the shrinkage strain from experimental test results are also covered. Special attention is paid on the loss of moisture in concrete i.e. moisture diffusion as this is the main mechanism driving long term drying shrinkage in structures. Finally, this chapter reviews the most noteworthy literature on numerical and analytical modelling to quantify long term deflections of reinforced concrete (RC) members such as beams or slabs due to the effect of creep and shrinkage.

2.1 Shrinkage and its types

Shrinkage is the volumetric changes of concrete due to loss of water from the concrete into the atmospheric environment or by internal chemical reactions. Concrete shrinkage is a time-dependent strain and occurs in an unloaded and unrestrained specimen. There are various types of shrinkage and that occurred in two stages one is in early ages (< 24 hours) and another one is in the long term (> 24 hours).

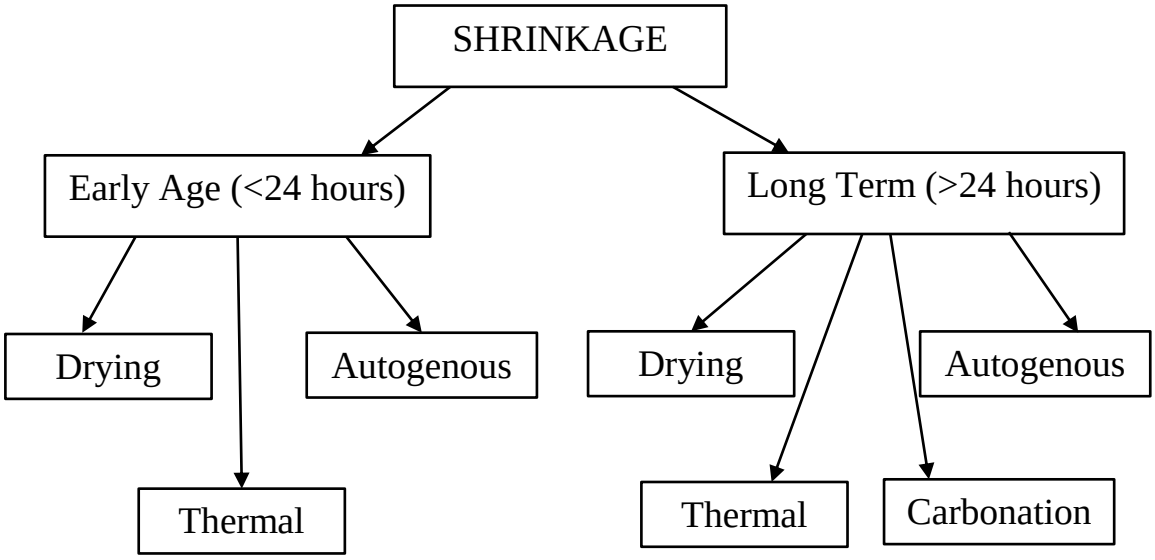

Figure 2.1: Shrinkage stages and types of concrete

According to Gribniak, Kaklauskas et al. (2008), Gilbert and Ranzi (2011) and Lam (2002) shrinkage of concrete can be considered to consist of four major forms: (i)plastic shrinkage, (ii)chemical or autogenous shrinkage, (iii)carbonation shrinkage and (iv) drying shrinkage. Plastic shrinkage occurs in the fresh concrete due to loss of moisture from the freshly poured concrete to its surroundings whereas autogenous, carbonation and drying shrinkage all occur in hardened concrete after setting. Autogenous or chemical shrinkage occurs at the early stages due to chemical reactions within the cement paste and binder includes the hydrations of cement without any moisture movement outside to the environment. Carbonation shrinkage occurs due to the chemical reaction with carbon dioxide in the air with various products of cement hydration. Thermal shrinkage is another type of shrinkage which occurs in first few hours or days after setting time as the heat of hydration dissipates gradually and the term endogenous shrinkage is used to refer to the part of shrinkage of hardened concrete which is not related with drying that means the sum of autogenous and thermal shrinkage. According to Holt and Leivo (2004), shrinkage

types and stages are as illustrated in the above Figure 2.1 where drying shrinkage in early ages has a negligible effect compare to the long term.

Drying shrinkage in concrete increases with time at a gradually decreasing rate and takes place in the long run even along the life time duration of a structure. The magnitude and rate of development of drying shrinkage depend on all the factors that affect the drying of concrete including the atmospheric relative humidity, the mix proportions such as water content, water to cement ratio, types of cement, aggregate types, fine to coarse aggregate ratio and also the shape and sizes of the member.

In terms of analysis of concrete structures two types of shrinkage are need to be considered: drying shrinkage and autogenous shrinkage (Holt and Leivo 2004, Gribniak, Kaklauskas et al. 2008). The ratio of drying and autogenous shrinkage is illustrated in the Figure 2.2 below (Sakata and Shimomura 2004) and it can be found that drying shrinkage is the governing one should be considered and autogenous shrinkage is negligible compare to the total long term shrinkage after drying and which is only 10% to 20% of the long term shrinkage strain (Silliman and Newtson 2006).

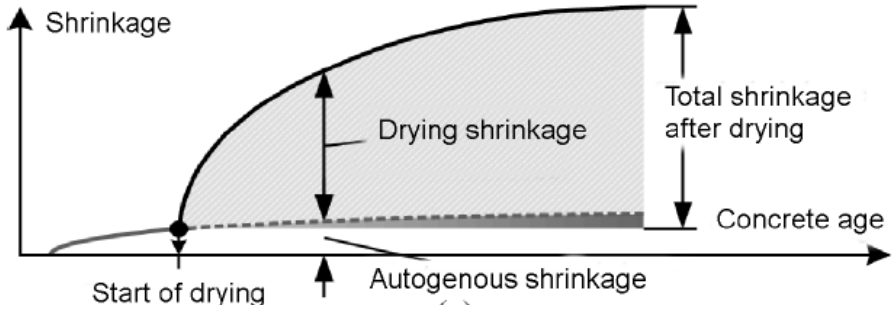

Figure 2.2: Shrinkage strain components in normal strength concrete (Sakata and Shimomura 2004 cited in Gribniak et al., 2008)

2.2 Effect of Shrinkage and Creep on Structures

Reinforced concrete members such as beams or slabs are embedded with reinforcements and also supported with joints which may provide the restraining effect to the shrinkage and can produce shrinkage induced curvature in an unsymmetrically reinforced concrete member. Hence, this shrinkage induced curvature can often leads to the significant deflection of the member and which is load independent. Therefore, shrinkage is one of the major concerning factors and that affects the time dependent deflection in RC flexural members (Jayasinghe 2011, Jafarifar 2012, Gilbert and Ranzi 2011).

The effect of shrinkage on structural members depends on the drying conditions at the exposed surfaces of RC members where the shrinkage profile should considered to be non-linear during the long term analysis of concrete structures (Terrill, Richardson et al. 1986, Mu and Forth 2009, Gilbert, Bradford et al. 2012) and will be discussed briefly at later sections of this chapter.

Creep of concrete can be defined as the time dependent strain in hardened concrete subjected to sustained stress and this is both time dependent and stress dependent. Creep is obtained normally by subtracting instantaneous strain after application of load and shrinkage strain in an unloaded specimen from the measured total strain with the change of time in a loaded specimen. Creep can be classified into two types, one is basic creep and another one is drying creep. Basic creep is the time dependent deformation which occurs in a loaded specimen without any moisture movement from the specimen to the surrounding environment. Hence the drying creep is the additional creep which occurs in a drying specimen due to the moisture movement between the specimen and the environment (Gilbert 1988, ACI209R-92 1992, He 2013).

The magnitude and the rate of development of creep are influenced by many factors such as concrete mix properties, aggregate type and sizes, water to cement ratio in the concrete, environmental humidity and temperature, member sizes and the loading conditions.

Creep decreases with increase in concrete strength and better quality of concrete provides lesser amount of creep. Creep also decreased with increment of aggregate content, maximum aggregate sizes and using of stiffer aggregate in the concrete mixes. Reduced water cement ratio uses in concrete mix composition may reduce the creep of concrete.

The magnitude of creep depends on the age of concrete and it decreases as the age at first loading increases. Creep decreases as the relative humidity increases and shows vice versa. Temperature rises also increases the creep as the deformability of cement paste is increased by a temperature rise and drying being accelerated.

Creep is also dependent on the sizes of the members and it increases in thinner specimen such as in a thin slab specimen as surface area to volume ratio increases. Creep is mainly dependent on the stress level and when the sustained stress is less than half of the compressive strength of concrete the creep strain is proportional to the stress level and is known as linear creep (Gilbert 1988, Gilbert and Ranzi 2011).

There are several methods to analyse the creep effects on structural members are available which includes the effective modulus method (EMM), the age adjusted effective modulus method (AEMM), the rate of creep method (RCM) and the rate of flow method (RFM) and among these first two of them used widely for the analysis of structures with regards to the effect of creep (Jayasinghe 2011). However, in this thesis we will discuss about the EMM which has been used to analyse the creep effect in RC members to quantify the long term deflections.

The effective modulus method (EMM) suggested by Faber (1928) is the simplest and oldest method applied in this research and the elastic modulus of concrete in a time t after first loading at time t_0 at any point can be defined as $E_c\,(t, t_0)$ and using effective modulus method can be written as

$$E_C(t, t_0) = \frac{E_c(t, t_0)}{1 + \varphi(t, t_0)} \qquad \text{Equation 2.1}$$

Where t_0 is the time at initial loading and φ is the creep coefficient of concrete at time t after initial loading at time t_0. Hence the change in elastic modulus in concrete due to creep would be applied to both in compression and tension zone of concrete at the segmental analysis in chapter 5 for time dependent deformations of the RC members (Gilbert and Ranzi 2011).

2.3 Prediction of Shrinkage Strains

Several models have been developed to predict shrinkage strains in concrete based on the results of experimental studies by the prominent researchers. These models have been adopted by codes of practices in different countries can be named as code based model and rest of them are remained as research based model which also can be used to predict the shrinkage strain in concrete specimens. These model including ACI 209R-92 model, ACI model modified by Huo, AS 3600-2009, AASHTO LRFD 2012 model, Bazant-Baweja B3 model, CEB MC90, CEB MC90-99, FIB 2010 model, GL2000 model and Sakata 1993 model are been discussed and compared with experimental shrinkage test results from Bazant NU-ITI database (Bazant and Li 2008) and shrinkage test results of concrete prisms by Al-Saleh and Al-Zaid (2006).

Concrete deformations due to shrinkage is quite difficult to predict as the actual behaviour of concrete with the effect of shrinkage are very complex and involves several physical mechanisms; also influenced by so many parameters associated with it. Numerous research has been done to quantify and predict the deformation of concrete due to shrinkage effect and also various analytical and empirical models have been developed to predict the shrinkage strain in concrete specimens (Al-Saleh 2014). Ten of the most utilised shrinkage prediction models including the current code of practices are described and also considered for the comparison with experimental test results of two rectangular concrete prisms, one is plain concrete prism and the other one is standard prism having sizes of 80 mm × 150 mm × 500 mm and 50 mm × 50 mm × 300 mm respectively (Al-Saleh and Al-Zaid 2006).

Figure 2.3 below represents the measured and calculated shrinkage strains in a rectangular plain concrete prism of sizes 80 mm × 150 mm × 500 mm and which are cured in a humidity and temperature control room having humidity of 50% and temperature of 28^0C. It can be seen from the figure that the theoretical shrinkage strains calculated by using ACI 209, ACI 209 model modified by Huo and AASHTO LRFD 2012 model provide well prediction of shrinkage strain. Whereas CEB FIP MC90, CEB MC90-99, FIB 2010, B3 model shown similar trend by achieving good correlation with measured values at the beginning of drying but underestimated at later ages. GL2000 and Sakata 1993 model exhibit closer estimation to the test results initially but as drying period increases the shrinkage strain also increases with increasing rate and finally overestimates the experimental shrinkage strains. AS 3600-2009 is found to have the worst approximation from early age up to the end of drying.

Figure 2.4 depicts the comparison between measured and calculated shrinkage strains in standard concrete prism having sizes of 50 mm × 50 mm × 300 mm stored in a similar environmental conditions with the rectangular concrete prism. Similar trends for shrinkage strains in rectangular plain concrete prism can be seen in this standard specimen except for the GL2000 model shows higher estimation than the Sakata 1993 model compared to rectangular plain prisms and however, both of them provide the overestimation of shrinkage strain. Hence finally, AS 3600-2009 gives the poorest approximation of shrinkage strain among all the models and code approaches.

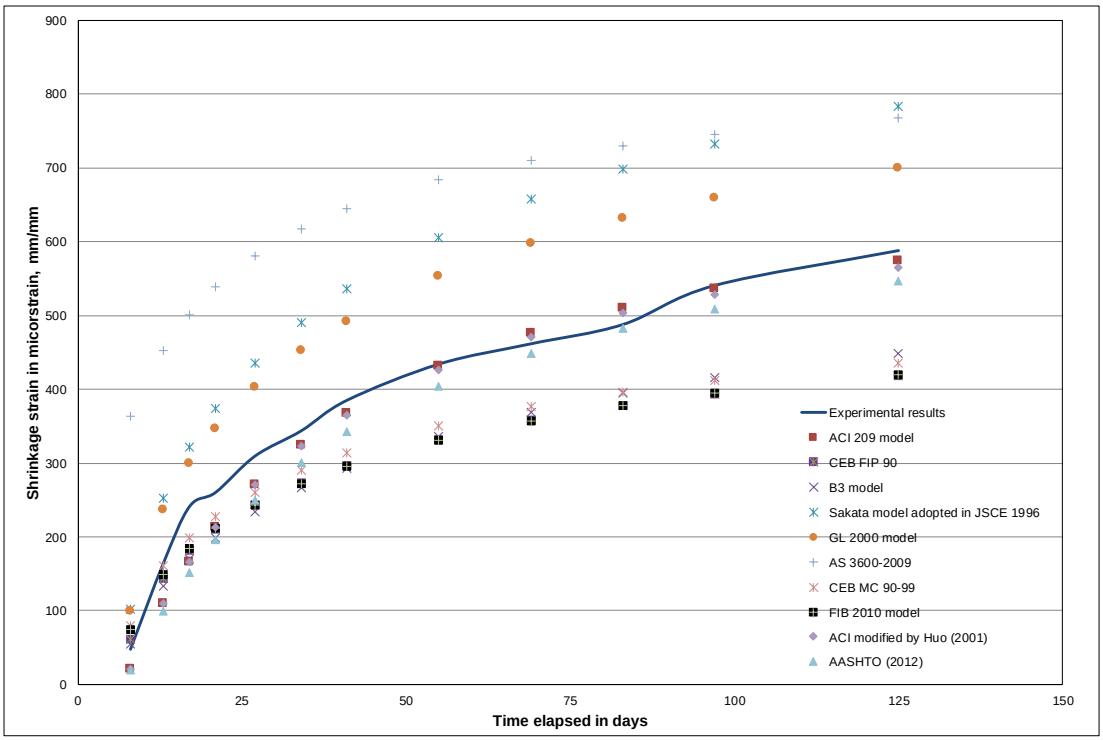

Figure 2.3: Experimental and predicted shrinkage strain in a plain rectangular concrete prism (80 mm × 150 mm × 500 mm) using different codes and shrinkage prediction models

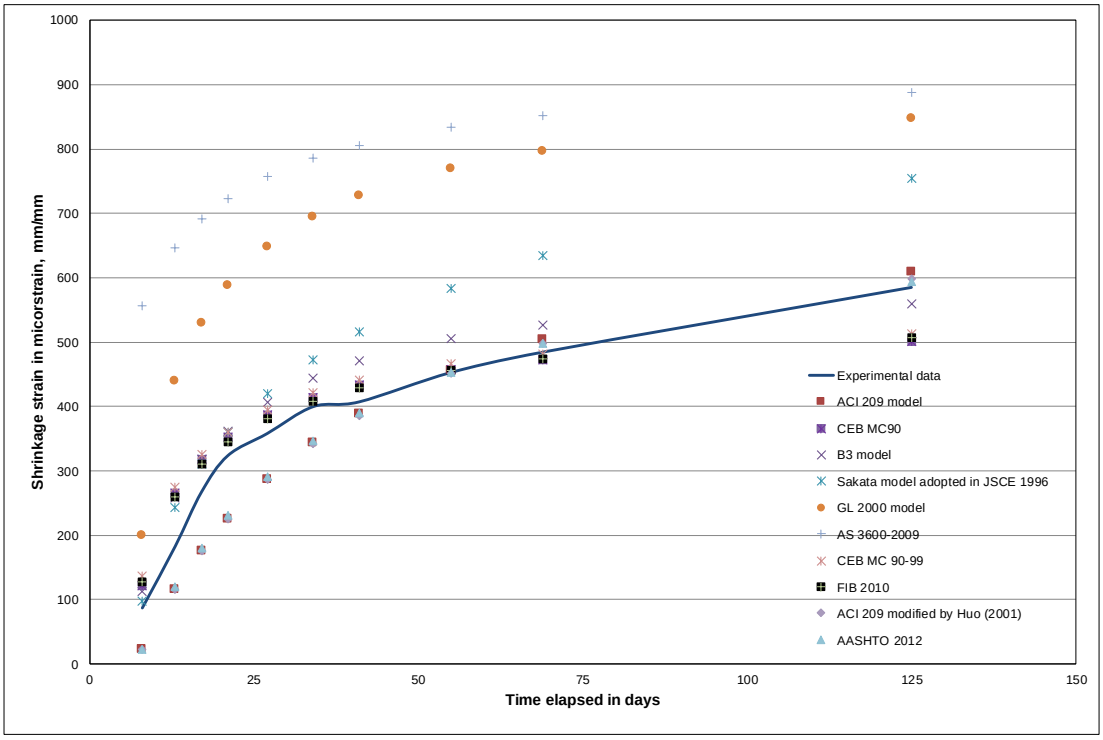

Figure 2.4: Experimental and predicted shrinkage strain in a standard concrete prism (50 mm × 50 mm × 300 mm) using different codes and shrinkage prediction models

2.4 Using Moisture Diffusion to quantify Shrinkage

Shrinkage occurs in the concrete mainly due to moisture diffusion from inner surface of the concrete to the outside environment due to the effect of ambient relative humidity. Many researchers have investigated the moisture diffusion of concrete experimentally and numerically will be described in this chapter. Hence due to the moisture diffusion, concrete exhibits the shrinkage strain which can be extracted by applying a mathematical relationship in between them.

2.4.1 Moisture and Humidity Diffusion in Concrete

Moisture diffusion is affected by moist curing period of concrete and it shows higher diffusion rate for poorly cured concrete and lower diffusion rate for properly cured concrete. Since self-desiccation has significant role in the early ages of concrete so this need to be considered especially for high strength concrete. Furthermore, moisture diffusion progresses more rapidly at high temperature compare to the low temperature environment conditions. Both finite difference and finite element method using moisture diffusion equation has shown good agreement with experimental results for one direction and two directional moisture diffusion processes (Kim and Lee 1999, Kang, Kim et al. 2011).

An experimental and numerical simulation of one direction moisture movement (exposed top surface only and rest of the surfaces are sealed) modelled for 180 mm ×150 mm ×150 mm plain conventional concrete (CC), plain rolling compacted concrete (RCC) and steel-fibre-reinforced (SFR) concrete. This investigation was performed in a chamber of constant relative humidity and temperature of 40±3% and 25±3ºC respectively and gravimetric method was used for measuring the moisture content inside the concrete specimen. ABAQUS 3D 8-noded solid element called DC3D8 was used for finite element (FE) simulation with the experimental test results and moisture diffusion coefficient and surface factors were back-calculated by using FE analysis. It can be seen that higher moisture diffusivity achieved when moisture content is above 90% and surface factor does not have significant effect except near the drying surface of the concrete specimen. Moisture diffusivity and surface factor varies from 0.001 to 30 mm^2/day and 3 to 10 mm/day for plain CC and 5-10 mm/day for plain RCC. Figure 2.5 below depicts the comparison of experimental and numerical non-uniform moisture profiles for four

different types of concrete. It can be found that moisture content increases through the depth of the concrete block away from the drying top surface and decreases over the drying period in days. Hence it can also be seen that numerical model results shown good agreement with experimental test results (Jafarifar 2012).

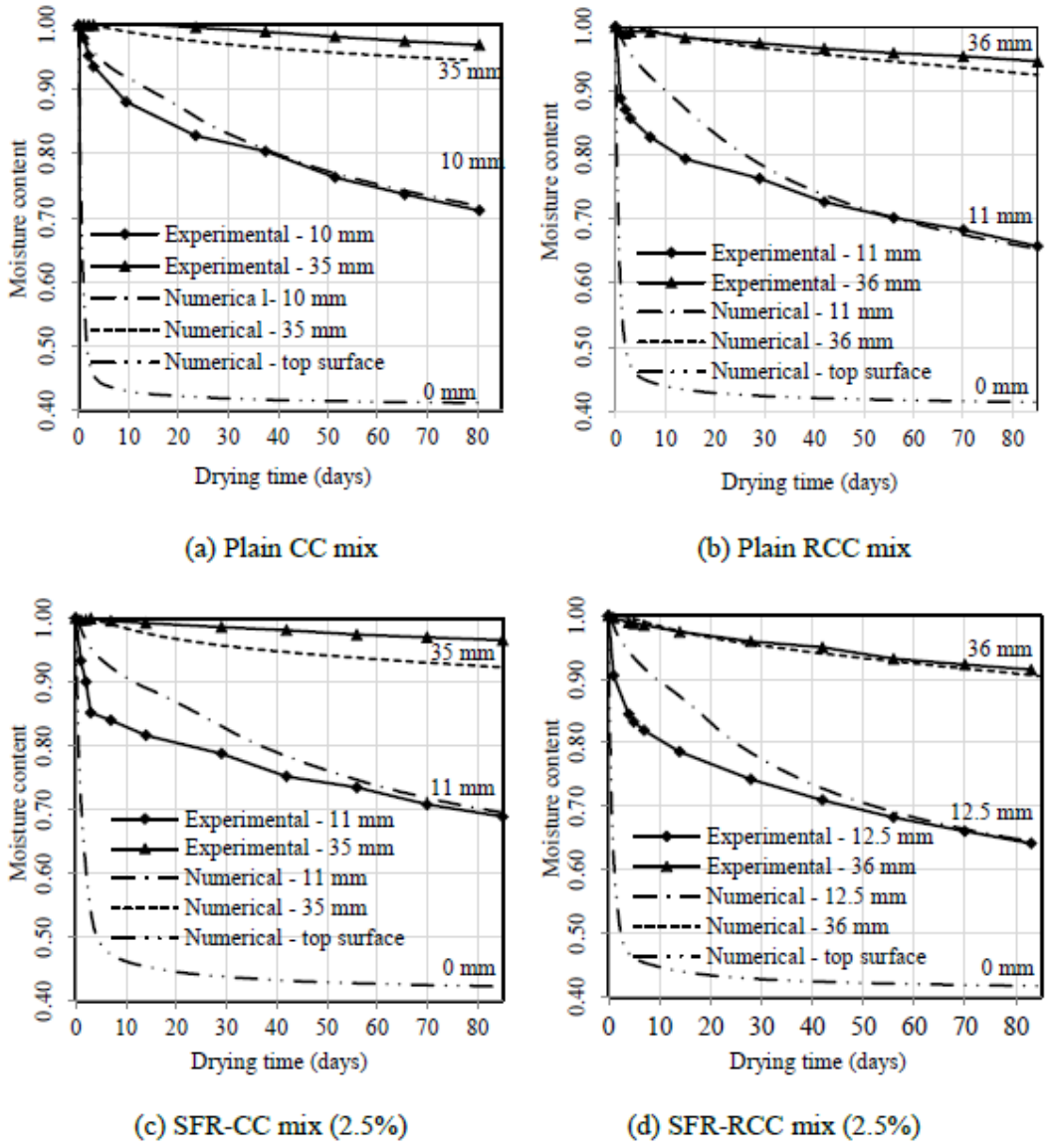

Figure 2.5: Numerical moisture profiles compared with the experimental test results: (a) Plain CC mix; (b) Plain RCC mix; (c) SFR-CC mix (2.5%); (d) SFR-RCC mix (2.5%) (Jafarifar 2012)

Zhang, Qi et al. (2009) also performed experimental investigation with 200 mm × 200 mm × 800 mm concrete prism for measuring the relative humidity at early ages in various depths starting from 2.5 cm to 18 cm exposed from drying top surface only and rest of the five surfaces are sealed. A numerical model considering both the cement hydration and moisture diffusion was also developed. It can be found that good agreement achieves with numerical modelling and finite difference method and which well predicts with the experimental results. Furthermore, the model results revealed that self-desiccation is more significant in high strength concrete compare to the normal strength concrete in the reduction of relative humidity. It can also be seen that humidity reduction is mainly due to the moisture diffusion for normal strength concrete but for high strength concrete, it is affected by both cement hydration and moisture diffusion together. Moisture diffusion coefficient is a critical parameter to identify and is required for measuring the changes of internal relative humidity due to water movement in concrete. Therefore, Zhang, Hou et al. (2011) determined the moisture diffusion coefficient at early ages for low and high strength concrete. It can be found that this coefficient decreases with increasing of drying periods and provide higher values for low strength concrete compare to the high strength one. Moisture diffusion coefficient varies from 8×10^{-8} to 7×10^{-10} m^2/s for low strength concrete and 2×10^{-8} to 4×10^{-10} m^2/s for high strength concrete from 3 to 28 days drying period after concrete casting.

However non-linear shrinkage exhibits with the effect of non-uniform moisture loss and it increases linearly with the increment of moisture losses in concrete. The exposed surfaces of concrete provide higher shrinkage than the inner part as because of higher moisture lost from the surface layer compare to the central region of concrete. Volume/surface ratio has a significant effect in shrinkage of concrete which reflects larger

the specimen size slower the moisture loss and hence lower the shrinkage strain and vice versa. Non-linear diffusion theory demonstrates non-linear diffusion of concrete and moisture diffusivity greatly depends on the pore relative humidity (RH) of concrete. Experimental investigation revealed to express the diffusion coefficient as a function of moisture content and the diffusion coefficient value of $0.23cm^2$/day and $0.30cm^2$/day was suggested by different authors (Pickett 1946, Bazant and Najjar 1972, Sakata 1982, Mu and Forth 2009). Moisture diffusion coefficient is also been determined by Akita, Fujiwara et al. (1997) with respect to the relative mass decreases during certain drying period for one-face and six-face drying of prismatic specimens and they revealed that the diffusion coefficient was a function of moisture content.

Hence Bažant and Najjar (1971) have proposed non-linear diffusion theory over the linear theory which can predict drying more realistically. They also provide mathematical formulation of moisture/pore relative humidity dependent moisture diffusivity/ diffusion coefficient which is then adopted by CEB-FIP model code applied in this study and also used by other researchers (Kim and Lee 1998, Kim and Lee 1999, Kang, Kim et al. 2011) to incorporate with their moisture diffusion model. This moisture diffusion coefficient decreases sharply at the early stages of drying in between 90 to 60% of pore humidity while it approaches approximately constant values below 60% of pore humidity inside the concrete specimens. However, there is a scarce in literature to predict the variation of moisture or relative humidity inside the concrete specimens with effect to the exposed surfaces and ambient humidity and therefore more extensive research is required to achieve the non-linear moisture profile in concrete with varying the specimen sizes and surface conditions. Hence this moisture profile can be used to quantify the shrinkage variations in concrete members and will be discussed in later sections.

2.4.2 Shrinkage strain in Concrete

Diffusion of moistures in concrete which varies with space and time yielded shrinkage strain and it provides non-uniform shrinkage profile along the depth of the concrete from exposed surfaces of concrete structures. Drying shrinkage strain was measured in a concrete specimen having size of 30 cm × 30 cm × 15 cm. Five sides of the specimen were covered with paraffin wax to avoid the moisture losses. Embedded strain gauges were used to measure the strain along the exposed surface of the specimen at 2 cm, 5 cm, 8 cm and 12 cm. Concrete specimen was kept at a constant temperature and humidity of 20±1ºC and 68±2% RH after being moist cured for 7 days. Two types of concrete, one is with admixture and another one is without admixture having the compressive strength of 44 and 28 MPa respectively was used for performing the test.

From Figure 2.6 (a) and (b), it can be seen that drying shrinkage strain varies significantly along the depth from exposed surface and the shrinkage strain decreases from the exposed surface to the inner part of the specimen. It can also be seen that the shrinkage strain exhibits slow increment inside the concrete while it increases quickly near the exposed surface of the specimen.

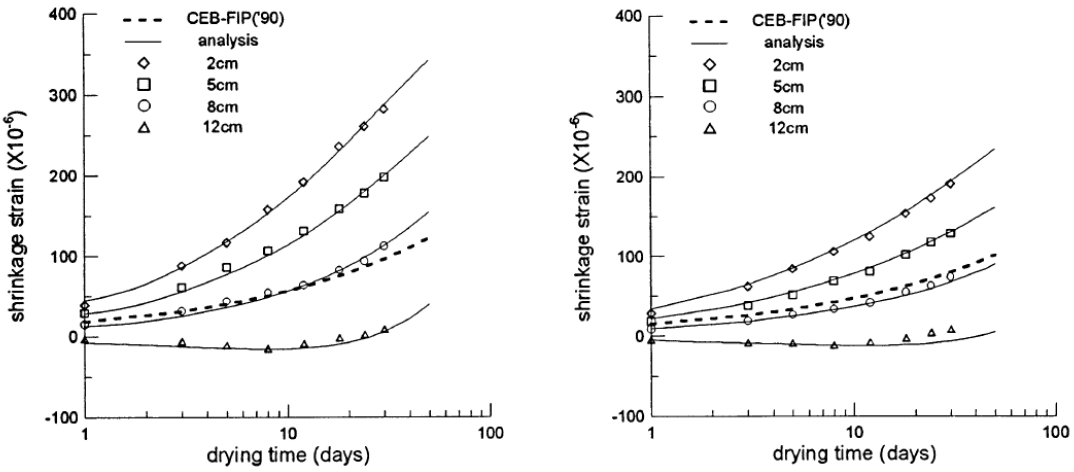

(a) Mix I (w/c=0.65) (b) Mix II (w/c=0.40)

Figure 2.6: Shrinkage strain variation along the thickness of concrete specimen for two different mixes and comparison with the analytical results (Kim and Lee 1998)

The analytical calculation also been performed with consideration of the creep of concrete. Hence the suggested analysis method able to quantify the differential drying shrinkage strain which is then compared with the test results. Thus the analysis method reflects well agreement with the test results. Furthermore, it has been recommended by the authors to consider the differential drying shrinkage strain for the analysis of thick structures and the method of analysis with the diffusion equation and embedded strain gauges is also suitable for measuring the differential drying shrinkage strain (Kim and Lee 1998).

Gilbert, Bradford et al. (2012) has also performed experimental investigation of shrinkage strain for composite concrete slab specimens for a period up to 322 days. A total of 10 specimens divided into two categories, type A (with restrained using steel deck) and type B (without restrained). Three different types of deck profiles which are re-entrant profile RF55 and two trapezoidal or wave-form profiles KF40 and KF70 were used. Vibrating wire strain gauges placed through the thickness of the slab were used to measure the concrete strain and a DEMEC gauge was used to measure the strains by placing at the upper and lower surface of the specimen. According to the test results, it can be seen that

the steel deck has provided significant restraint effect compare to the unrestrained one. An analytical calculation using age adjusted effective modulus method considering non-linear shrinkage profile for restrained specimen was performed to measure the shrinkage-induced long term deflection and curvatures. The predicted concrete stress at bottom of each slab is found almost 60% of the flexural tensile strength of concrete and that quantified the significant reduction of cracking moment. Hence it can be concluded that analytical method has shown excellent agreement with the experimental results.

According to Ong, Chandra et al. (2010) early age shrinkage strains varies along the depth of mortar specimens with using image analysis technique. Two types of specimens having the size of 75 mm × 75 mm × 285 mm and 100 mm × 100 mm × 285 mm were casted with three different water/cement (w/c) ratios of 0.25, 0.30 and 0.35. Shrinkage strains was measured from the top (trowelled/ exposed) surface along the depth (3 mm, 20 mm, 40 mm and 60 mm) of the mortar prism specimen started 30 minutes after adding water and end up to 24 hours with using the innovative image analysis technique for both sealed and unsealed specimen. The temperature and relative humidity during the whole test period was kept constant at 30 ± 0.5ºC (86 ± 0.9ºF) and 65 ± 2%. From the test results, it can be found that shrinkage strains along the depth of the specimen shows minor differences for the sealed specimens but it has shown significant variation for the unsealed specimens. In unsealed specimens, shrinkage strains decreased from the exposed top surface to the depth of the mortar specimens. Moreover, it can be also seen that higher shrinkage strains occurred to the lower w/c ratio specimens compared to the higher one. That means high level of early-age shrinkage strains achieved for the lower w/c ratios mortar specimens and vice-versa. However, a limited number of research has been found on non-linear shrinkage behaviour in concrete and hence a further investigation is required

to quantify the non-linear shrinkage profile in concrete specimens with varying the sizes and surface boundary conditions.

2.4.3 Correlations in between with Moisture loss, Humidity and Shrinkage strain of Concrete

Shrinkage strain is directly related to the moisture/ humidity loss of concrete to the atmospheric environment and many researchers investigated the relationship in between them to quantify shrinkage strain from moisture /humidity loss of concrete will be discussed in this section.

Figure 2.7 (a) and (b) below represents the relative humidity at 3 cm, 7 cm and 12 cm distance of 10 cm × 10 cm × 20 cm prism specimens measured after 3 and 28 days moist curing. These Figures shown the relative humidity occurred only for moisture diffusion that been achieved by subtract the humidity due to self-desiccations. It can be found that the effect of water/cement ratio on moisture diffusion is substantial and high water/cement ratio concrete shows higher diffusion rate compare to the low water/cement ratio concrete. Numerical finite element analysis been performed using non-liner moisture diffusion theory and maximum moisture diffusion coefficient (which provides the best fit with experimental results) which shows well agreement with experimental results.

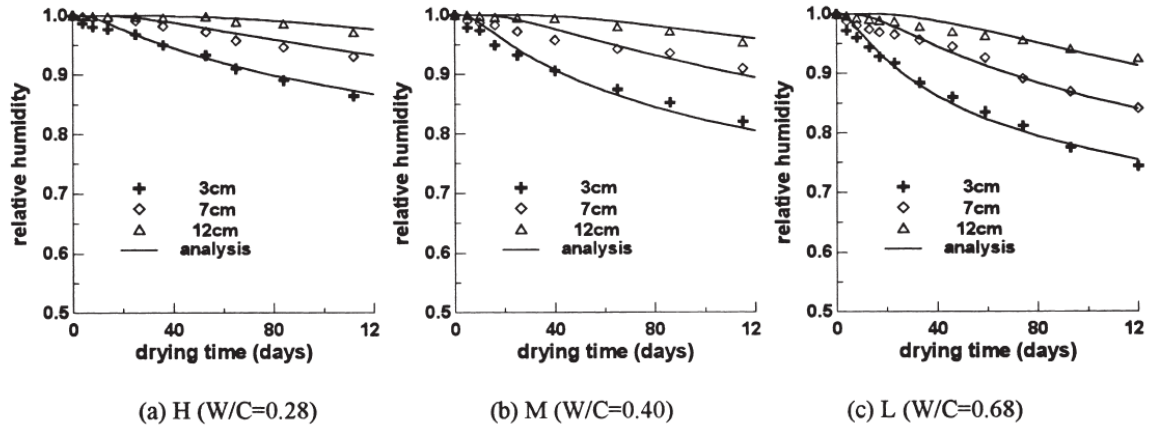

(a)

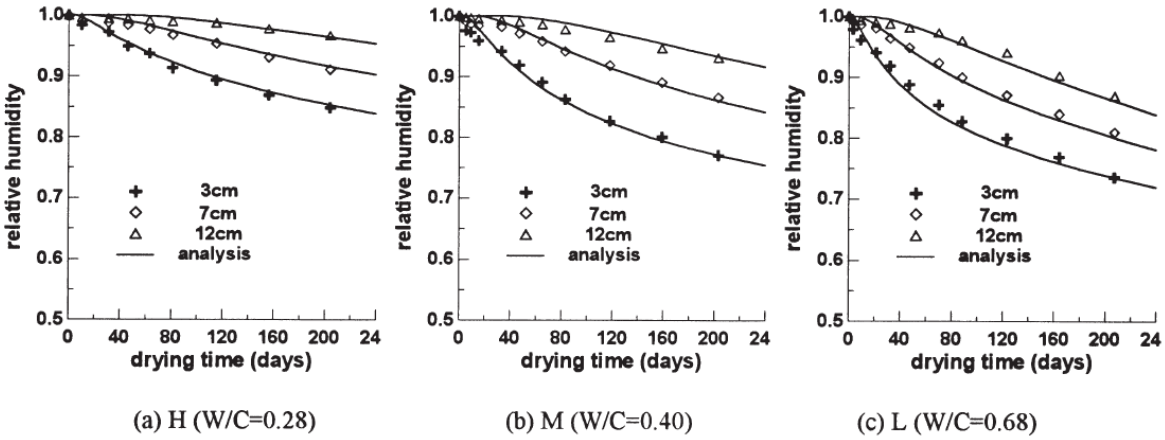

(b)

Figure 2.7: Calculated relative humidity compared to modified experimental results due to moisture diffusion only a) curing period = 3 days b) curing period = 28 days (Kim and Lee 1999)

Hence the linear relationship between humidity and moisture diffusion in concrete and it exhibits significant effect on moist curing periods and which is illustrated in Figure 2.8. Internal relative humidity occurred only due to moisture diffusion varied slowly at each location for 28 days moist curing compare to the 3 days moist cured concrete. Concrete microstructure is affected by curing periods which effects the moisture diffusion as well.

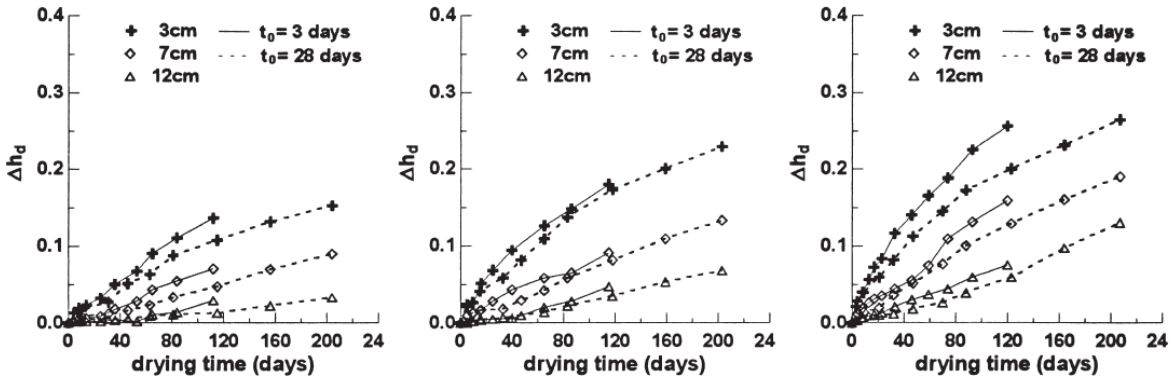

(a) H (W/C=0.28) (b) M (W/C=0.40) (c) L (W/C=0.68)

Figure 2.8: Relationship between relative humidity and moisture diffusion on different moist curing period (Kim and Lee 1999)

Moisture loss has direct relationship with moisture diffusion and indirect relationship with self-desiccation. Hence according to Figure 2.9, high water/cement ratio concrete provides higher amount of water loss in terms weight per unit exposed area compare to the low water/cement ratio one. Moist-curing time has also significant effect on moisture loss of concrete and it can be found that 3 days moist-cured concrete gives higher moisture loss as because of high amount of evaporable free water content in capillary pore with comparison of 28 days moist cured one (Kim and Lee 1999)

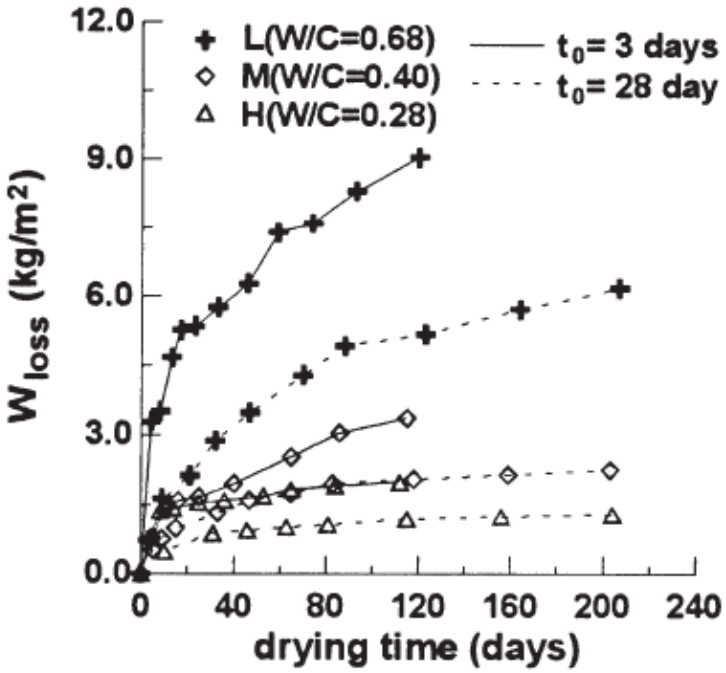

Figure 2.9: Loss of moisture in concrete due to drying (Kim and Lee 1999)

Finite difference method using moisture diffusion coefficient considering the concrete porosity and temperature effect applied to compare with experimental results performed by Kim & Lee, 1999 as illustrated in Figure 2.10. Gradient boundary conditions were used using environmental humidity, surface humidity and surface factor of concrete. It can be seen that numerical investigation shown good agreement with experimental results as shown in Figure 2.10 (Kang, Kim et al. 2011).

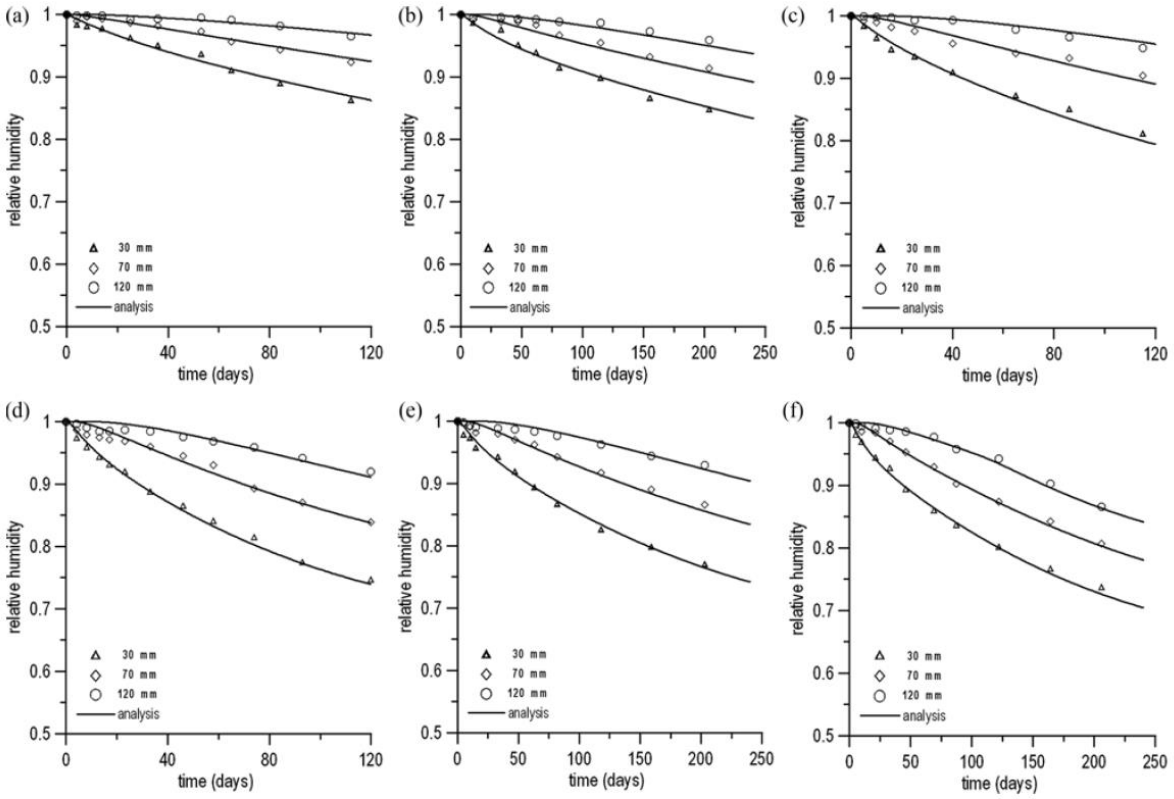

Figure 2.10: Comparisons between experimental and numerical results (ambient temperature 200 C): a) Exposed at 3 days (w/c = 0.28) b) Exposed at 28 days (w/c = 0.28) c) Exposed at 3 days (w/c = 0.40) d) Exposed at 28 days (w/c = 0.40) e) Exposed at 3 days (w/c = 0.68) f) Exposed at 28 days (w/c = 0.68) (Kang et al 2012)

Hence the relationship between shrinkage and relative humidity for both cement paste and mortar specimens represents in Figure 2.11. It can be seen that shrinkage has linear relationship with relative humidity in between 48 to 100% for cement pastes. For mortar specimens, the slope between 48 to 75% is lower and then it exhibits increment in between the relative humidity range of 75 to 100% and the effect of water/cement ratio is negligible. So it can be said that drying shrinkage is inversely proportional to the environment relative humidity. Hence it can be observed that drying shrinkage is approximately proportional to the water loss of specimens as shown in Figure 2.12 (Bissonnette, Pierre et al. 1999).

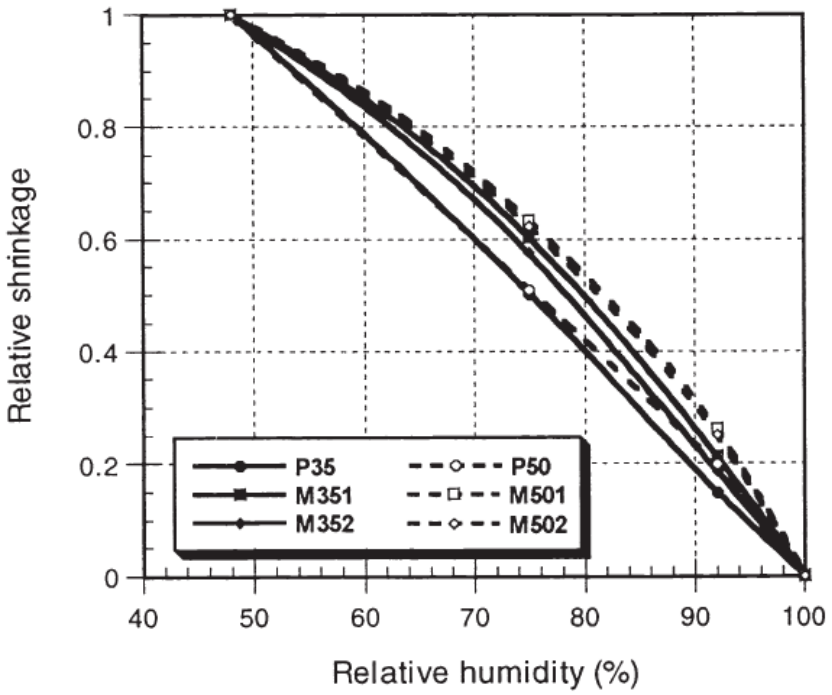

Figure 2.11: Relationship between ultimate shrinkage and relative humidity for cement paste and mortar specimens (Bissonnette, Pierre et al. 1999)

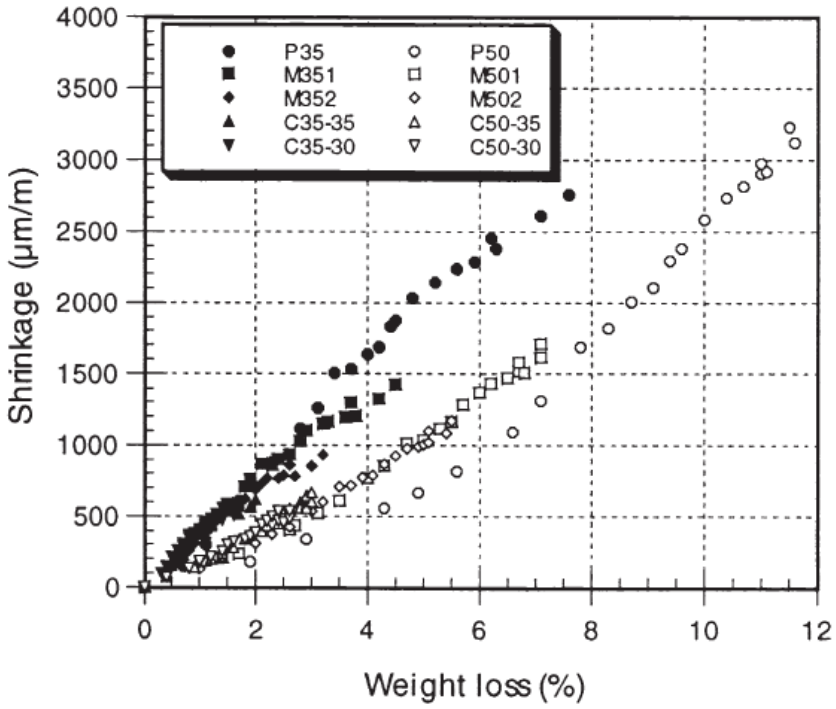

Figure 2.12: Relation between shrinkage and weight loss for various types and sizes of paste, mortar and concrete specimens (Bissonnette, Pierre et al. 1999)

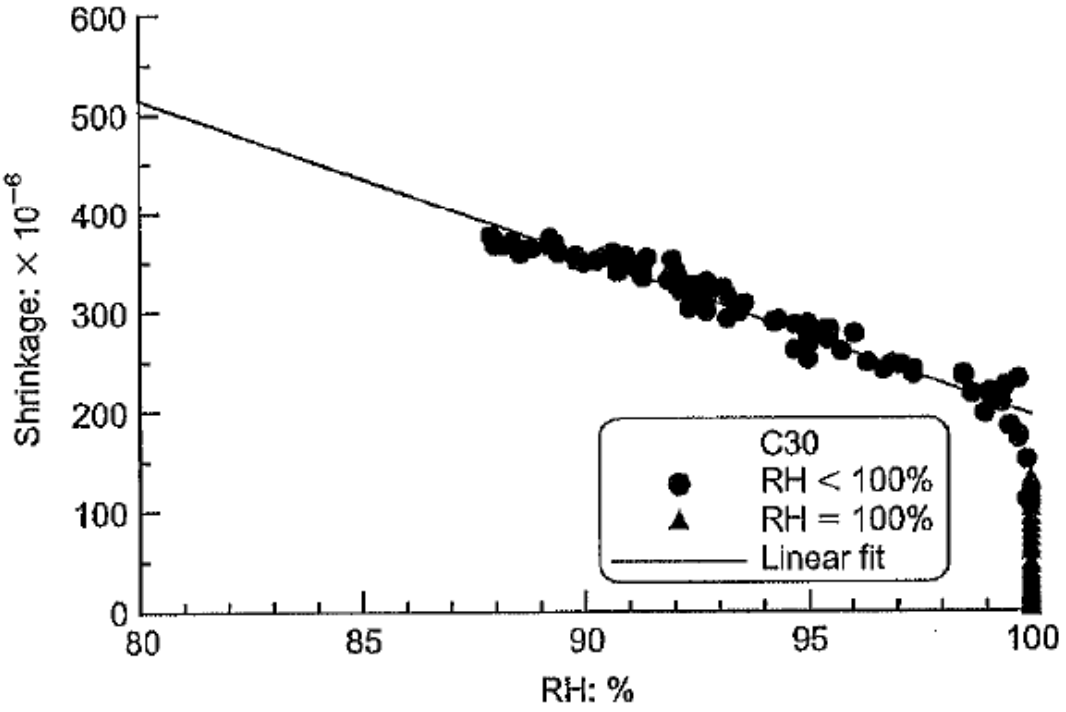
600
500
400
300
200
100
0
Shrinkage: × 10⁻⁶
80
85
90
95
100
RH: %
C30
RH < 100%
RH = 100%
Linear fit

(a)

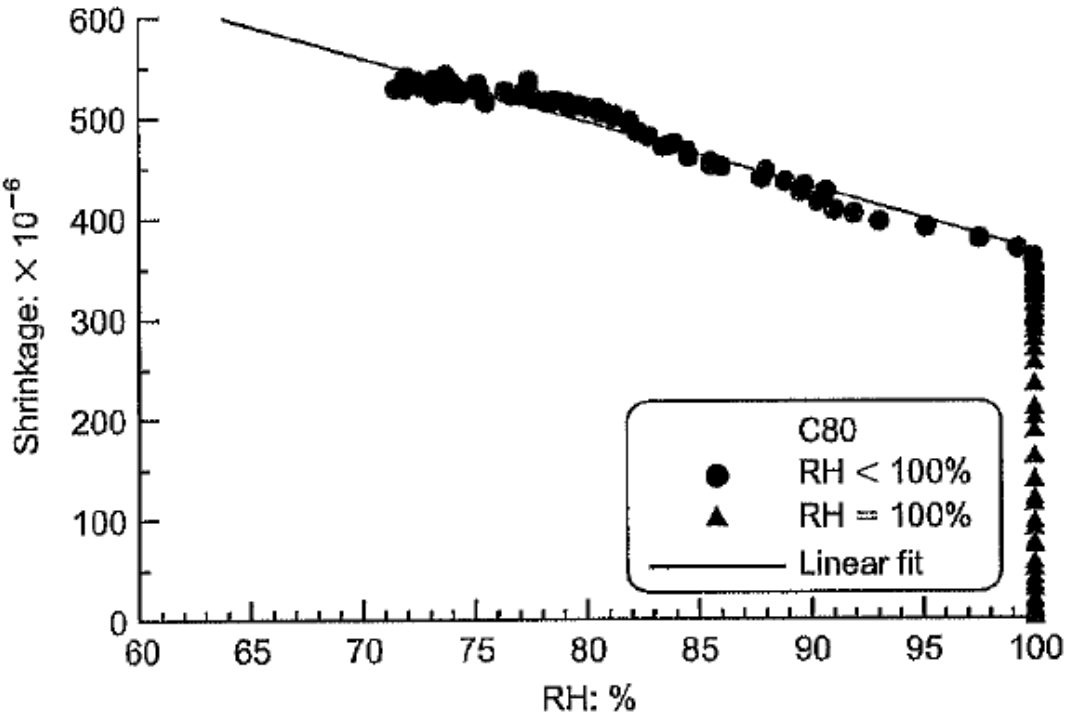
600
500
400
300
200
100
0
Shrinkage: × 10⁻⁶
60
65
70
75
80
85
90
95
100
RH: %
C80
RH < 100%
RH = 100%
Linear fit

(b)

Figure 2.13: Relationship between free shrinkage strain and interior relative humidity (RH) of a) C30 concrete and b) C80 concrete (Zhang, J, Dongwei and Wei 2010)

Relationship between free shrinkage strain (ε_w) and interior relative humidity of concrete has shown in above Figure 2.13 for two different types of concrete having 28 days compressive strength of 34 MPa (C30) and 88 MPa (C80). Free shrinkage results can be split into two parts whereas free shrinkage induced at stage I (RH = 100%) and free shrinkage induced at stage II (RH < 100%). Linear relationship between shrinkage strain and internal relative humidity can be achieved at stage II for both C30 and C80 concrete and the relationship can be expressed as

$\varepsilon_w = \varepsilon_0 + k$ (100-RH) for RH < 100% Equation 2.2

Where ε_w is the free shrinkage strain, ε_0 is the shrinkage at stage I (RH = 100%), k is the shrinkage strain occurred due to one-unit humidity reduction. For this case, ε_0 = 197 & 367 μm/m and k = 15.8 & 6.4 μm/m per percentage for C30 and C80 concrete respectively.

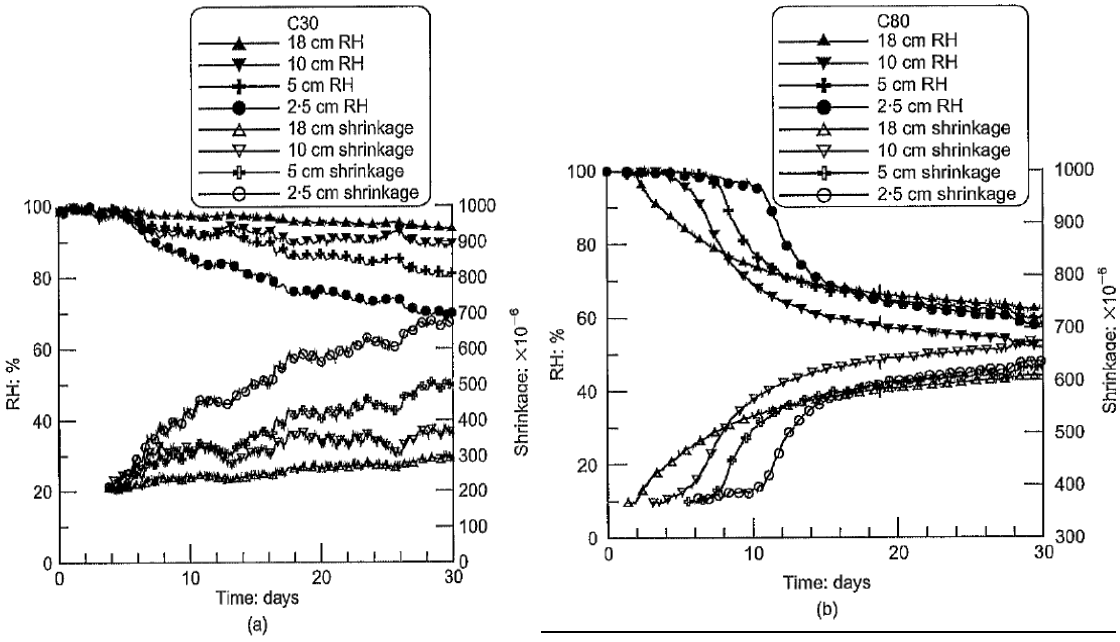

Figure 2.14: Calculated free shrinkage strains and measured relative humidity at different depths of the slab from exposed surface against drying period (Zhang, J, Dongwei and Wei 2010)

Figure 2.14 displays above the analytical free shrinkage strain calculated by using Equation 2.2 and internal relative humidity measured at various depths of 2.5, 5, 10 and 18 cm of 200×200×800 mm slab specimens sealed at five sides except top surface against moisture movement for two types of concrete C30 and C80. Significant variation of humidity reduction and shrinkage strain exhibits through the depth of slab. It should be noted that shrinkage strain has been achieved only for stage II (RH < 100%) by using Equation 2.2 but moisture induced shrinkage also occurred at stage I when RH = 100%. Therefore, author recommend for further investigation in complete exploration of non-linear relationship between internal relative humidity and shrinkage strain of concrete (Zhang, Dongwei et al. 2010).

A series of experimental tests for different types of concrete (low, medium and high strength) in sealed and dry conditions of concrete prism been performed for validation of a theoretical model that including pore correction factor, developed both for autogenous and drying shrinkage strain predictions and it provides well agreement with the experimental results (Jun, Dongwei et al. 2010, Zhang, Hou et al. 2012, Zhang, Hou et al. 2012).

Experimental investigated moisture loss at a depth of 1 cm from drying surface is plotted against free shrinkage strain in Figure 2.15. Hence it can be seen that the relationship between free shrinkage strains and moisture loss in non-linear. It can be expressed by this Equation based on a regression model:

$$(\varepsilon_{sh})_M = [M^{2.5}/ (195 + M^{2.5})] \times (\varepsilon_{sh})_{ult} \qquad \text{Equation 2.3}$$

This Equation is very similar to the form of ACI committee 209 Equation for the variation of shrinkage with time (ACI209R-92 1997). Here, ε_{sh} is the free shrinkage strain, M is the loss of moisture in percentage starting from 0% and $(\varepsilon_{sh})_{ult}$ is the ultimate free shrinkage strain which is considered 1600 micro strain for this case. The free shrinkage strain can be able to predict with using Equation 2.3 for different values of moisture loss in concrete (Asad 1995).

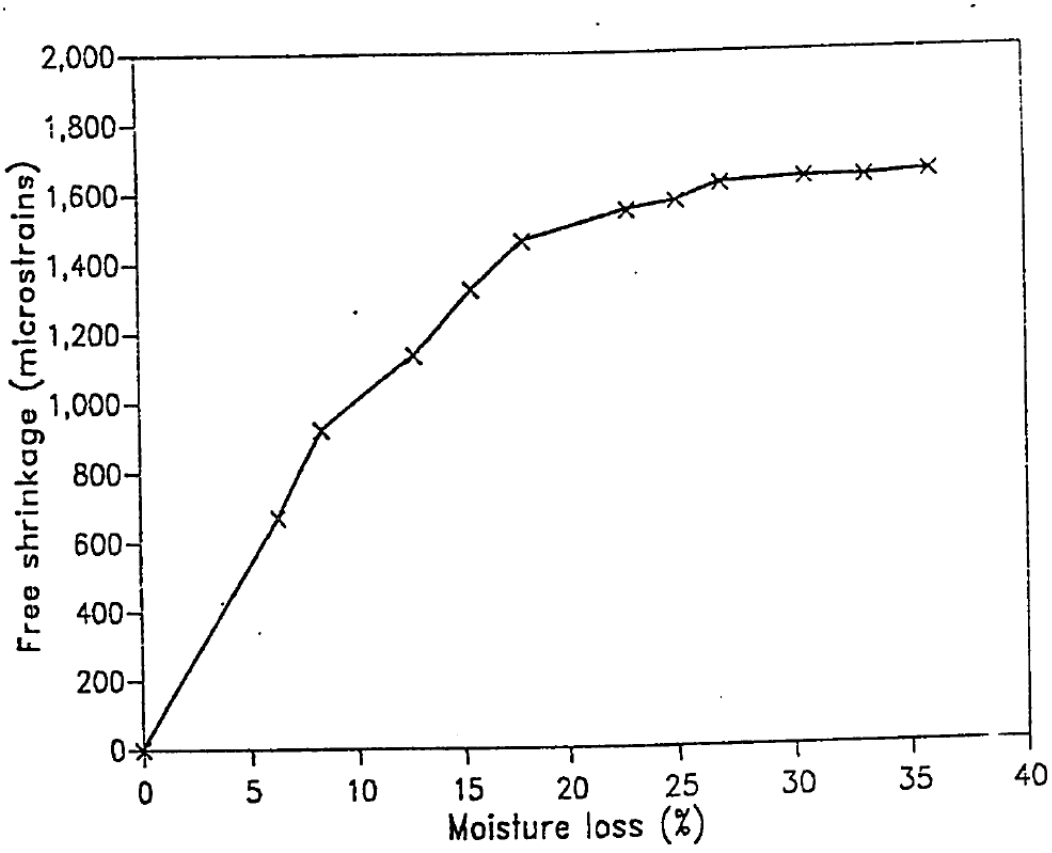

Figure 2.15: Relationship between free shrinkage strain and moisture loss (ACI209R-92 1997; Asad, M 1995)

Suwito, Ababneh et al. (2006) has performed analytical and numerical investigation on moisture diffusivity and its effect on drying shrinkage of concrete. Finite element method been used for the analysis of concrete slab specimen having a depth of 20 cm and 100 cm long. The slab is considered to be fully saturated at the initial stage (RH = 100%) and

environmental humidity at the exposed top surface is 50% (rest of the surfaces are sealed). It can be seen from the finite element mesh consisting of 3000 quadrilateral elements that RH decreases from sealed surface to the exposed surface along the depth of the slab over the period of 365 days and its converging to the boundary conditions at RH = 50%. Shrinkage strain is increased through the depth from sealed surface to exposed face over the total period of a year. Two types of curves have shown one is damaged and another one is undamaged. Damage curve has given higher effect than the undamaged one. As because drying shrinkage occurs due to moisture loss and it generates damage. In consequence, damage increased the concrete diffusivity which accelerates the moisture dissipation. Bazant, Sener et al. (1987) has also performed experimental and analytical studies cracking effect on drying permeability and concrete diffusivity. They found that cracked specimen dried more rapidly than the uncracked one and simultaneously cracked specimen showed more weight loss compared to the uncracked one. Granger, Torrenti et al. (1997) has developed a model which is in good agreement with shrinkage as a function of moisture loss. Previous experimental result reveals that concrete loses its weight with the effect of drying shrinkage and it shows non-linear relationship between shrinkage strain and weight loss of concrete.

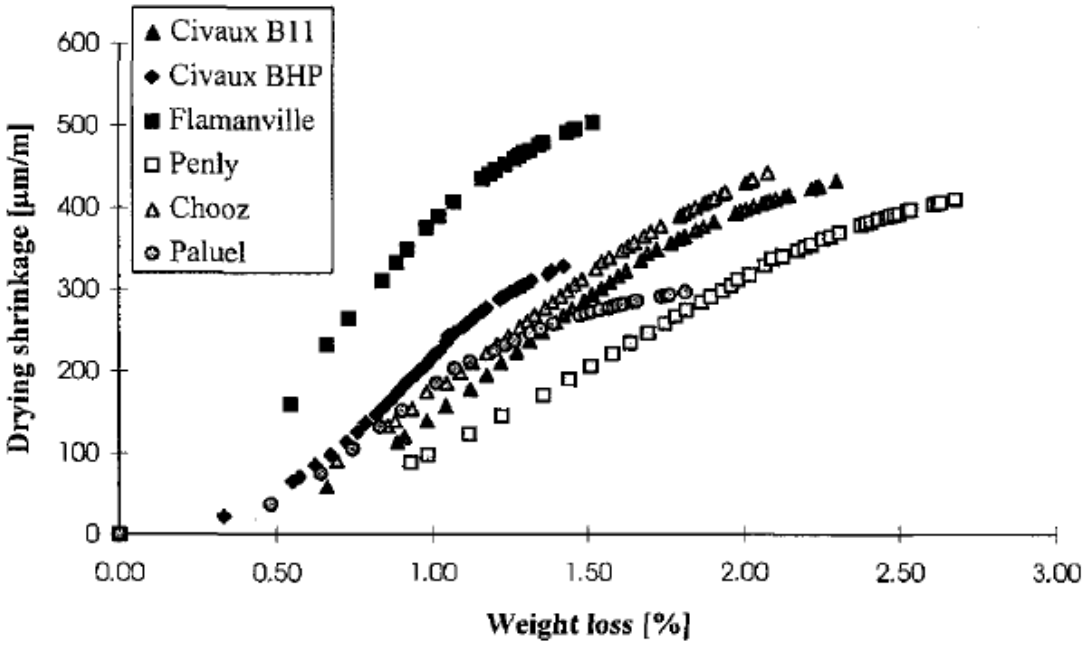

Figure 2.16: Experimental results of different concrete specimens drying shrinkage as a function of weight loss (Granger, Torrenti and Acker 1997)

Above Figure 2.16 represents the drying shrinkage as a function of weight loss for six different types of concrete having 28 days compressive strength of 30 MPa to 65 MPa. Concrete specimens of having 16 cm diameter and 100 cm height are kept at controlled ambient conditions of 50±5% RH and 20º±1º C. End of the specimens were sealed with self-adhesive aluminium layers for preventing any loss of moisture. Only radial drying was allowed and the shrinkage measurement was taken at the middle of 50 cm of the cylinders. Drying shrinkage was achieved by subtracting the autogenous shrinkage measured from completely sealed specimen by two self-adhesive aluminium layers to prevent drying and kept under the same environment conditions. Shrinkage test was began after 28 days when the cylinders were covered with a polyane film and itself covered with two self-adhesive aluminium layers to prevent from moisture before 28 days. Among all the six types of concrete, if we closely concentrate on Penly concrete having 28 days compressive strength of 24.3 MPa; it can be seen that 1% weight loss occurred at the

drying shrinkage strain value of 100 micro strains. Concrete is gradually losing its weight as the shrinkage strain increases and the graph shows linear behaviour up to the value of 2% weight loss then non-linear relationship exhibits to the maximum drying shrinkage of 400 micro strains at an amount of 2.7% weight loss of concrete.

However, the free shrinkage strain of concrete is a function of pore relative humidity and can be described using Equation 2.4 from Bažant and Yunping (1994) has been used in this current study.

$$\varepsilon_{sh} = k_{sh} f_s(h) = k_{sh}(1-h);\ k_{sh} = \varepsilon_s^0 g_s(t) \qquad \text{Equation 2.4}$$

Where, k_{sh} is the shrinkage coefficient; ε_s^0 is the ultimate shrinkage strain and $g_s(t)$ is the ratio of elastic modulus with time, i.e., $g_s(t) = \frac{E_{(t0)}}{E_{(t)}}$ and $E(t)$ can be estimated by

$E(t) = E(28)\sqrt{\frac{t}{4+0.85t}}$ with $E(28) = 33w^{1.5}\sqrt{f_c'}$

2.5 Member Behaviour

The shrinkage induced deformation affects the serviceability of structures by producing initial cracks even before application of loading and increases the crack widths after loading as drying commences that accelerates shrinkage and finally enhances shrinkage induced excessive deformations in a concrete member at a later period and which may cause the serviceability failure of a RC member.

2.5.1 Models to predict long term Deflections

There are several models to quantify long term deflections of RC members such as beams or slabs. The prediction of long term deflections in a concrete member depends on so many parameters including nonlinear concrete material properties, history of loading, flexural cracking, time dependent effects due to creep and shrinkage, loading ages in

concrete and reinforcement ratios. Some codes such as AS 3600-2009 (Standards Australia 2009), CEB FIP model code 90 (CEB-FIP 1990) and ACI 318-08 (American Concrete Institute 2008) provide simplified method to quantify instantaneous and long term deflection of RC members.

The instantaneous deflection using these methods are computed with using effective second moment of area, I_{eff} or mean curvature of the member, K_m and that are provided by empirical equations. The long term deflection calculation due to creep and shrinkage can be determined from the material properties of concrete i.e. design shrinkage strain and creep coefficient of concrete and the principles of mechanics. The other simplified method to quantify the time dependent long term deflection is to multiply the instantaneous deflection by a deflection multiplying factor λ which is also given by an empirical equation.

These simplified methods do not consider the ageing of concrete, loading history, bond slip behaviour between steel and concrete, flexural cracking variation with time, tension stiffening behaviour of concrete prism and steel in the cracked region. Hence according to Gilbert (1999), the present simplified method may not be able to calculate the instantaneous and time dependent long term deflection perfectly especially for lightly reinforced concrete beams and slabs. Hence, there is a need to provide a better deign procedures to predict the short and long term deflections of RC members with incorporation of ageing of concrete, loading history, bond slip characteristics between steel and concrete, crack propagation with time, steel in between cracked concrete need to be considered (Gilbert and Ranzi 2011, Jayasinghe 2011).

Numerical models are also been developed to compute the long term deflection of reinforced concrete beams or slabs where non-linear material properties of concrete,

flexural cracking, tension stiffening and bond slip behaviour between reinforcement and concrete are been considered in the analysis. In such analysis RC member is divided into elements and each elements containing flexural cracks been initiated. In this method the RC member is divided into block element and each block is having two flexural cracks where a bond slip relationship between steel and concrete can be presented and can be said that there is no perfect bond between steel and concrete been applied (Fantilli, Ferretti et al. 1998, Gravina and Warner 2003, Gravina and Smith 2008).

Gravina (2002) proposed a block model where a linear variation of strain is considered at crack faces to compute the stress and tensile steel and tensile concrete strains are been used to quantify the deflections of the member. This model is applicable for one layer of reinforcement to predict the crack formation of RC beams and the similar trend can be observed from the block model developed by Fantilli, Ferretti et al. (1998).

Oehlers, Liu et al. (2005) proposed a model to predict the deflection of RC beams due to instantaneous loading considering the formation of flexural cracks, interaction between steel and concrete, allowing slip of the bars and can be applicable for multiple layers of steel but unable to predict long term deflection considering the effect of creep and shrinkage.

A finite element method proposed by Pulmano and Shin (1987) to predict the instantaneous and long term deflections of simply supported, continuous RC and prestressed concrete beams using empirical equations to compute the effective bending stiffness and the creep and shrinkage curvatures.

Bazant and Oh (1984) proposed a model to quantify the short term deformations of members up to ultimate load and long term creep deformations of cracked beams by making an assumption of concrete having nonzero tensile capacity and characterized by a

uniaxial stress strain diagram that has progressive micro cracking behaviour due to strain softening. Prasada Rao, Jayaraman et al. (1994) proposed a model to calculate the time dependent stress and strain distribution in concrete due to the effect of creep and shrinkage and the relaxation of prestressing steel in a cracked prestressed concrete member without considering the tensile strength of concrete.

Jayasinghe (2011) developed an analytical model to predict the long term deflections of post-tensioned beams and one way spanning slabs under sustained loading conditions including its rotations, crack widths and crack spacing considering the effect of creep and shrinkage, bond slip behaviour between steel and concrete and prestress losses over time. Gribniak (2009) proposed an innovative numerical model to derive a free of shrinkage tension stiffening relationships using test data of shrunk bending RC members and applying moment curvature relationships to investigate the short-term deformation of RC flexural members due to the effect of shrinkage.

All of these mentioned above numerical and analytical models and simplified methods to quantify the instantaneous and long term deflection of RC members are mainly based on moment curvature (M/χ) approach where there is a linear strain profile and the full interaction (FI) between reinforcement and concrete that is reinforcement does not slip relative to the concrete is been considered. Therefore in these assumptions, it can be found that the analysis techniques are unable to describe the crack widths and crack spacing or widening properly as because these techniques are relied on the effective flexural rigidity (EI_{eff}).

Hence, a numerical model has been developed using partial interaction (PI) moment rotation (M/θ) approach to predict the instantaneous deflection of RC flexural members and that taken into consideration the bond slip behaviour in between with concrete and

steel, tension stiffening of the concrete prism and considering the flexural cracking behaviour with crack widths and crack spacing of the member accurately (Oehlers, Mohamed Ali et al. 2011, Visintin, Oehlers et al. 2012, Visintin, Oehlers et al. 2013). This numerical partial interaction (PI) moment rotation (M/θ) analysis technique has been extended by Visintin, Oehlers et al. (2013) to quantify the long term deflection of RC members incorporating the effect of creep and shrinkage. But in this case, linear shrinkage strain profile of the member has been considered which is quite straight forward to do the analysis and in the practice shrinkage strain profile should be strongly non-linear as mentioned earlier and also varies along the depth and width of the member. Therefore, there is a need to develop a new model to quantify the long term deflection of RC members with incorporation of creep and non-linear shrinkage variations in concrete member.

2.6 Summary

Based on the critical reviewing of all the literatures stated above the following conclusion can be drawn:

The most common cause of cracking in concrete structures occur due to shrinkage. Direct tension cracks due to restrained shrinkage can penetrate through the member and these are always difficult to control and can create serviceability and durability problems to the structures. In addition, shrinkage is detrimental to the structures which may result in significant deflections to the member and the restrained shrinkage can cause tension in the concrete and that result the cracks and if not controlled properly can lead to durability and serviceability failures to the members. Current design techniques assume uniform shrinkage profile but in practice it is strongly non-linear and also influence of member size has significant effect in shrinkage strains. A limited number of research been conducted to quantify the non-linear shrinkage behaviour of concrete. Therefore, a

numerical moisture diffusion model been developed to predict the non-linear shrinkage behaviour of concrete along both its depth and width of the member. Hence an experimental program has also been proposed to quantify the shrinkage behaviour of concrete member varying the exposed surfaces with considering the member size effect as well.

Finally, it can be clearly stated that a lack of research and knowledge is existing in this shrinkage effect in RC structures and we can briefly mention that although a lot of research has been performed on this time dependent shrinkage behaviour of concrete but still these behaviours are not been clarified properly. However, there is a need to do more research to explore completely the shrinkage effect of concrete which will be able to quantify the shrinkage induced deformation of RC members effectively. There is no research been conducted on using non-linear shrinkage profile along the depth and width of the member to examine the influence of non-linear shrinkage on member behaviour and there are also no design guidelines available for long term member deflection allowing for non-linear shrinkage. Hence, a numerical partial interaction (PI) segmental moment rotation (M/θ) approach is been developed to quantify the long term deflection of RC members and which also considers the non-linear shrinkage behaviour along the depth and width of the member.

Chapter 3 Journal Paper on Non-linear Shrinkage

This chapter deals with the journal article prepared from this study titled "Mechanics of simulating the serviceability deflection of RC beams allowing for partial interaction and non-linear shrinkage".

In this chapter, it is shown that the mechanics of simulating the long term serviceability deflection of RC beams is very complex as it requires four specific mechanics models:

(1) A diffusion model to quantify the variation of shrinkage strain with: time; environmental conditions; beam shape; beam surface conditions; and with the width and depth of the beam.

(2) A full interaction flexural segmental analysis that can cope with the variations in shrinkage strain from the diffusion model to quantify: the behaviour of the beam in uncracked regions; and also to predict the onset of flexural cracking that is the start of partial interaction behaviour.

(3) A partial-interaction tension stiffening analysis that can cope with imposed shrinkage strains from the diffusion model to quantify: primary crack spacings and widths; the onset of secondary cracks and their spacings and widths; and crack opening stiffnesses.

(4) A partial interaction flexural segmental analysis that can cope with any imposed variation in shrinkage strain to quantify the behaviour of the cracked sections of the beam. This analysis gives: the moments at which primary and secondary cracks occur; variations in crack spacings and widths; and mechanically correct moment-curvatures for quantifying the deflections.

This research provides mechanics solutions for all the facets that control the serviceability time dependent behaviour of RC beams. It is envisaged that these numerical mechanics solutions can provide researchers with the tools to develop simple design procedures.

Publication:

Mechanics of simulating the serviceability deflection of RC beams allowing for partial interaction and non-linear shrinkage

[1]Noor Md. Sadiqul Hasan, [2]Terry Bennett, [3]Phillip Visintin

and [4]Deric John Oehlers

[1]Noor Md. Sadiqul Hasan

PhD Candidate

School of Civil, Environmental and Mining Engineering

The University of Adelaide

South Australia 5005

AUSTRALIA

[2] Dr. Terry Bennett

Senior Lecturer,

School of Civil, Environmental and Mining Engineering

The University of Adelaide

South Australia 5005

AUSTRALIA

Corresponding Author:

[3]Dr.Phillip Visintin

Senior Lecturer,

School of Civil, Environmental and Mining Engineering

The University of Adelaide

South Australia 5005

AUSTRALIA

email: phillip.visintin@adelaide.edu.au

Tel. +61 8 8313 3710

Fax. +61 8 8303 4359

[4]Emeritus Professor Deric J. Oehlers

School of Civil, Environmental and Mining Engineering

The University of Adelaide

South Australia 5005

AUSTRALIA

Submitted to Proceedings of the Institution of Civil Engineers – Structures and Buildings

Statement of Authorship

Mechanics of simulating the serviceability deflection of RC beams allowing for partial interaction and non-linear shrinkage
Submitted to Proceedings of the Institution of Civil Engineers – Structures and Buildings

Noor Md. Sadiqul Hasan (Candidate)

Performed all analysis of the paper and wrote the manuscript.

I hereby certify that the statement of contribution is accurate and give permission for the inclusion of the paper as thesis chapter

Signed.....Date.....

Terry Bennett

Helped in analysis of the paper and manuscript evaluation.

I hereby certify that the statement of contribution is accurate and give permission for the inclusion of the paper as thesis chapter

Signed.....Date.....

Phillip Visintin

Supervised the work development and edit the manuscript.

I hereby certify that the statement of contribution is accurate and give permission for the inclusion of the paper as thesis chapter

Signed.....Date.....

Deric John Oehlers

Helped in evaluation and in editing the manuscript.

I hereby certify that the statement of contribution is accurate and give permission for the inclusion of the paper as thesis chapter

Signed.....Date.....

Mechanics of simulating the serviceability deflection of RC beams allowing for partial interaction and non-linear shrinkage

Noor Md. Sadiqul Hasan, Terry Bennett, Phillip Visintin and Deric John Oehlers

Abstract

Existing analysis and design techniques to quantify serviceability member deflection of reinforced concrete (RC) beams are generally built on two major premises: (1) full interaction (FI) through the use of moment curvature approaches; and (2) a uniform longitudinal shrinkage strain ε_{sh} within the member to simplify the analysis. Both premises are gross approximations. With regard to the first premise, RC beams are subject to flexural cracking and the associated partial interaction (PI) behaviour of slip between the reinforcement and adjacent concrete. Furthermore with regard to the second premise, numerous tests have shown that ε_{sh} varies along both the width and depth of the beam that is, it is far from uniform. Hence the quantification of the serviceability deflections of RC beams for design is subject to two major sources of error: that due to the PI mechanisms that occur in practice; and that due to the time dependent material properties of shrinkage and creep. This paper deals with the development of PI numerical mechanics models with non-linear shrinkage strain variations required to simulate the PI behaviour of RC beams in order to considerably reduce the source of error due to the mechanics model. This new mechanics model will allow: the development of better design mechanics rules for serviceability deflection; and also assist in the better quantification of creep and shrinkage by removing or considerably reducing the existing mechanics source of error.

Keywords: reinforced concrete beams; deflection; concrete shrinkage; concrete creep; partial interaction mechanics; segmental approach.

List of notation

A_c cross sectional area of concrete in prism

A_r cross section area of reinforcement

A_{rc} total A_r in compression

A_{rt} total A_r in tension

B bond force at reinforcement/interface

B_n B in n^{th} prism segment

b width of beam

C moisture diffusion coefficient

C_1 maximum value of C

C_n force in concrete on left hand side of n^{th} segment

D displacement of reinforcement relative to position at unstressed state

$D_{b\text{-}long}$ long term deflection of beam at mid-span

$D_{b\text{-}short}$ short term deflection of beam at mid-span

D_{FI} D from full interaction analysis

D_{PI} D from partial interaction analysis

d full depth of beam

d_{rt} distance of tension reinforcement to tension face of beam; half depth of reinforced concrete prism

d_{NA} depth of neutral axis from compression face

$d_{NA\text{-}c}$ d_{NA} for concrete section

d_{NA-cn} d_{NA} for concrete slice n

d_{NA-r} d_{NA} for all the longitudinal reinforcement

$d\Delta/dx$ slip strain

E_c concrete modulus allowing for creep

E_r reinforcement modulus

$E_{(t)}$ concrete elastic modulus at a given time

$E_{(t0)}$ initial elastic modulus of concrete

EI flexural rigidity

F force profile

F_{cc} resultant force in concrete in compression

F_{ccn} F_{cc} in $n^{th\ slice}$

F_{ct} resultant force in concrete in tension

F_{ctn} F_{ct} in n^{th} slice

F_{rc} resultant force in compression reinforcement

F_{rt} resultant force in tension reinforcement

FI full interaction

f surface factor

f_c compressive strength of concrete

f_{ck} Characteristic compressive strength

f_{ct} tensile strength of concrete

$g_s(t)$ $E_{(t0)}/E_t$

H pore humidity

H_c H when $C(H) = 0.5C_1$

H_{en} environmental humidity

H_s surface humidity

k_{sh} shrinkage coefficient

L_b length of beam

L_{def} half length of symmetrically loaded segment; half length of concrete prism prior to straining

L_{per} length of reinforcement perimeter

L_s length of prism segment

L_T total length of prism after straining

m empirical constant for the diffusion coefficient

M moment

M_{cr} moment to cause cracking

$M_{cr\text{-}in}$ M_{cr} to cause initial crack in uncracked beam

$M_{cr\text{-}pr}$ moment to cause primary cracks

$M_{cr\text{-}sec}$ moment to cause secondary cracks

n number of slices per half width

P resultant longitudinal force in reinforcement

P_{cr} resultant force in reinforcement at a flexural crack

$P_{cr\text{-}pr}$ P_{cr} at the formation of primary cracks

$P_{cr\text{-}sec}$ P_{cr} to cause secondary cracks

P_{cr}/Δ_{cr} crack opening stiffness

P_n P on left side of n^{th} element

PI partial interaction

RC reinforced concrete

S_{cr} crack spacing

$S_{cr\text{-}pr}$ primary crack spacing

T temperature

t time

w width of crack; $2\Delta_{cr}$

α_0 empirical constant for the diffusion coefficient

χ curvature

Δ slip of reinforcement

Δ_{cr} Δ relative to crack face; w/2

Δ_n slip at n^{th} segment

δ deformation profile

δ_b interface bond slip

$\delta_{c\text{-}n}$ concrete deformation within n^{th} slice

δ_{rc} contraction of compression reinforcement

δ_{rt} extension of tension reinforcement

$\delta\Delta_n$ change in slip in n^{th} segment

ε strain profile; strain

ε_c concrete strain distribution

$\varepsilon_{c\text{-}sh}$ strain in concrete due to shrinkage

ε_{cn} ε_c in n^{th} slice; mean concrete strain in n^{th} prism segment

ε_{ct} fracture strain of concrete; f_{ct}/E_c

ε_r reinforcement strain distribution

ε_{rc} strain in compression reinforcement

ε_s^0 magnitude of the ultimate shrinkage strain

ε_{rt} strain in tension reinforcement

ε_{rn} mean reinforcement strain in n^{th} prism segment

$\varepsilon_{r\text{-}sh}$ strain in reinforcement due to shrinkage

ε_s^0 ultimate concrete shrinkage strain

ε_{sh} shrinkage strain

ε_{shn} shrinkage strain distribution in n^{th} slice of concrete or n^{th} prism

θ rotation

σ stress profile

σ_c concrete stress distribution

σ_{cc} stress in concrete at level of compression reinforcement

σ_{ct} stress in concrete at level of tension reinforcement

σ_r reinforcement stress distribution

σ_{rc} stress in compression reinforcement

σ_{rt} stress in tension reinforcement

τ_b interface bond stress

τ_{bn} τ_b in n^{th} segment

1. Introduction

Prior to flexural cracking, the deflection of an RC beam can be derived from strain based approaches (Faber 1927; Whitney 1932; Bresler and Selna, 1964; Ghali et al., 1967; Bazant 1972, Branson 1977; Gilbert 1988; Gilbert and Ranzi, 2011) , such as the use of FI flexural rigidities (*EI*) or FI moment-curvatures (M/χ), and it is fairly straightforward

to incorporate constant values of shrinkage strain ε_{sh} (Visintin et al., 2013a). This can be used to predict the initial flexural crack and the deflection up to the formation of the initial flexural crack. The mechanics is correct, that is there is no error associated with the FI M/χ mechanics, and the only major source of error is in estimating the shrinkage strain ε_{sh} and in particular the assumption of a uniform distribution.

Once the initial flexural crack occurs, then the behaviour is governed by tension-stiffening as this PI behaviour controls the crack spacing and crack widths that have a major effect on the deflection (Visintin et al., 2013a; Visintin et al., 2013b; Knight et al., 2013; Knight et al., 2015). A constant shrinkage strain, that is a longitudinal shrinkage strain ε_{sh} that is constant along both the depth d and width b of the member, can be added to these PI analyses (Visintin et al., 2013b; Knight et al., 2013; Knight et al., 2015) to determine the effect of shrinkage. However numerical analyses and tests have shown that the shrinkage strain does vary along the depth and width of the member (Terrill et al., 1986; Mu and Forth, 2009; Gilbert et al., 2012).

The main purpose of this paper is to develop a mechanics based numerical procedure for quantifying the serviceability deflection that directly simulates all regions of the RC beam and that allows for non-linear shrinkage strains and creep as happens in practice. It is shown that the following four distinct mechanics models are required to simulate the long term serviceability deflection of RC beams:

Model 1. A Standard Diffusion Model (Kim and Lee, 1998; Kim and Lee, 1999; Kang et al., 2011) to quantify the variations in the shrinkage strains ε_{sh} within

beams for any environmental condition and for a variety of surface boundary conditions. It is shown how the diffusion coefficients (Bazant and Najjar, 1971; CEB-FIP 1990) can be derived from the CEB FIP model code 1990 using concrete material properties.

Model 2. A FI Segmental Model (Visintin et al., 2013b; Knight et al., 2015) that can incorporate the variations in ε_{sh} derived from Model 1 above. It may be worth noting that a standard FI M/χ analysis gives exactly the same results as this FI segmental analysis. However the FI segmental model is described as it can easily incorporate PI as explained later. This FI segmental model quantifies the occurrence of the first or initial flexural crack M_{cr} and, consequently, the serviceability deflection prior to M_{cr}. After the initial flexural crack has formed, reinforcement slip occurs at and adjacent to the crack so that the following PI tension-stiffening model is required to predict the occurrence and spacing (S_{cr}) of subsequent flexural cracks (Visintin et al., 2013a; Visintin et al., 2013b; Knight et al., 2013; Knight et al., 2015).

Model 3. A PI Tension Stiffening Model (Visintin et al., 2013a; Visintin et al., 2013b; Knight et al., 2013; Knight et al., 2015) that can incorporate the non-linear shrinkage strains ε_{sh} from Model 1. This model predicts the occurrence of subsequent cracks such as primary and secondary cracks and their crack spacings S_{cr}. Furthermore, it quantifies the crack opening stiffness P_{cr}/Δ_{cr}, that is the force in the reinforcement at a crack P_{cr} as a proportion of the half crack width Δ_{cr}. To complete the analyses, the PI properties S_{cr} and P_{cr}/Δ_{cr} are required in the following PI segmental model.

Model 4. A PI Segmental Model (Visintin et al., 2013a; Knight et al., 2015) can now be used to predict the deflection of RC beams with the shrinkage strains ε_{sh} from Model 1 for any environmental conditions and a variety of RC surface conditions. These analyses are then used to simulate 6 RC test specimens by Gilbert and Nejadi (2004).

2. Diffusion model

2.1 Diffusion analysis

Drying of concrete can be represented in terms of pore humidity H at constant temperature T and can be written as follows

$$\frac{\partial H}{\partial t} = div(C\ grad\ H) \tag{1}$$

where the dependence of the moisture diffusion coefficient C on the pore humidity H in the concrete specimen can be determined empirically such as by the following

$$C(H) = C_1\left(\alpha_0 + \frac{1-\alpha_0}{1+[(1-H)/(1-H_c)]^m}\right) \tag{2}$$

where C_1 is the maximum value of the diffusion coefficient, H_c is the pore relative humidity when $C(H) = 0.5\,C_1$. For typical dense concretes having low water-cement ratios, the model parameters have the following values $H_c = 0.8$, $\alpha_0 = 0.05$, $m = 15$ (CEB-FIP 1990). The maximum diffusion coefficient is calculated as

$$C_1 = \frac{C_{1,0}}{f_{ck}/f_{ck0}} \quad (3)$$

where $C_{1,0}$ = 0.864 cm^2/day, f_{ck0} = 10 MPa and the characteristic compressive strength f_{ck} may be estimated as 8 MPa less than the mean.

At high saturations, the process of moisture migration will involve bulk liquid transport in addition to diffusion and these processes can be modelled using a two phase, liquid and water vapour, formulation (Lewis et al., 1998). However for efficiency, a surface factor f representing the relationship between moisture transfer from the concrete surface to the atmosphere, can be applied to reduce the system to a single field equation. Therefore, the boundary conditions for the one dimension case can be expressed as follows (Kang et al., 2011)

$$C(H)\frac{\partial H}{\partial x} = f \cdot (H_{en} - H_s) \quad (4)$$

where H_s is the surface humidity and H_{en} is the environmental humidity. A value of 0.55 cm/day is assumed for the surface factor f for normal strength concrete (Sakata 1982).

The free shrinkage strain of concrete is a function of pore relative humidity (Bazant and Yunping, 1994)

$$\varepsilon_{sh} = k_{sh}(1 - H) \quad (5)$$

where k_{sh} is the shrinkage coefficient which is time dependent as follows

$$k_{sh} = \varepsilon_s^0 g_s(t) \quad (6)$$

with ε_s^0 is the ultimate shrinkage strain and $g_s(t)$ is the ratio of the initial elastic modulus $E(t_0)$ to the elastic modulus at a given time $E(t)$ where t is the time in days and $E(t)$ can be estimated by

$$E(t) = E(28)\sqrt{\frac{t}{4+0.85t}} \quad (7)$$

where $E(28)$ is equal to $33w^{1.5}\sqrt{f_c}$, w is the unit weight of concrete in lb.ft^{-3} and $E(t)$ and $E(28)$ are in psi. In using Eq.7 units were converted to SI.

2.2 Flow in rectangular beams

The diffusion analysis has been applied to the test beams of Gilbert and Nejadi (2004) which were subjected to a sustained loading for 400 days. The beams had the following properties: length L_b = 3500 mm, effective depths d = 325 to 340 mm, width b = 250mm, reinforced with either 2 No. 16 mm or 3 No. 16 mm diameter bars and a compressive cylinder strength f_c of 24.8 MPa. From these beam properties and using CEB-FIP Model Code (1990) was derived the relationship between moisture diffusivity (moisture diffusion coefficient) with moisture content (pore relative humidity of concrete) in Figure 1.

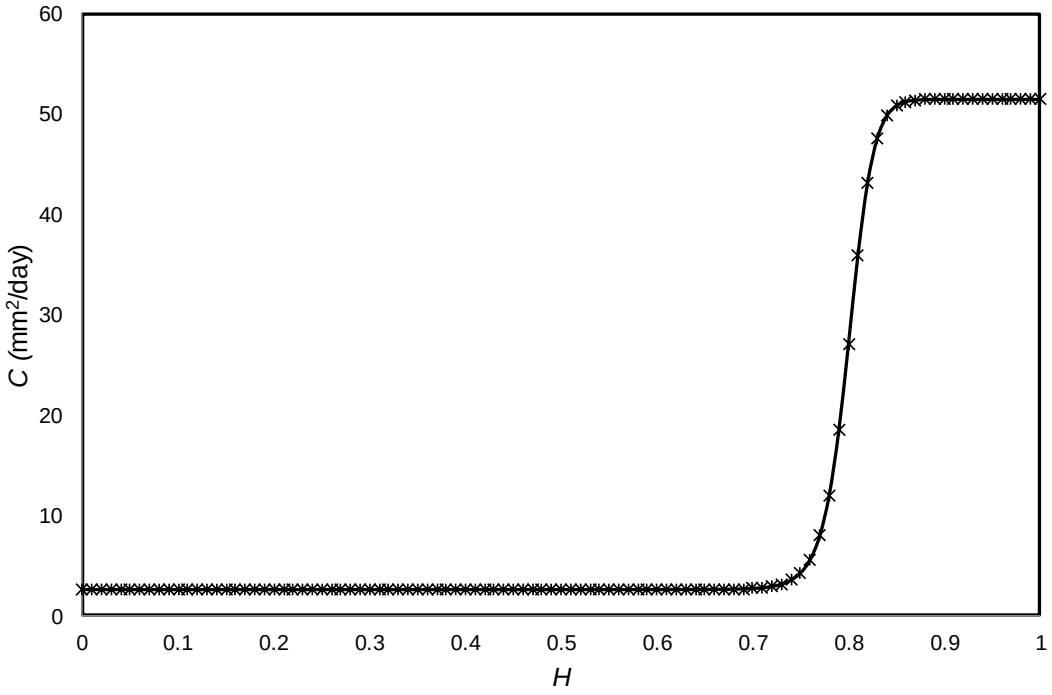

Figure 1. Variation in moisture diffusion coefficient

The beams were divided into *n* slices per half width as in Figure 2 such that the behaviour within one half was the mirror image of the other. The length of the beam L_b was considered to be much larger than either the depth *d* or width *b* so that there was only lateral moisture flow that is no moisture flow along the length. The environmental humidity was taken as 40% and the ultimate shrinkage strain as 1800με.

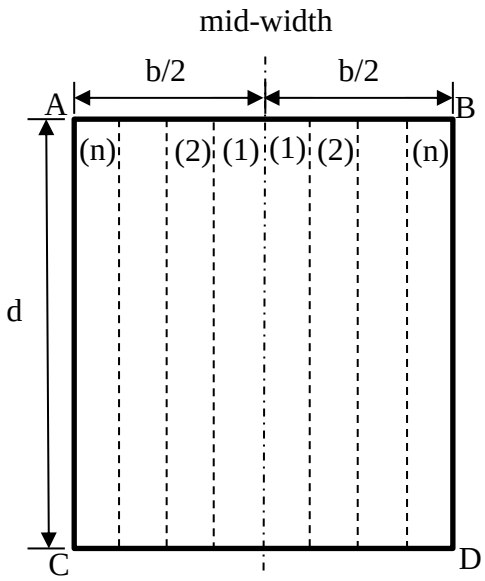

Figure 2. Beam cross-section for diffusion analysis

The results from a diffusion analysis when moisture could flow through all four boundaries in Figure 2 are shown in Figure 3 at 400 days. In this analysis the cross-section in Figure 2 has 4 slices per half width. The slice nearest to the mid-width is labelled 1 in Figure 3 and that adjacent to the boundary A-C in Figure 2 labelled 4 in Figure 3. As would be expected, the shrinkage strain distributions are: symmetrical about mid-depth; they are greatest adjacent to the sides A-C and B-D in Figure 2 shown as Slice 4 in Figure 3 in comparison to those at mid-width that is Slice 1; and they are a maximum at the upper and lower boundaries A-B and C-D in Figure 2.

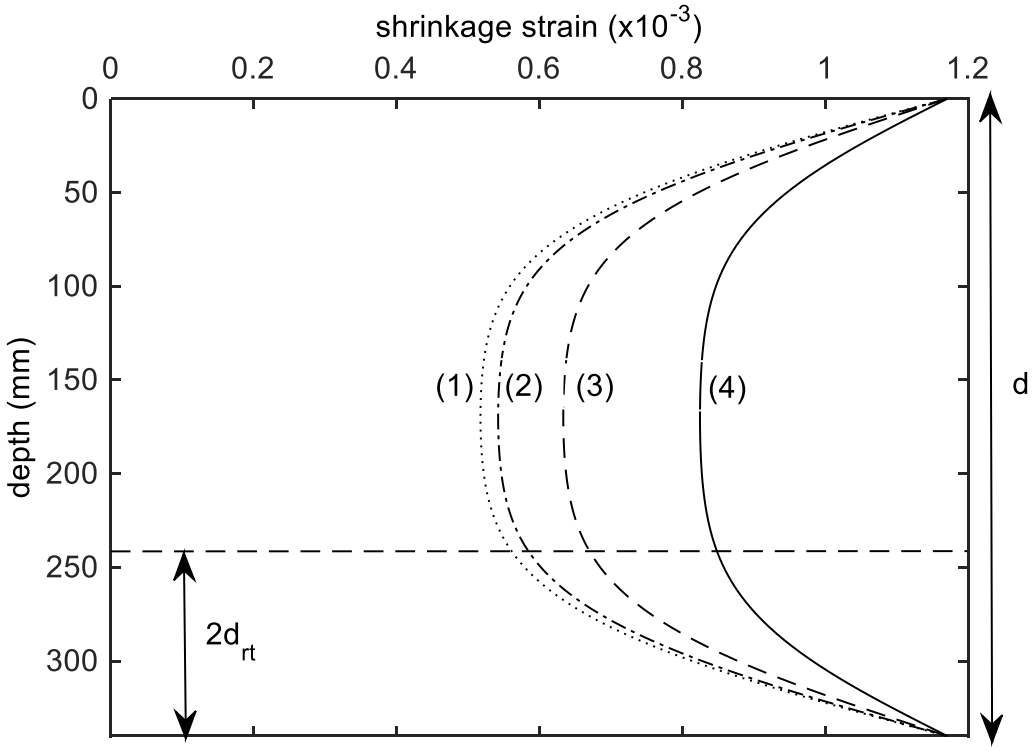

Figure 3. Variation in shrinkage strain along beam width and depth

Importantly: the shrinkage strains in Figure 3 have the greatest magnitude and greatest variations in the tension stiffening region labelled $2d_{rt}$; and above the tension stiffening region they are not even close to uniform as assumed in current design.

Sealing the side A-B in Figure 2 gives the variation in shrinkage strain in Figure 4 for three intervals of time and where there are two slices per half width. Once again the critical tension stiffening region within $2d_{rt}$, critical as it controls crack spacing and crack widths, has the greatest shrinkage strain and variation in shrinkage strain. However in the remaining region the shrinkage strain can be considered to be uniform.

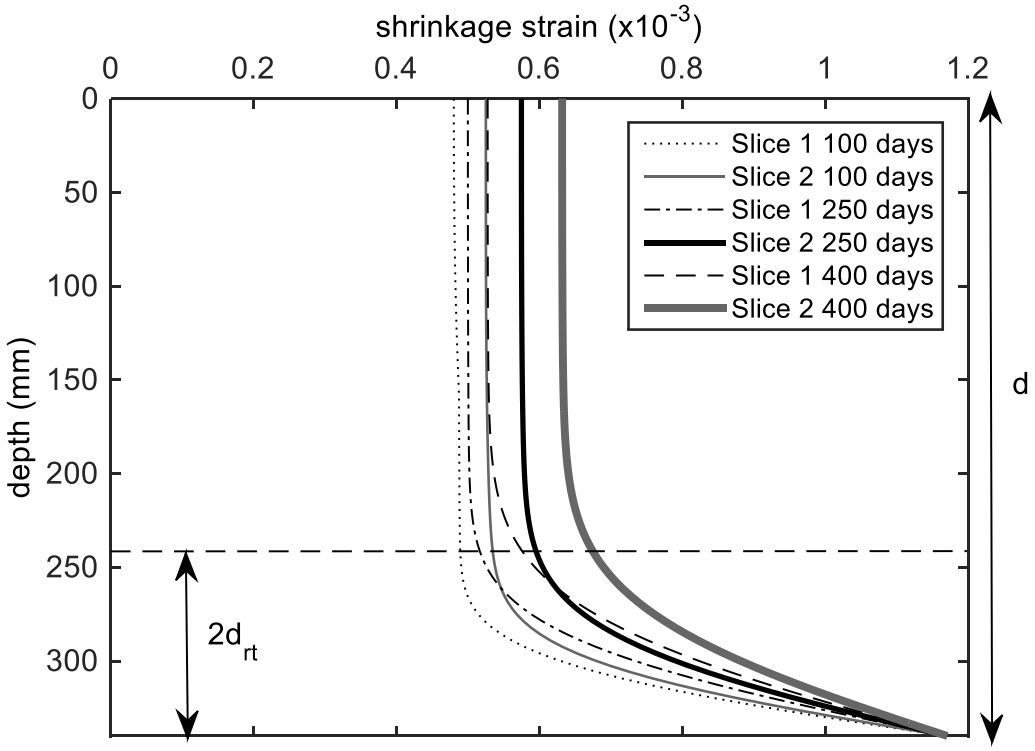

Figure 4. Variation in shrinkage strain with time

Finally sealing A-C, A-B and B-D in Figure 2 so that flow is only one way gives the shrinkage strain after 400 days in Figure 5 labelled 'One way'. These are compared with the previous two cases to further emphasis that a uniform shrinkage strain is a very crude assumption and that the critical tension stiffening region has the greatest variation and magnitude.

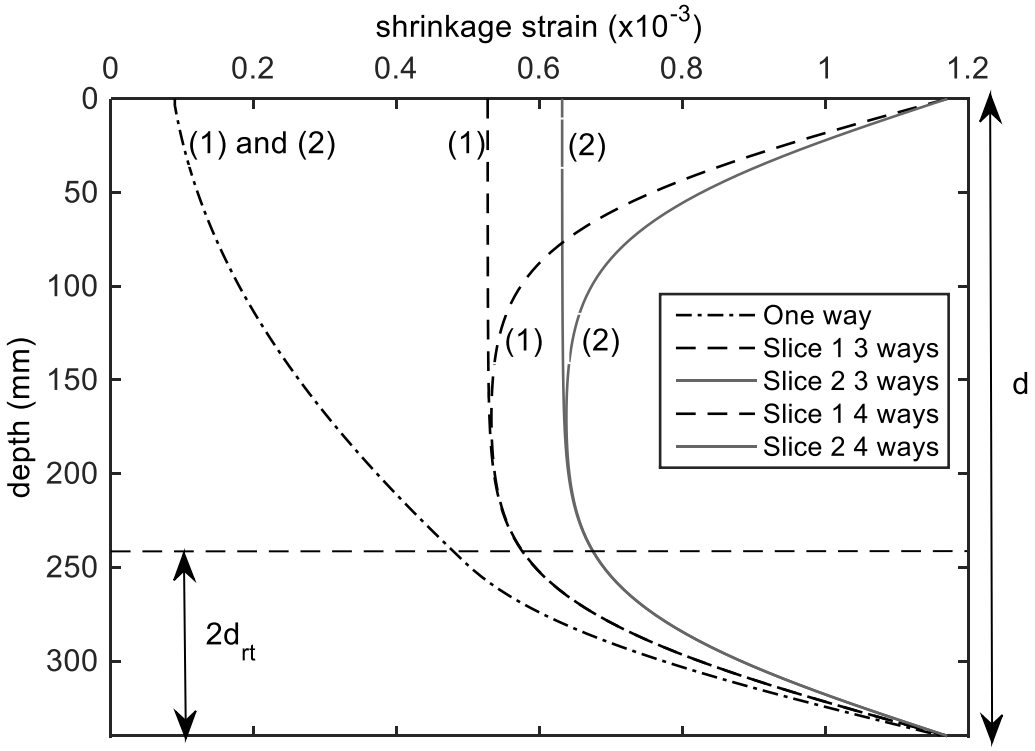

Figure 5. Variation in shrinkage strain with sealed surfaces

It has been shown that the diffusion model can be used to quantify the longitudinal shrinkage strains ε_{sh} in an RC beam. It is now a question of incorporating these shrinkage strains in a flexural analysis of a beam to determine their effect on deflection. Let us start with the behaviour prior to the onset of flexural cracking. As flexural cracking has not occurred there is no slip between the reinforcement and the adjacent concrete so that the beam has a full interaction behaviour as follows.

3. Full-interaction segmental model

Consider a small length $2L_{def}$ of a beam of length L_b as in Figure 6(b). The segment length L_{def} can be of any length and has the cross-section in Figure 6(a) where: b is the width of

the beam; d is the full depth; A_{rc} is the total area of reinforcement in compression; and A_{rt} is the total area of reinforcement in tension at a distance d_{rt} from the tension face. To determine the flexural properties of the beam, such as its M/χ relation or its flexural rigidity EI, the segment is subjected to a constant moment M as shown by applying the symmetric Euler-Bernoulli deformations A-A as shown in Figure 6(b). The deformations cause rotations θ of the segmental faces which have a neutral axis depth d_{NA}.

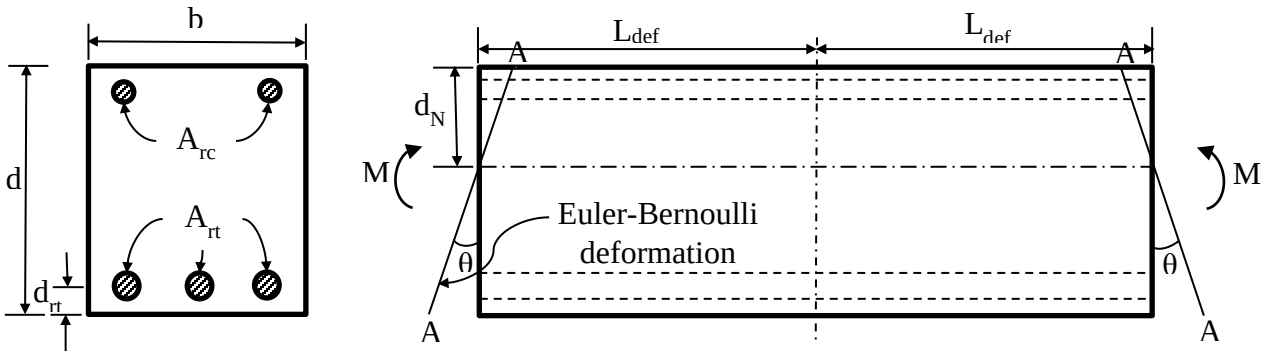

(a) (b)

Figure 6. Uncracked segment

As the segment in Figure 6(b) is symmetrically loaded, consider the left hand side as in Figure 7(a). To illustrate the segment approach, it is first subjected to uniform concrete shrinkage strain ε_{sh} such that the shrinkage strain does not vary along the width b nor along the depth d (Visintin et al., 2013a; Knight et al., 2015). If the concrete were free to shrink, that is it is unrestrained by the reinforcement, then the concrete face would move from B-B to C-C that is a distance $\varepsilon_{sh}L_{def}$ as shown, whereas, the face of the reinforcement would remain at B-B. Hence the Euler-Bernoulli deformation A-A would cause the compression

reinforcement to contract δ_{rc} and the tension reinforcement to extend δ_{rt}. Dividing these deformations by L_{def} gives the strain profile ε_r in Figure 7(b) in which the neutral axis depth is $d_{NA\text{-}r}$ as shown in Figure 7(a). Furthermore the Euler-Bernoulli deformation causes the concrete at the compressive face to contract A-C and expand C-A on the tension face such that the neutral axis depth is $d_{NA\text{-}c}$; dividing these deformations by L_{def} gives the concrete strain profile ε_c in Figure 7(b).

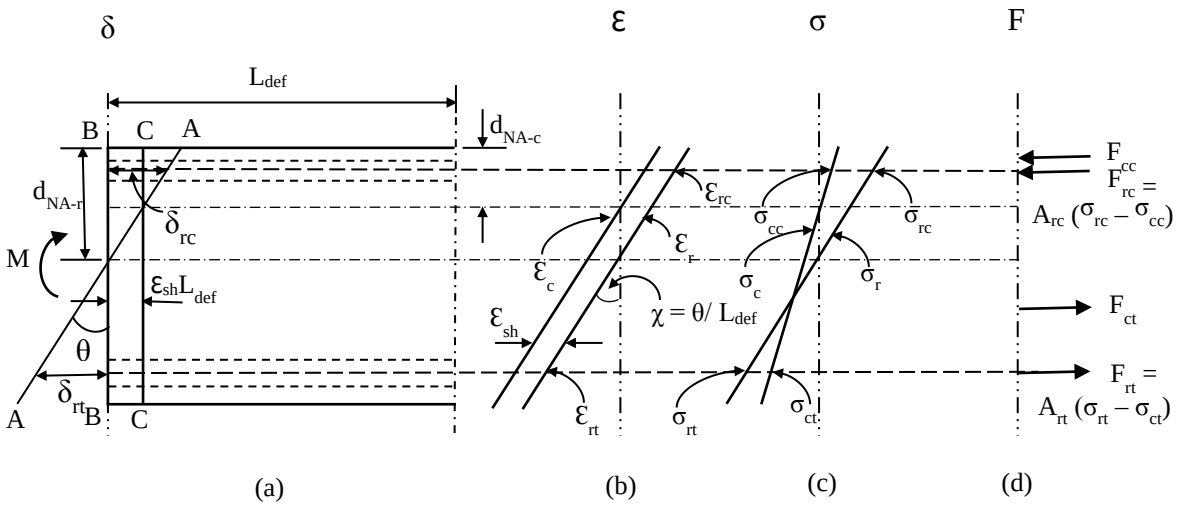

Figure 7. Uncracked segmental analysis with uniform shrinkage strains

The Euler-Bernoulli deformation in Figure 7(a) gives the strain distributions in Figure 7(b) that are offset by ε_{sh} as shown. This is exactly what would be obtained from a standard FI M/χ analysis but is presented in this form as it can later cope with non-linear strain profiles and with flexural cracking. Having quantified the strain distributions in Figure 7(b), in which the slope is the curvature χ which is θ/L_{def}, the concrete stress profile σ_c and reinforcement stress profile σ_r in Figure 7(c) can be derived from their material moduli. Furthermore from the stress profiles, can be derived the resultant forces F in

Figure 7(d). To simplify the analysis, the concrete cross section in Figure 6(a) has an area *bd* that is the concrete 'voids', at the position of the reinforcement, have been allowed for by reducing the reinforcement force. Hence in Figure 7(d): F_{cc} is the resultant force in the concrete in compression; F_{rc} is the resultant force in the compression reinforcement that is the cross sectional area of the compression reinforcement A_{rc} multiplied by the reinforcement stress σ_{rc} less the stress in the concrete at the level of the reinforcement σ_{cc}; F_{ct} is the resultant force in the concrete in tension; and F_{rt} is the resultant force in the reinforcement in tension.

For a fixed rotation θ in Figure 7(a), it is a question of varying the neutral axis depth d_{NA-r} until there is longitudinal equilibrium in Figure 7(d) after which moments can be taken to derive M for that particular θ. Dividing θ by L_{def} gives the equivalent curvature χ and the slope of M/χ gives the equivalent flexural rigidity EI.

The above analysis is adapted in Figure 8 to incorporate non-linear shrinkage strain distributions such as those in Figure 3. In this case, the cross-section in Figure 8(a) is divided into four slices. It will be assumed that the shrinkage strains to the left of the mid-width are a reflection of those to the right, that is there is symmetrical drying. Hence in this example there are only two variations in shrinkage to consider which are labelled ε_{sh1} and ε_{sh2}. Multiplying the shrinkage strains, such as those in Figure 3 but for two slices per half width, by L_{def} gives the concrete deformations δ_{c1} for Slice 1 and δ_{c2} for Slice 2 in Figure 8(b). An Euler-Bernoulli deformation A-A at neutral axis depth d_{NA-r} is applied where it can now be seen that there are now two concrete neutral axis depths d_{NA-c1} and

$d_{NA\text{-}c2}$ that is a neutral axis depth for each slice. The analysis follows the same procedure as outlined in Figure 7.

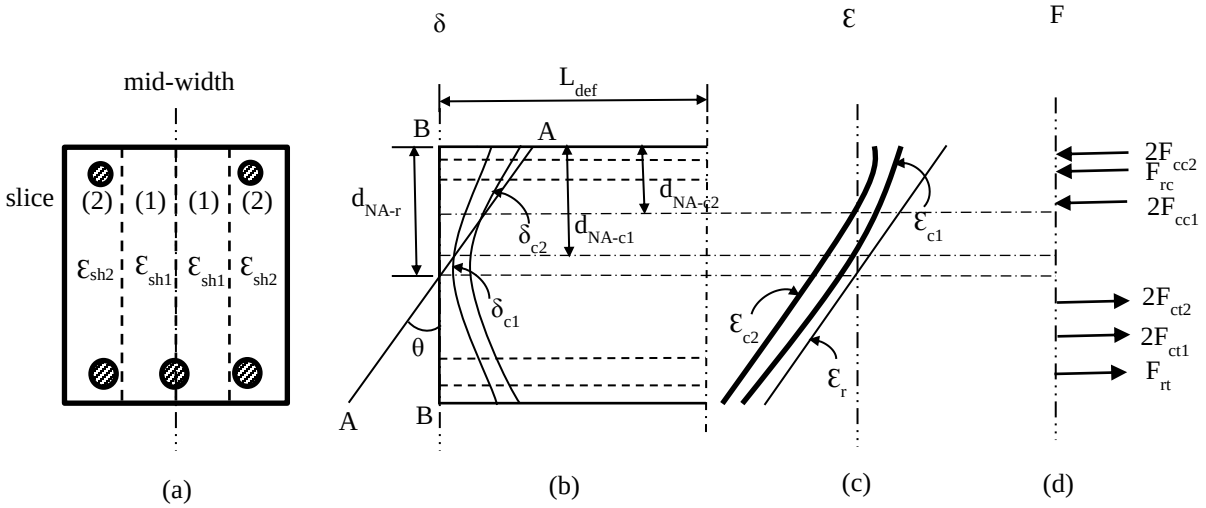

Figure 8. Uncracked segmental analysis with non-linear shrinkage strains

The above analyses give the moment at which flexural cracking starts or initiates $M_{cr\text{-}in}$ and of course the flexural properties of uncracked members up to $M_{cr\text{-}in}$. As illustrated in Figure 8, shrinkage causes a reduced moment at cracking as would be expected. In Figure 8(b), flexural cracking without shrinkage will occur when the strain (A-B)/L_{def} equals the fracture strain capacity of the concrete ε_{ct} which can be taken as the concrete tensile strength f_{ct} divided by its modulus. However shrinkage increases the strain to (A-C_2)/L_{def} so that cracking will occur at a lower moment.

The above analyses can also be used until the tip of the flexural crack extends above the tension reinforcement after which the tension reinforcement slips relative to the concrete

such that there is partial interaction. Once this occurs, behaviour is governed by the tension stiffening mechanism as explained below.

4. Partial interaction tension stiffening model

The segment required to allow for partial interaction tension stiffening (Visintin et al., 2013a; Knight et al., 2015) is illustrated in Figure 9(b). In this case, the length of the segment $2L_{def}$ is equal to the flexural crack spacing S_{cr}. Furthermore, it is common practice to allow for tension stiffening through the use of axially loaded RC prisms (Knight et al., 2013) as shown where the depth of the prism $2d_{rt}$ is twice the distance of the tension reinforcement from the tension face. The mean shrinkage strain within each prism ε_{shn} in Figure 9(a) is determined from the results of a diffusion analysis as in Figures 3-5 that is the mean shrinkage within the depth $2d_{rt}$.

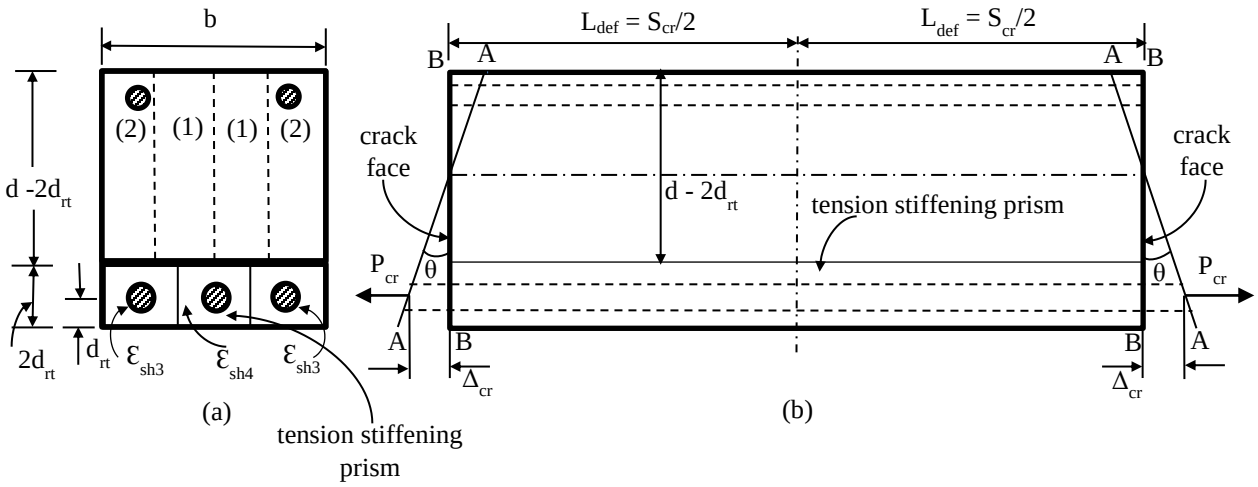

Figure 9. Cracked segmental analysis

Consider the tension stiffening prism in the segment in Figure 9(b), half the length of which L_{def} is shown by itself in Figure 10(b). To understand the mechanics, the prism is divided into x segments of a very short length L_s that is $L_s << L_{def}$. The cross section is shown Figure 10(a) where the perimeter length of the interface between the reinforcement and adjacent concrete is L_{per}. The bond-slip properties (τ_b-δ_b), that is the relationship between the interface bond shear stress τ_b and interface bond slip δ_b, control the behaviour across this interface of area $L_{per}L_s$. For example, if the bond stress between the reinforcement and adjacent concrete is τ_b such that the slip is δ_b, then the bond force B over the segment length is $\tau_b L_{per} L_s$ and the bond stiffness is τ_b/δ_b.

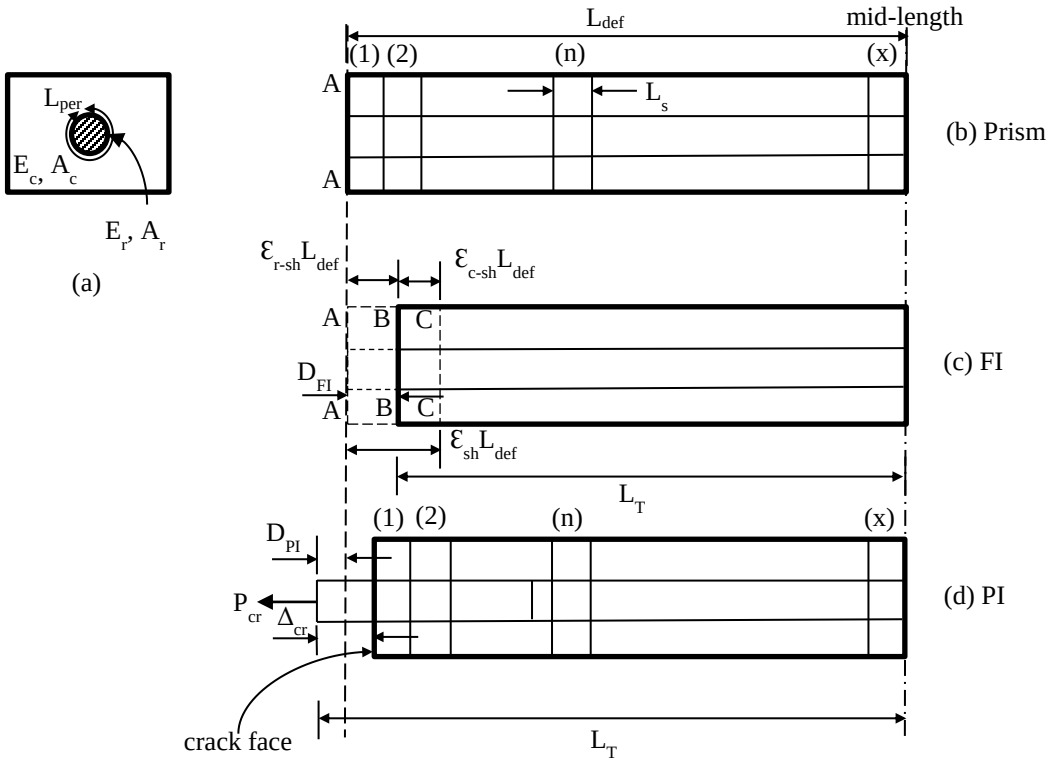

Figure 10. Tension stiffening prism

First consider the FI case where the bond stiffness τ_b/δ_b is infinite which is shown in Figure 10(c) and in which the concrete shrinkage strain is ε_{sh}. If there were no bond, that is no

restraint from the reinforcement, then the concrete face which was originally at A-A in Figure 10(b) would shrink by $\varepsilon_{sh}L_{def}$, that is slip relative to the reinforcement $\varepsilon_{sh}L_{def}$, to C-C in Figure 10(c) as shown. However, an infinite bond stiffness prevents interface slip such that the concrete and reinforcement face B-B lies between the unstressed face of the reinforcement A-A and the unstressed face of the concrete C-C. Applying equilibrium and compatibility (Visintin et al., 2013a), it can be shown that the residual compressive strain in the reinforcement due to shrinkage is given by

$$\varepsilon_{r-sh} = \frac{\varepsilon_{sh}}{1+\frac{E_r A_r}{E_c A_c}} \tag{8}$$

where: E_rA_r is the axial rigidity of the reinforcement; E_cA_c the axial rigidity of the concrete prism; the shrinkage strain is taken as positive; and tensile strains are also taken as positive. From compatibility in Figure 10(c), it can be shown (Visintin et al., 2013a) that the residual tensile strain in the concrete due to shrinkage is

$$\varepsilon_{c-sh} = \varepsilon_{sh} - \varepsilon_{r-sh} \tag{9}$$

Furthermore, the displacement of the reinforcement face relative to its original position whilst there is FI is given by

$$D_{FI} = L_T - L_{def} = \varepsilon_{r-sh}L_{def} \tag{10}$$

in which D_{FI} is negative when in contraction.

Now consider the effect of PI that is slip between the reinforcement and concrete as illustrated in Figure 10(d). The n^{th} segment in Figure 10(b) which is also shown in Figure 10(d) is displaying now in Figure 11. At the position of the n^{th} segment, the reinforcement force and concrete force to the left of the segment is P_n and C_n respectively, the slip relative to the concrete is Δ_n and the bond force due to this slip Δ_n is B_n. The parameters P_n, C_n and Δ_n depend on the behaviour of the whole prism and will be determined later. As the chosen segment length L_s is very small compared with L_{def}, mean strains will be dealt with. The force in the reinforcement to the left P_n reduces due to the bond to P_n-B_n. Hence the mean strain in the reinforcement ε_{rn} is due to the average of the forces P_n and P_n-B_n. Similarly the mean strain in the concrete ε_{cn} is due to the mean of the forces C_n and C_n+B_n.

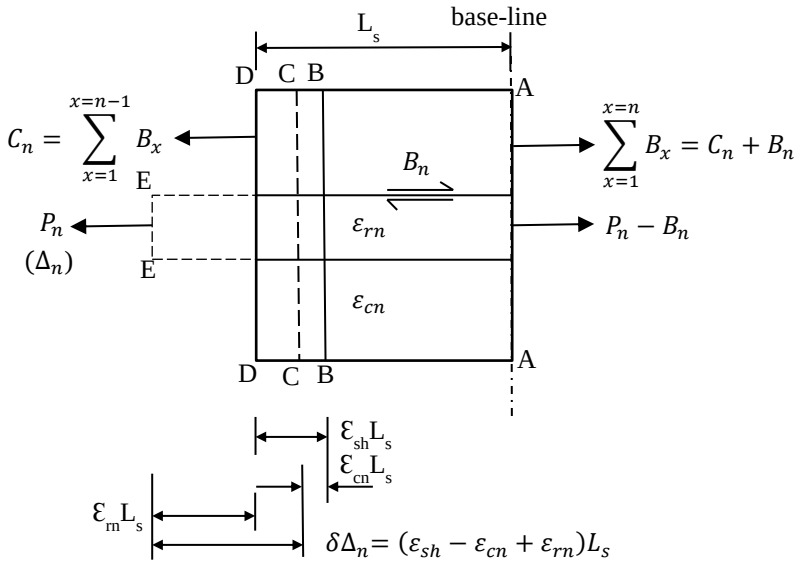

Figure 11. Local deformation of n^{th} segment in prism

The concrete shrinkage strain causes the concrete face to displace $\varepsilon_{sh}L_s$ from D-D to B-B as shown in Figure 11. The stress in the concrete ε_{cn} increases this by $\varepsilon_{cn}L_s$ as shown to C-

C. Similarly the strain in the reinforcement ε_{rn} increases it by $\varepsilon_{rn}L_s$ to E-E as shown. Hence the increase in the slip in the n^{th} segment is given by the following in which the term in brackets is often referred to as the slip strain dΔ/dx.

$$\delta\Delta_n = (\varepsilon_{sh} - \varepsilon_{cn} + \varepsilon_{rn})L_s \tag{11}$$

The application of the analysis depicted in Figure 11 to the first two segments in Figure 10(d) are shown in Figure 12. The initial crack is to the left of Segment 1, hence the force in the concrete on the left hand side C is zero. Let the force in the reinforcement at the crack be P_{cr} and the slip Δ_{cr} such that the width of the crack w is $2\Delta_{cr}$. From Δ_{cr} and the bond-slip properties τ_b-δ_b can be derived the bond force B_1 as shown in the equations below. Hence the forces on the right of the prism and consequently the material strains ε_{c1} and ε_{r1}, also in the equations below. Finally the slip-strain $d\Delta_1/dx$, and increase in slip of Segment 1 that is $\delta\Delta_1$. The forces on the left hand side of Segment 2 are those already derived on the right hand side of Segment 1. The analysis then follows the same steps as for Segment 1 which are listed below Segment 2. And so on with further segments.

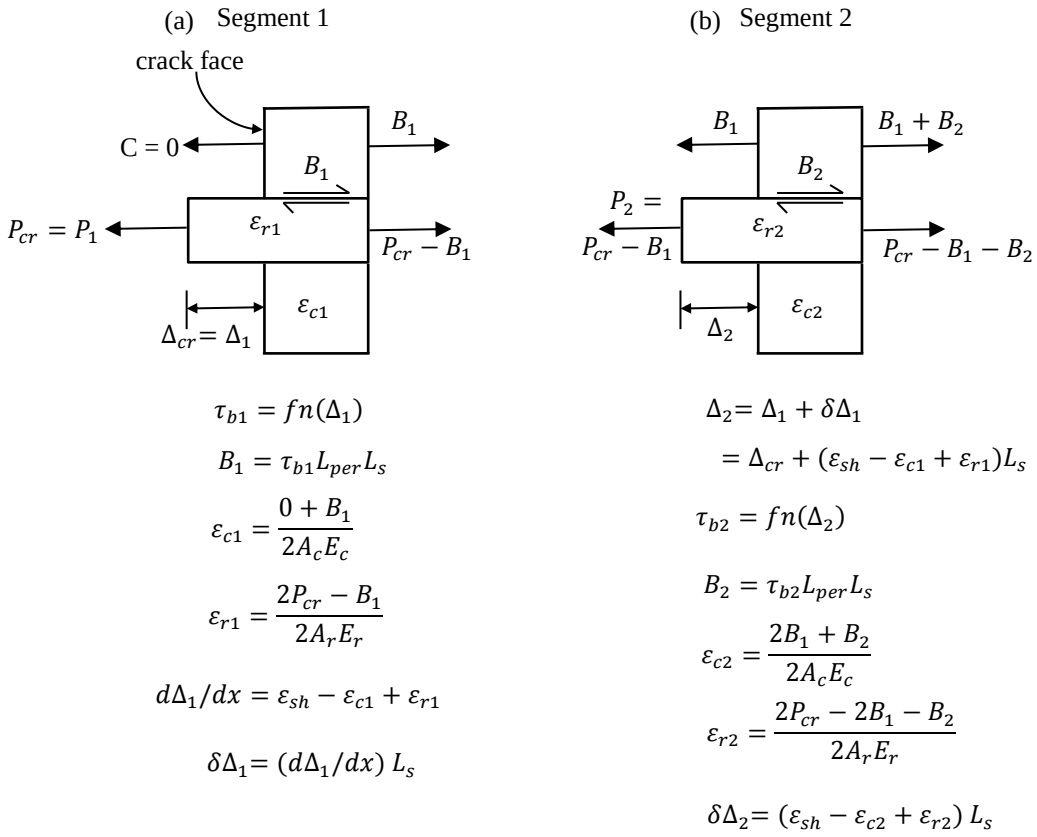

$$\tau_{b1} = fn(\Delta_1)$$

$$B_1 = \tau_{b1} L_{per} L_s$$

$$\varepsilon_{c1} = \frac{0 + B_1}{2A_c E_c}$$

$$\varepsilon_{r1} = \frac{2P_{cr} - B_1}{2A_r E_r}$$

$$d\Delta_1/dx = \varepsilon_{sh} - \varepsilon_{c1} + \varepsilon_{r1}$$

$$\delta\Delta_1 = (d\Delta_1/dx)\, L_s$$

$$\Delta_2 = \Delta_1 + \delta\Delta_1$$

$$= \Delta_{cr} + (\varepsilon_{sh} - \varepsilon_{c1} + \varepsilon_{r1}) L_s$$

$$\tau_{b2} = fn(\Delta_2)$$

$$B_2 = \tau_{b2} L_{per} L_s$$

$$\varepsilon_{c2} = \frac{2B_1 + B_2}{2A_c E_c}$$

$$\varepsilon_{r2} = \frac{2P_{cr} - 2B_1 - B_2}{2A_r E_r}$$

$$\delta\Delta_2 = (\varepsilon_{sh} - \varepsilon_{c2} + \varepsilon_{r2})\, L_s$$

Figure 12. Tension stiffening analysis

An iterative shooting method is used to find a solution. The first case to consider is when only the initial crack has occurred from the analysis of the uncracked segment in Figure 6. Hence there is only one crack on the left hand side of the prism in Figure 10(d). For a given force P_1 in Figure 12(a) an estimated slip Δ_1 is chosen. At each segment the slip Δ_n and the slip-strain $d\Delta_1/dx$ are derived. It is a question of finding the x_{th} element where FI occurs which in this case is that the slip is zero and the slip-strain is $\varepsilon_{r\text{-}sh}$-$\varepsilon_{c\text{-}sh}$, which can be derived from Eqs. 8 and 9, is also zero. The estimate Δ_1 is varied until this occurs. Once this boundary condition is achieved the position of the x_{th} segment is the first primary crack spacing $S_{cr\text{-}pr}$. When the concrete strain in this x^{th} segment ε_{cx} reaches the concrete strain capacity ε_{ct} the reinforcement force to cause primary cracks $P_{cr\text{-}pr}$.

Having formed primary cracks at known spacings $S_{cr\text{-}pr}$, this is used in a tension stiffening analysis in which L_{def} in Figure 10 is equal to $S_{cr\text{-}pr}/2$ to determine the tension stiffening behaviour between primary cracks. The analysis depicted in Figure 10 still applies except that the boundary condition is no longer that for FI but instead that at mid-length, that is $S_{cr\text{-}pr}/2$ from the crack faces, the slip is zero. This analysis gives the relationship between P_{cr} and Δ_{cr} in Figure 10(d) that is the crack opening stiffness P_{cr}/Δ_{cr} required for the segmental analysis. Furthermore it gives the reinforcement force to cause secondary cracks $P_{cr\text{-}sec}$ that is when ε_c is equal to ε_{ct} should they occur and if so an analysis with a prism length of $S_{cr\text{-}pr}/4$ gives the behaviour in regions where there are secondary cracks.
It can be seen in Figure 11 and Eq. 11 that the shrinkage strain ε_{sh} causes a more rapid build up of slip and therefore bond force, so that shrinkage will reduce the crack spacings and also the reinforcement force to cause cracking.

5. Partial-interaction segmental model

After flexural cracking from the segmental analysis in Figure 6, the properties of the beam within the cracked regions are determined from a segmental analysis of a segment between two adjacent cracks as shown in Figure 9.

Starting with primary cracks, the length of the segment in Figure 9 is $S_{cr\text{-}pr}$ which is obtained from the above tension stiffening analysis and which allows for the effects of shrinkage. Euler-Bernoulli deformations A-A are applied. Within the tension stiffening region of depth $2d_{rt}$, the force in the tensile reinforcement P_{cr} is now determined from Δ_{rt} that is from the crack opening stiffness P_{rt}-Δ_{rt} also previously obtained from the tension

stiffening analysis and which also allows for shrinkage within the tension stiffening region. For the region of depth d-$2d_{rt}$ above the tension stiffening analysis, the segmental analysis follows that depicted in Figure 8 except that flexural cracking of the concrete can occur at ε_{ct} that is the progression of a flexural crack tip can continue. When the force in the reinforcement is $P_{cr\text{-}pr}$ that was obtained from the above tension stiffening analysis, this gives the moment to cause primary cracks $M_{cr\text{-}pr}$. Hence the moment to cause primary cracks is the lesser of $M_{cr\text{-}pr}$ and $M_{cr\text{-}in}$ (Visintin et al., 2013b) as both can occur in a FI region. When the force in the reinforcement in Figure 9 reaches $P_{cr\text{-}sec}$, this gives the moment to cause secondary cracks $M_{cr\text{-}sec}$ should they occur. Hence in regions of the beam where $M_{cr\text{-}sec}$ is exceeded both primary and secondary cracks occur where the crack spacing is now $S_{cr\text{-}pr}/2$.

The analysis in Figure 9 can be used to derive the M/θ at serviceability loads in members with non-linear shrinkage strains not only along the depth of the beam d but also along the width of the beam b. Dividing the rotations by L_{def} gives the equivalent M/χ; this is not an approximation in mechanics terms but in mechanics terms an exact solution that directly copes with variations in shrinkage. The equivalent M/χ can then be used in the analysis of a loaded beam to determine its deflection and can cope with any shape of beam, any cross-section properties, any environmental conditions and any surface conditions.

6. Application of shrinkage analyses

The above shrinkage analyses were applied to beams tested by Gilbert and Nejadi (2004). The segmental analyses depicted in Figure 8 were first used to quantify the variation in moment-curvature with time as follows

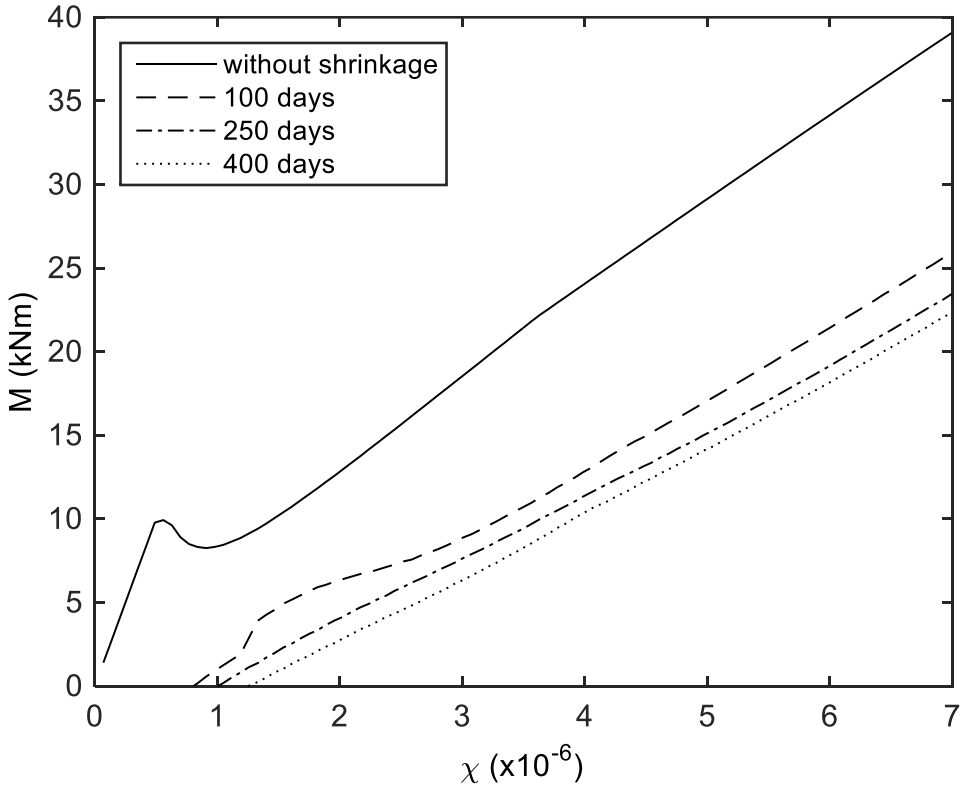

Figure 13. Moment-curvature with time

These were then used to quantify the deflection with time and compared with test results in the following figure. It can be seen in Figure 14 that there is a reasonable correlation. To further show the significance of the incorporation of a non-linear shrinkage profile, the analysis for beam B1b in Figure 14 has been repeated in Figure 15(b) but with various different shrinkage profiles as shown in Figure 15(a). That is the non-linear shrinkage profile is compared to an assumed constant shrinkage strain of magnitude equal to that of the minimum, maximum and mean obtained from the diffusion analysis. Finally these

values are compared to that obtained from a standard shrinkage test conducted on a concrete prism with cross sectional dimensions of 600 mm by 160 mm. The results of the analysis show the best fit with experimental data is obtained by considering a non-linear shrinkage profile and that taking an average result from the diffusion analysis may lead to a poor correlation with test data. While in the scenario considered the constant shrinkage strain obtained experimentally yield reasonable correlation with test results this may not always hold in practice. For example, as the beams exposed surfaces are changed a significant variation in the shrinkage profile in Figure 5 is observed and this leads to a substantial variation in long term deflection as in Figure 16.

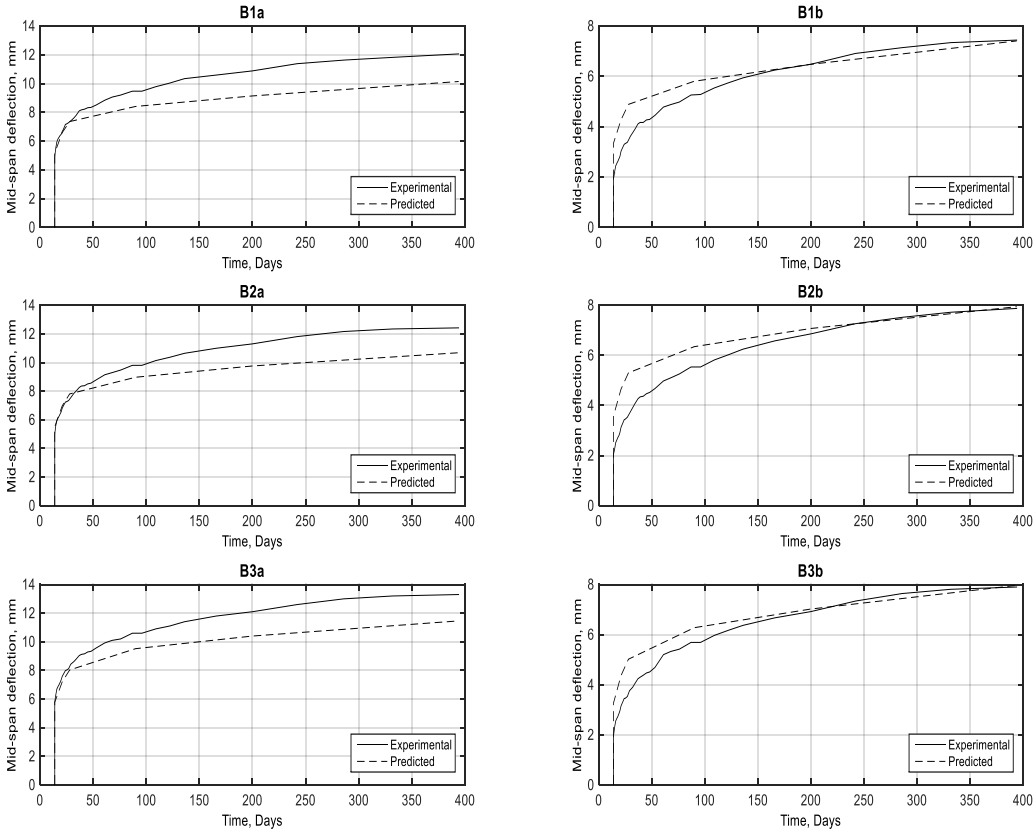

Figure 14. Comparison of deflections with test results

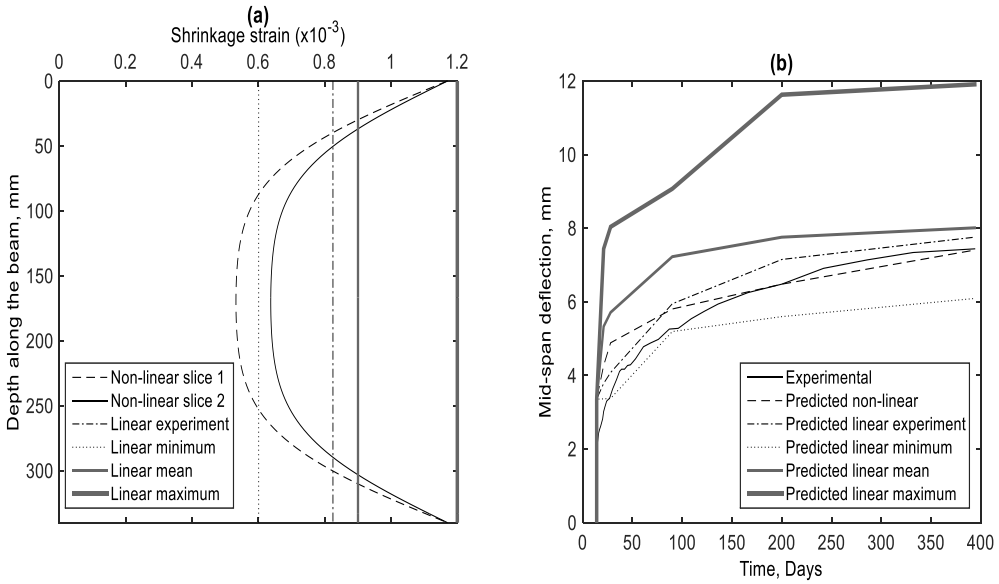

Figure 15. a) Various shrinkage strain profiles used in the analysis at 400 days and b) Deflection of beam B1b over time

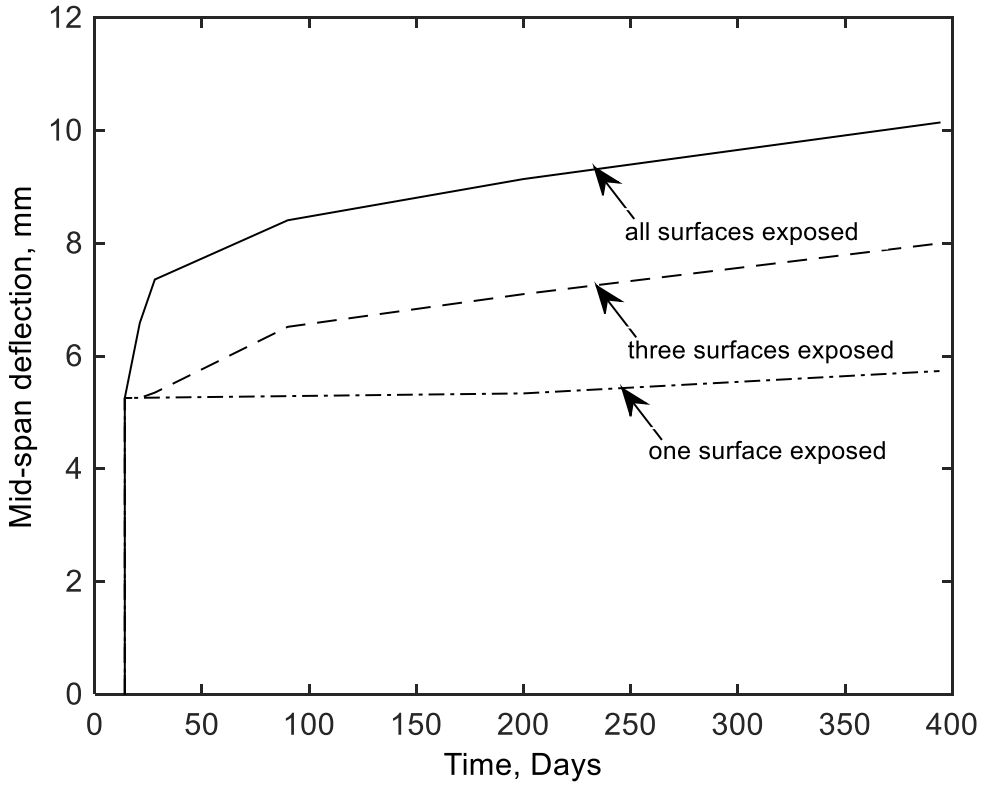

Figure 16. Variation in deflection with exposed surfaces

7. Conclusion

It has been shown that the mechanics of simulating the long term serviceability deflection of RC beams is very complex as it requires four specific mechanics models:

(1) A diffusion model to quantify the variation of shrinkage strain with: time; environmental conditions; beam shape; beam surface conditions; and with the width and depth of the beam.

(2) A full interaction flexural segmental analysis that can cope with the variations in shrinkage strain from the diffusion model to quantify: the behaviour of the beam in uncracked regions; and also to predict the onset of flexural cracking that is the start of partial interaction behaviour.

(3) A partial-interaction tension stiffening analysis that can cope with imposed shrinkage strains from the diffusion model to quantify: primary crack spacings and widths; the onset of secondary cracks and their spacings and widths; and crack opening stiffnesses.

(4) A partial interaction flexural segmental analysis that can cope with any imposed variation in shrinkage strain to quantify the behaviour of the cracked sections of the beam. This analysis gives: the moments at which primary and secondary cracks occur; variations in crack spacings and widths; and mechanically correct moment-curvatures for quantifying the deflections.

Importantly, this research provides mechanics solutions for all the facets that control the serviceability time dependent behaviour of RC beams. It has been shown that the problem is very complex. However it is envisaged that these numerical mechanics solutions although not suitable for routine design can provide researchers with the tools to develop

simple design procedures as they simulate the major mechanisms influencing cracking and tension stiffening in reinforced concrete beams.

References

Bresler, B and Selna, L (1964) Analysis of Time Dependent Behaviour of Reinforced Concrete Structures. Symposium of Creep in Concrete ACI Special Publication *SP-9*(5): 115-128.

Bazant Z and Najjar L (1971) Drying of concrete as a nonlinear diffusion problem. Cement and Concrete Research 1(5): 461-473.

Bazant, ZP (1972) Prediction of Concrete Creep Effects using Age-Adjusted Effective Modulus Method. ACI Journal 69: 212-217.

Branson, DE (1977) *Deformation of Concrete Structures*. McGraw Hill, New York.

Bazant ZP and Yunping X (1994) Drying creep of concrete: constitutive model and new experiments separating its mechanisms. Materials and Structures 27(1): 3-14.

CEB-FIP. CEB-FIP model code (1990) Design code 1994. Thomas Telford, London.

Faber, O (1927) Plastic Yield, Shrinkage and Other Problems of Concrete and their Effects on Design. *Minutes of the Proceedings of the Institute of Civil Engineers*. 225(1928). Part I, London, pp. 27-73.

Ghali, A, Nevile, AM and Jha, PC (1967) Effect of Elastic and Creep Recoveries of Concrete on Loss of Prestress. ACI Journal 64(12): 802-810.

Gilbert, RI (1988) *Time Effects in Concrete Structures*. Elsevier Science Publishers B.V..

Gilbert RI and Nejadi S (2004) An experimental study of flexural cracking in reinforced concrete members under sustained loads. UNICIV Report No. R-435, School of Civil and Environmental Engineering, University of New South Wales, Sydney, Australia.

Gilbert RI and Ranzi, G (2011). *Time-dependent behaviour of concrete structures.* Spoon Press.

Gilbert RI, Bradford MA, Gholamhoseini A and Chang ZT (2012) Effects of shrinkage on the long-term stresses and deformations of composite concrete slabs. Engineering Structures 40: 9-19.

Kim JK and Lee CS (1998) Prediction of differential drying shrinkage in concrete. Cement and Concrete Research 28(7): 985-994.

Kim JK and Lee CS (1999) Moisture diffusion of concrete considering self-desiccation at early ages. Cement and Concrete Research 29: 1921-1927.

Kang ST, Kim JS, Lee Y, Park YD and Kim JK (2011) Moisture diffusivity of early age concrete considering temperature and porosity. KSCE Journal of Civil Engineering 16(1): 179-188.

Knight, D, Visintin, P, Oehlers, D and Jumaat, M (2013) Incorporating residual strains in the flexural rigidity of RC members with varying degrees of prestress and cracking. Advances in Structural Engineering 16(10): 1701-1718.

Knight, D, Visintin, P and Oehlers, DJ (2015) Displacement-based simulation of time-dependent behaviour of RC beams with prestressed FRP or steel tendons. Structural Concrete 16(3): 406-417.

Lewis RW, Schrefler BA and Abd Rahman N (1998) A finite element analysis of multiphase immiscible flow in deforming porous media for subsurface systems. Communication in Numerical Methods in Engineering 14: 135-149.

Mu R and Forth J (2009) Modelling shrinkage of concrete from moisture lost. Magazine of Concrete Research 61(7): 491-497.

Sakata K (1982) A Study on moisture diffusion in drying and drying shrinkage of concrete. Cement and Concrete Research 13: 216-224.

Terrill J, Richardson M and Selby A (1986) Non-linear moisture profiles and shrinkage in concrete members. Magazine of Concrete Research 38(137): 220-225.

Visintin P, Oehlers DJ and Haskett M (2013a) Partial-interaction time dependent behaviour of reinforced concrete beams. Engineering Structures 49: 408-420.

Visintin, P, Oehlers, DJ, Muhamad, R and Wu, C (2013b) Partial-interaction short term serviceability deflection of RC beams. Engineering Structures 56: 993-1006.

Whitney, CS (1932) Plain and Reinforced Concrete Arches. ACI Journal 28: 479-519.

Chapter 4 Simulating Shrinkage Strain using Moisture Diffusion

4.1 Introduction

This chapter describes the usage of the diffusion process to predict the non-linear variation in shrinkage of a concrete prism. Firstly, the basic mechanics of moisture diffusion are presented in a mathematical form and it is shown how the finite difference method can be used to solve and develop a numerical solution to describe the diffusion process. It is then shown how the material properties and boundary conditions required to describe the diffusion process that can be extracted using generic concrete material properties and which is described in the CEB-FIP model code 90. Hence it is also shown how these properties relate the moisture or pore relative humidity of concrete to the shrinkage strain. Finally, the diffusion model developed is then used to predict the shrinkage strain variations of RC beam tested by Gilbert and Nejadi (2004) with varying the surface boundary conditions. A wider validation is then conducted to show the general accuracy of the approach to a wide range of concrete material properties.

4.2 Moisture diffusion equation

Moisture diffusion can be used to simulate with the movement of moisture in concrete and taking drying shrinkage to be proportional to the moisture content or pore relative humidity, h of concrete specimens it follows that it can also be used to predict concrete shrinkage strains. According to Bažant and Najjar (1971), the specific water content of concrete, w (mass per unit volume) should satisfy the partial differential Equation 4.1 which is known as Fick's law,

$$\frac{\partial w}{\partial t} = div(D\ grad\ w)$$ Equation 4.1

where t = time and D = diffusion coefficient as a function of w and this Equation is only applicable when the degree of hydration is uniform throughout the body of the specimen and temperature T is constant and changing of material properties due to hydration is negligible especially in old concrete. Drying of concrete can also be represented in terms of pore humidity h at constant temperature T and a fixed degree of hydration, $dh = k\ dw$ where k = function of h which is equivalent to co-tangent of the slope of the desorption isotherm $w = w(h)$ and hence the equation can be expressed as,

$$\frac{dw}{dt} = \frac{1}{k}\frac{dh}{dt}$$ Equation 4.2

Hence from Equation 4.1 and 4.2, the mass balance equation can be expressed as follows,

$$\frac{\partial H}{\partial t} = k\ div(c\ grad\ w)$$ Equation 4.3

where $c = D/k$ which represent the permeability of the concrete and it is equal to the mass flux due to a unit gradient of h and D is the moisture diffusion coefficient. According to Powers and Brownyard (1946), k may be taken as a constant in the ranges of 0.20 to 0.95 for dense cement pastes and concretes. Hence from Equations 4.1, 4.2 and 4.3, the non-linear moisture diffusion equation can be obtained as follows:

$$\frac{\partial h}{\partial t} = div(D\ grad\ h)$$ Equation 4.4

Where D is the moisture diffusion coefficient and it is the same as that in Equation 4.1 except it is considered as a function of h rather than w. In Equations 4.1-4.4 the moisture diffusion coefficient D is dependent on the pore humidity h in the concrete specimen kept for drying and is been investigated to provide a fundamental mathematical formulation in Equation 4.4 used for diffusion modelling by finite the difference method.

4.3 Moisture diffusion coefficient

The moisture diffusion coefficient or moisture diffusivity, *D* is also dependent on the moisture content or pore relative humidity *h* of concrete. According to the CEB-FIP (1990) model code, the moisture diffusion coefficient is expressed as a function of the pore relative humidity 0 < h < 1 given in Equation 4.5,

$$D(h) = D_1\left(\alpha + \frac{1-\alpha}{1+[(1-h)/(1-h_c)]^n}\right) \quad \text{Equation 4.5}$$

where D_1 is the maximum of $D(h)$for h = 1.0, $\alpha = D_0/D_1$, D_0 is the minimum of *D(h)* for h = 0.0, h_c is the pore relative humidity at $D(h) = 0.5\ D_1$ and n is an exponent, α = 0.05, h_c = 0.80 and n = 15 are approximately assumed. D_1 may be estimated from Equation 4.6,

$$D_1 = \frac{D_{1,0}}{f_{ck}/f_{ck0}} \quad \text{Equation 4.6}$$

where $D_{1,0}$ = 0.864 cm^2/day, f_{ck0} = 10 MPa and the characteristic compressive strength f_{ck} may be estimated by the mean compressive strength f_{cm} and

$$f_{ck} = f_{cm} - 8\ MPa \quad \text{Equation 4.7}$$

By solving Equation 4.4, the boundary conditions which correlate the surface moisture with the environmental humidity at the atmosphere and on the exposed surface *S* must be defined and according to Kang, Kim et al. (2011) can be expressed as:

$$D\left(\frac{\partial h}{\partial x}\right)_s = f(h_{en} - h_s) \quad \text{Equation 4.8}$$

4.4 Finite difference method on moisture diffusion analysis

Moisture diffusion occurs in the concrete if concrete is exposed to an environmental humidity that is different than the internal humidity of concrete. A numerical analysis on the moisture diffusion of concrete specimen has been performed by formulating the moisture diffusion equation as in basic form given in an Equation 4.4 and the boundary condition expressed in Equation 4.8 by means of finite difference method. Considering the one dimensional case in Equation 4.4, moisture diffusion can also be expressed using the Laplace transform given in Equation 4.9 (Kang, Kim et al. 2011)

$$\frac{\partial h}{\partial t} = D(h)\frac{\partial^2 h}{\partial x^2} \qquad \text{Equation 4.9}$$

where h is the pore relative humidity of concrete, D is the moisture diffusion coefficient (mm^2/day), t is the drying period in days and x is the spaces (mm).

Using a Taylor's series of expansion, the Equation can be rewritten as follows in one dimension but can be readily exposed to multiple dimensions (varying the exposed surface conditions),

$$h_i^{t+1} = h_i^t + \lambda\,(h_{i+1}^t - 2h_i^t + h_{i-1}^t) \qquad \text{Equation 4.10}$$

where, $\lambda = D(h)\frac{\Delta t}{\Delta x^2}$ Equation 4.11

At high humidity's, the process of moisture migration will involve bulk liquid transport in addition to diffusion and these processes can be modelled using a two phase (liquid and water vapour) formulation according to Lewis, Schrefler et al. (1998), however for efficiency a surface factor expressed using Equation 4.12 below can be applied to reduce the system to a single field Equation for the one dimension case according to (Kang, Kim et al. 2011)

$$D(h)\frac{\partial h}{\partial x} = f \cdot (h_{en} - h_s) \qquad \text{Equation 4.12}$$

Where, h_{en} is the environmental humidity, h_s is the humidity at the surface of the concrete and the surface factor f represents the relationship between moisture transfers from concrete surface to the atmosphere at the exposed surfaces while drying and depends on the water to cement ratio, air flow speed, moisture gradient and surface textures of the concrete specimens (Sakata 1982). A value of 5.5 mm/day can be used for normal strength concrete which is determined by Sakata (1982) from experimental results.

Discretising h_{en} and h_s in Eq. 4.12 yields Equation 4.13 and 4.14 for left and right hand side boundary conditions respectively.

$$h_{i-1}^{t+1} = \frac{(-h_i^{t+1} - \frac{f\Delta x}{D(h)_i^{t+1}} h_{en})}{(-1 - \frac{f\Delta x}{D(h)_i^{t+1}})} \qquad \text{Equation 4.13}$$

$$h_{i+1}^{t+1} = \frac{(h_i^{t+1} + \frac{f\Delta x}{D(h)_i^{t+1}} h_{en})}{(1 + \frac{f\Delta x}{D(h)_i^{t+1}})} \qquad \text{Equation 4.14}$$

Which along with Equation 4.10 allow for the development of a numerical finite difference solution to the moisture diffusion problem.

4.5 Relationship between pore relative humidity and free shrinkage strain of concrete

According to Bažant and Yunping (1994) the free shrinkage strain of concrete is a function of pore relative humidity and can be described using

$$\varepsilon_{sh} = k_{sh} f_s(h) = k_{sh}(1 - h);\ k_{sh} = \varepsilon_s^0 g_s(t) \qquad \text{Equation 4.15}$$

Where, k_{sh} is the shrinkage coefficient; ε_s^0 is the ultimate shrinkage strain and $g_s(t)$ is the ratio of elastic modulus with time, i.e., $g_s(t) = \frac{E_{(t0)}}{E_{(t)}}$ and $E(t)$ can be estimated by

$E(t) = E(28)\sqrt{\frac{t}{4+0.85t}}$ with $E(28) = 33w^{1.5}\sqrt{f_c'}$

A flow chart diagram summarising the process of moisture diffusion modelling is shown below in Figure 4.1.

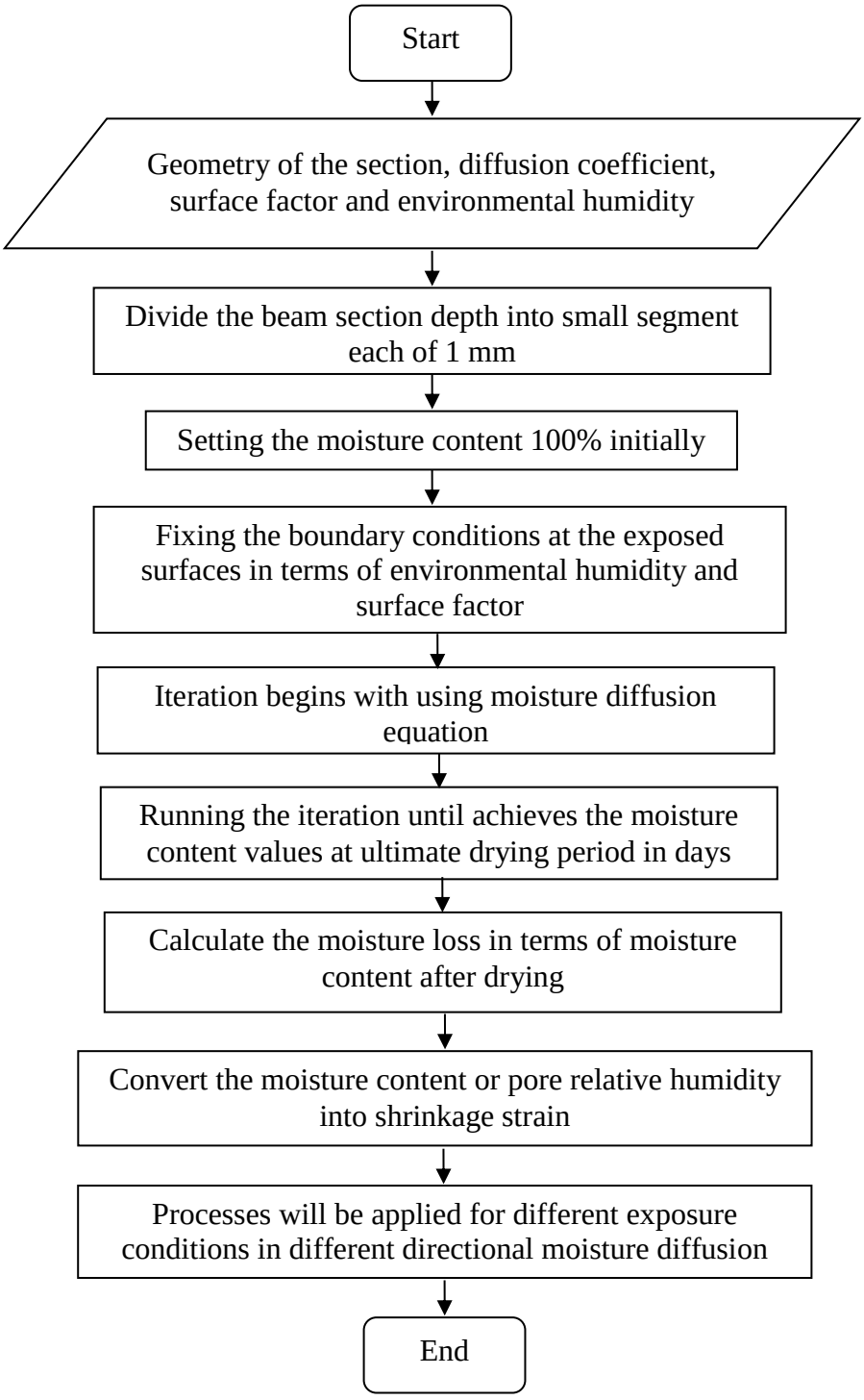

Figure 4.1: Flow chart diagram to perform moisture diffusion modelling process

4.6 Quantification of moisture diffusion coefficient

Moisture diffusion coefficient has been extracted from Gilbert's tested beam material properties with using Equation 4.5 from CEB-FIP ('90) model code where moisture diffusivity expressed as a function of pore relative humidity, *h* of concrete.

Gilbert and Nejadi (2004) tested six beams having same material properties of 25 MPa concrete under sustained loading for a period up to 400 days. All the beams were of length of 3500 mm, with a width of 250 mm and varying in depth from 325 to 340 mm. Beam B1a represented in Figure 4.2a and sectional elevation of this beam also shown in Figure 4.2b.

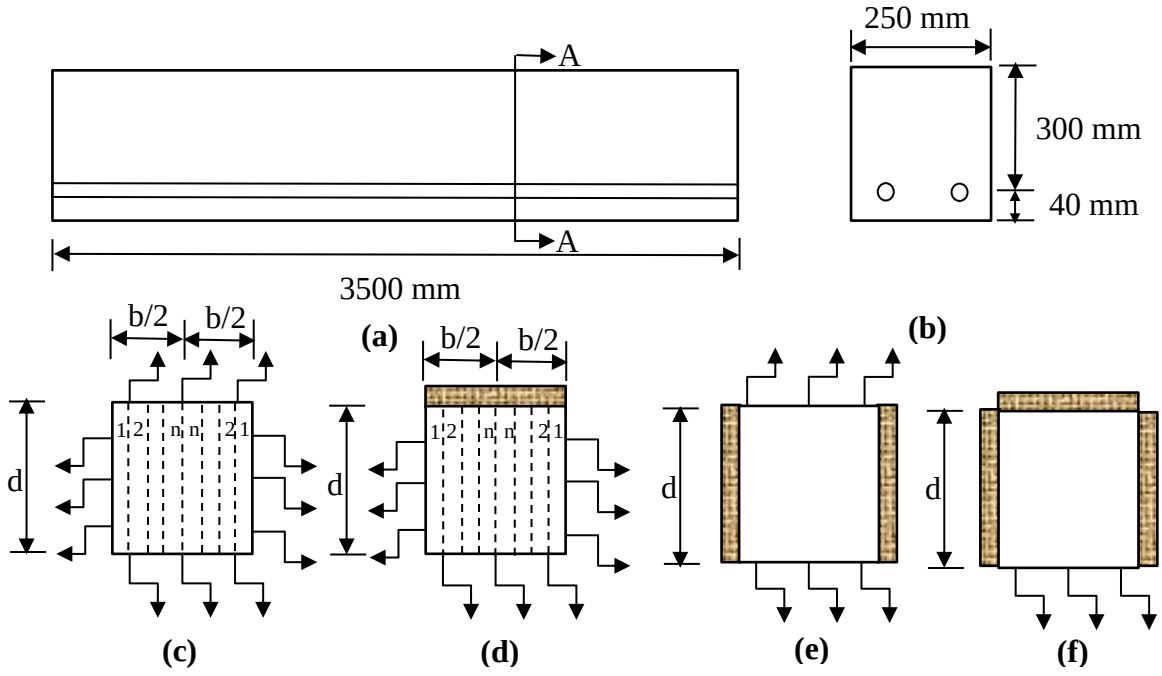

Figure 4.2: a) Gilbert and Nejadi (2004) Beam B1a b) Sectional elevation of beam B1a at A-A c) Four way flow in beam B1a d) Three way flow in beam B1a e) Two way flow in beam B1a f) One way flow in beam B1a

Now let the beam be divided into four slices along its width and allowed to diffuse moisture through the four surfaces of the beam except its two edges. As the beam is very long in length compare to its depth and width so considering there will be no moisture movement along the edges of the beam. Hence Figure 4.2c present the four way flow in the beam and Figure 4.2d shows the three way flow in the beam where top surface is sealed against moisture movement and moisture is moving through the three exposed surfaces of the beam. The two way flow in Beam represents in Figure 4.2e where moisture is moving along the top and bottom surfaces of the beam and rest of the surfaces are sealed against moisture movement and then Figure 4.2f depicts the one way flow in the beam where all the surfaces are sealed against moisture movement except the bottom surface and so the moisture is moving only through the bottom surface of the beam.

For analysis the characteristic compressive strength of concrete has been determined using Equation 4.7 for the concrete having mean compressive strength of 24.8 MPa. The maximum moisture diffusion coefficient D_1 for the relative humidity of h = 1.0 has then been calculated using Equation 4.6 which is then be used in Equation 4.5 to develop the relationship between moisture diffusion coefficient, D with moisture content or pore relative humidity, h of concrete shown in S-shaped curve in Figure 4.3.

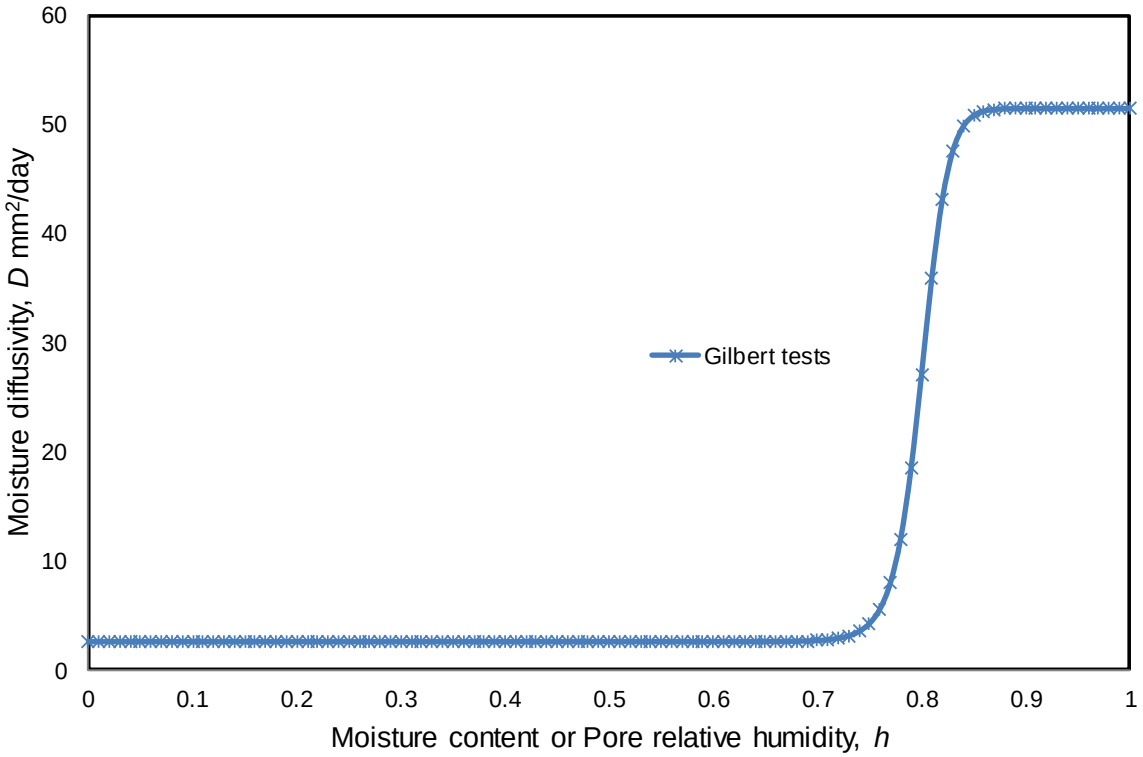

Figure 4.3: Moisture diffusivity vs moisture content or pore relative humidity, h for the beams tested by Gilbert and Nejadi (2004)

4.7 Four way flow in rectangular beam

As mentioned in earlier section, the beam in Figure 4.2a is very long in length L = 3500 mm compare to the depth d or width b of the beam and if this is the case, there will be no moisture flow along the length of the beam and therefore moisture will be flowing through the four surfaces except the edges of the beam. Hence moisture diffusion modelling has been performed by using finite difference method with using Equation 4.9 and the boundary conditions were used according to Equation 4.12 where environmental humidity is been considered as 40 percent. Relationship between moisture diffusivity with moisture content been achieved using Equation 4.5 from CEB-FIP (’90) model code as illustrated

in Figure 4.3. Then the moisture content can be converted into shrinkage strain of concrete with using Equation 4.15 from Bažant and Yunping (1994) where ultimate shrinkage strain is 1800με. According to Figure 4.2c, where concrete member can be sliced up to *n* components and may be considered into four slices along its width in this study and due to symmetry only half of the member would be used for analysis and hence shrinkage strain profile for slices named b1 and b2 is been plotted in Figure 4.4 after been drying for the period of 100, 250 and 400 days. Experimental investigation by Gilbert and Nejadi (2004) also confirms that the moisture diffusion model can reasonably well predict the shrinkage strain variations in a beam as displayed in Figure 4.4 where shrinkage strain increases over time while drying period accelerates. It can be found that shrinkage strains are symmetrical about mid-depth and they are of maximum at top and bottom sections of the beam. Also, they are greatest adjacent to the sides labelled 'slice b1'comparison to those at mid-width that is slice b2.

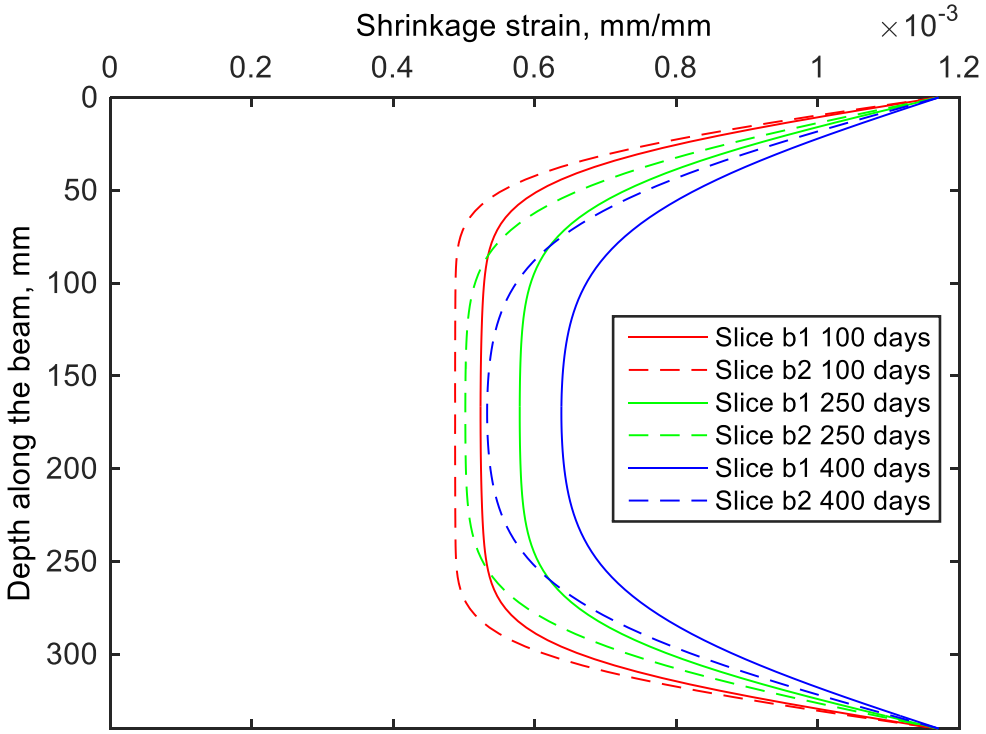

Figure 4.4: Shrinkage strain profile in a four way flow Gilbert and Nejadi (2004) Beam B1a after 100 days, 250 days and 400 days of drying

4.8 Three way flow in a beam

Let us now consider the beam shown in Figure 4.2a is sealed against moisture movement at the top surface and rest of the surfaces are exposed to moisture movement as it can be seen in Figure 4.2d. Therefore, moisture will be flowing through the sides and bottom surfaces of the beam. Boundary conditions are been used near to the exposed surfaces according to Equation 4.12 and Neumann boundary condition (Walker, Leonard et al. 2009) has also been applied to the sealed surface to allow diffusion to commence from the sealed surface over time. Using the Finite difference method and considering the relationship between moisture diffusivity and moisture content represented in Figure 4.3, the moisture content will be converted into free shrinkage strain of concrete according to Equation 4.15 that is displayed in Figure 4.5 and which shows the shrinkage strain profile at slices b1 and b2 for the three way moisture diffusion of a beam at the end of drying period for 100, 250 and 400 days. It can be seen that the shrinkage strain has the greatest variations and is the greatest magnitude at the bottom section of the beam and in the remaining region the shrinkage strain can be considered to be uniform in this case.

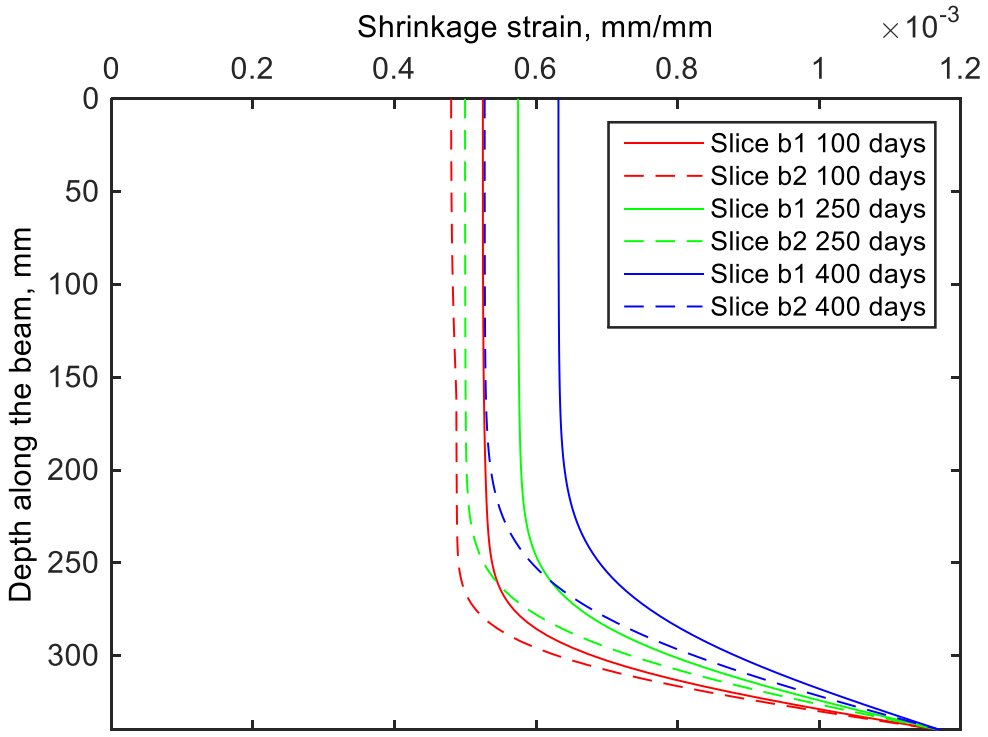

Figure 4.5: Shrinkage strain profile in a three way flow Gilbert and Nejadi (2004) Beam B1a after 100 days, 250 days and 400 days of drying

4.9 Two way flow in a beam

Let the beam in Figure 4.2a now be exposed form top and bottom surfaces to allow for moisture movement which is to cause shrinkage strain variations along the beam and rest of surfaces are sealed against moisture movement can be seen in Figure 4.2e. This moisture diffusion process can be treated as two directional flow or two way flow in a beam where identical values achieved along the slices of its width and the problem is become one dimensional (1D). The boundary condition expressed in Equation 4.12 can be applied to the top and bottom exposed surfaces at the moisture diffusion modelling purposes. Hence the finite difference method is applied with consideration of the relationship between moisture diffusion coefficient with moisture content or pore relative

humidity, *h* shown in Figure 4.3. Then the remaining moisture content after been drying of 100 days, 250 days and 400 days which causes of moisture losses in the member would be converted to the shrinkage strain variations along the depth of the beam as displayed in Figure 4.6 with using Equation 4.15. It can be found remarkable increment of non-linear shrinkage strain variations along the depth of the beam as the drying period increases.

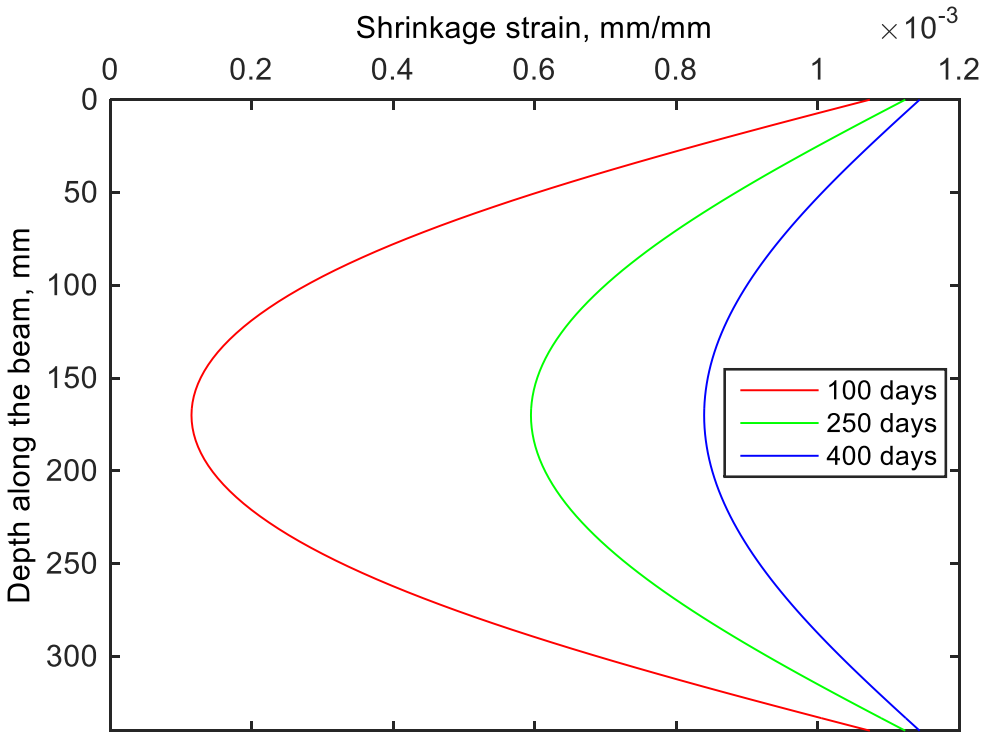

Figure 4.6: Shrinkage strain profile in a two way flow Gilbert and Nejadi (2004) Beam B1a after 100 days, 250 days and 400 days of drying

4.10 One way flow in a beam

Now let the beam in Figure 4.2a is been sealed all surfaces except bottom surface against any moisture movement to allow for shrinkage and so the moisture will be moving from top region of the member through bottom surface of the beam to cause shrinkage and that

can be treated as one directional or one way flow (1D) in a beam as shown in Figure 4.2f. As discussed earlier, Equation 4.12 would be used to set up the boundary conditions at the exposed bottom surfaces considering environmental humidity of 40 percent and surface factor *f* value of 5.5 mm/day (Sakata 1982). The Neumann boundary conditions (Walker, Leonard et al. 2009) would be applied at the sealed top surfaces to allow the moisture diffusion will be taking place from top which causes the shrinkage strain would be starting from top surfaces of the member which increases over time and representing a non-linear parabolic profile after 100, 250 and 400 days of drying displaying in Figure 4.7.

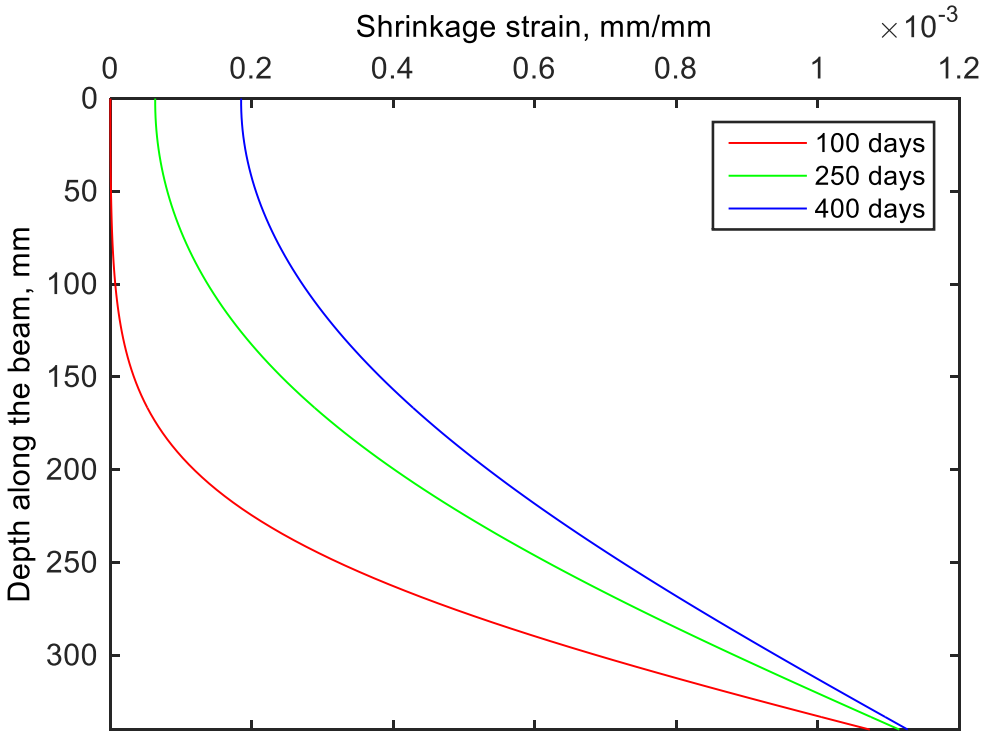

Figure 4.7: Shrinkage strain profile in a one way flow Gilbert and Nejadi (2004) Beam B1a after 100 days, 250 days and 400 days of drying

4.11 First simulation with Asad, Baluch et al. (1997)

According to Asad, Baluch et al. (1997), a concrete repair material mortar specimen having dimensions of 10 cm × 2 cm × 2 cm exposed one faces and rest of the surfaces are sealed. Moisture loss measured at 1cm from the drying surface and simulated with non-linear theory using non-linear moisture diffusivity provided by the author as expressed in Equation 4.16 and also displayed in Figure 4.8.

$$D(h) = D_0 + a\left(\frac{h}{1-h}\right)^b \qquad \text{Equation 4.16}$$

Where $D_0$is the moisture diffusivity at oven-dry condition when $h = 0$ % and is equal to 0.1175 cm^2/day, and the regression parameters *a* and *b* are 0.05 and 1.878 respectively.

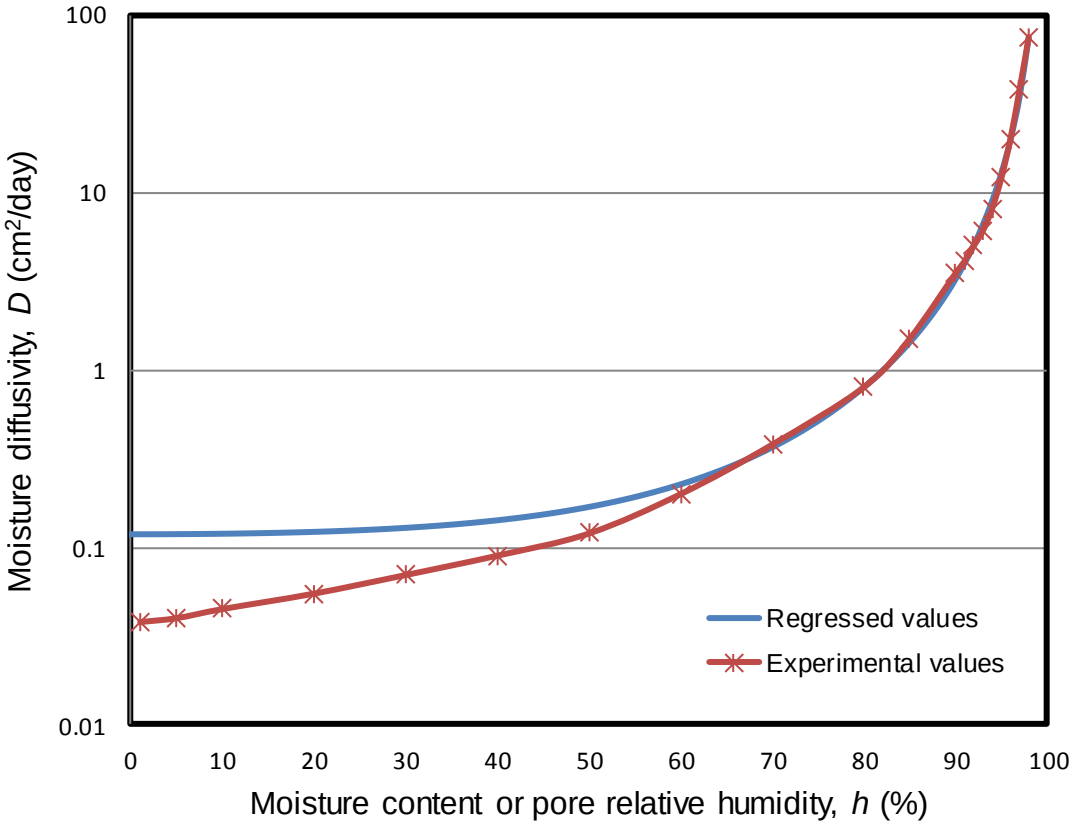

Figure 4.8: Relationship between moisture content or pore relative humidity, h and moisture diffusivity D

Experimental and predicted values of moisture loss at 1 cm from the drying surface can be represented in Figure 4.9 which has been simulated using the finite difference method considering the non-linear relationship between moisture diffusivity with moisture content from Figure 4.8 where the value of surface factor, f = 0.30 cm/day is the same used by the author. For linear theory, considering constant diffusivity D = 0.45 cm^2/day (where author used D = 0.30 cm^2/day) and f = 0.40 cm/day (where author used f = 0.30 cm/day) to achieve the best fit. It can be observed that the prediction of moisture loss is found to be in better agreement using moisture dependent diffusivity with comparison of constant diffusivity. At the initial stages of drying, moisture loss is high due to the high value of moisture diffusivity and after 10% of moisture loss the predicted value is in good agreement with experimental values and this is because the bulk water flux also participates in moisture transport in the form of pore water suction and elevation at the early stages for nearly saturated conditions though diffusion mechanism in unsaturated condition is mainly due to the vapour flux diffusion.

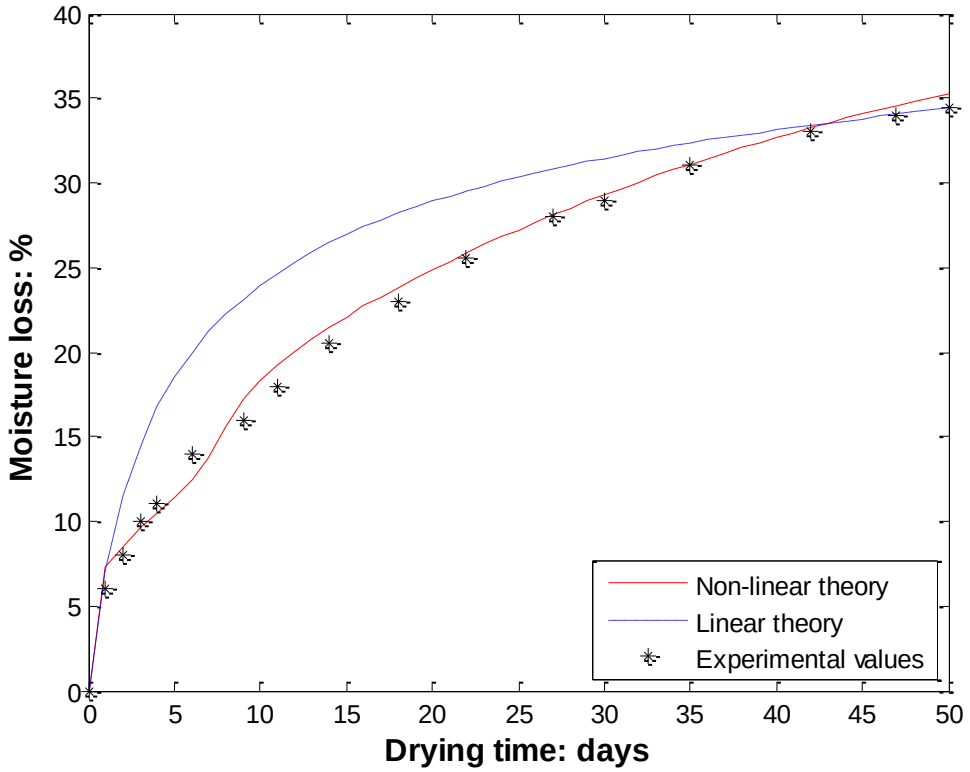

Figure 4.9: Numerical simulation of experimental and predicted values of moisture loss at 1 cm from the drying surface using finite difference method

4.12 Second simulation with Jafarifar (2012)

According to Jafarifar (2012), concrete specimens were cast in a dimension of 180 mm × 150 mm × 150 mm to measure the moisture content at various depths after 90 days of water curing and drying starts at 1, 3, 5, 7, 14, 28, 42, 56, 70 and up to 84 days. Specimens were kept at a chamber of constant humidity and temperature control room of 40 ± 3% and 25 ± 3°c. Moisture measurement for various types of concrete conducted for this experiment using the modified gravimetric method and moisture diffusivities as a function of moisture content determined from the experimental results using the inverse analysis technique as shown in Figure 4.10. The surface factor, *f* also derived from experimental test results using the technique of inverse analysis and found to be in the range of 3-10

mm/day for conventional concrete CC mixes, and 5-10 mm/day for rolling compacted concrete RCC mixes.

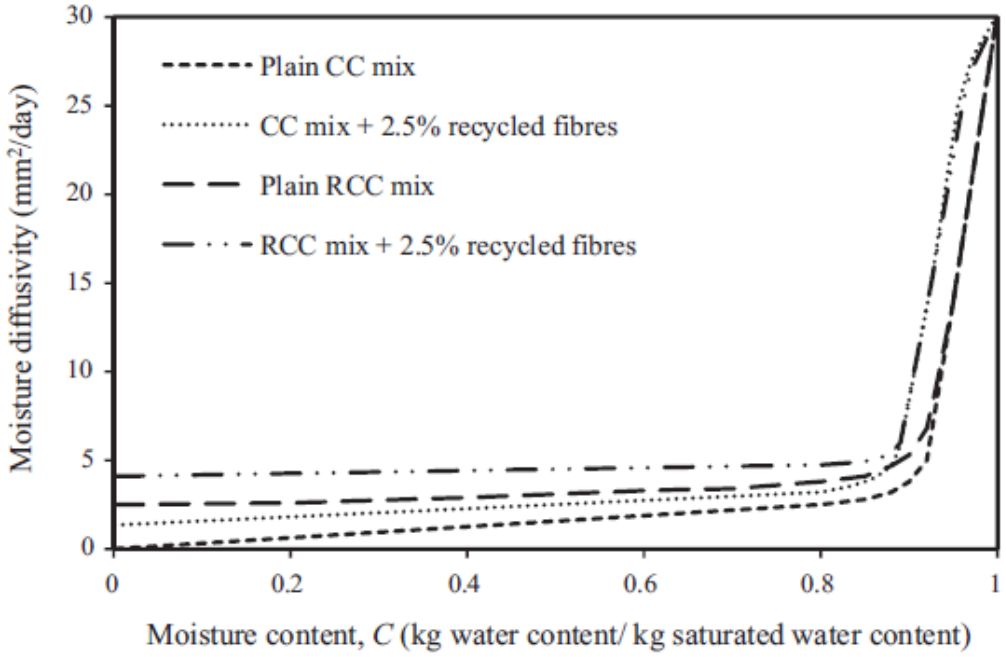

Figure 4.10: Moisture diffusivity versus pore relative humidity or moisture content for various types of concrete mixes (Jafarifar 2012)

Figure 4.11 represents the numerical simulation of experimental moisture profiles using the finite difference method with consideration of nonlinear relationship between moisture diffusivity and moisture content obtained from Figure 4.10 and the range of surface factor values for different concrete mixes derived by the author. These curves are the best fit plotting achieved from numerical simulations to the experimental results of moisture content values using the non-linear relationship of moisture diffusivity with moisture content and by changing the moisture diffusivity and range of surface factor values determined by the author.

It can be seen from Figure 4.11 (a) for plain CC mix, predicted moisture content values are in good agreement with experimental results and for rest of the mixes from Figure 4.11 (b) to (d) for plain RCC mix, SFR-CC mix and SFR-RCC mix, moisture content lower than 75-80%, it shows good accuracy with the test results. This is because the bulk water flux also responsible for moisture transfers in the form of pore water suction and elevation whereas vapour flux is considered only in the moisture diffusion mechanism.

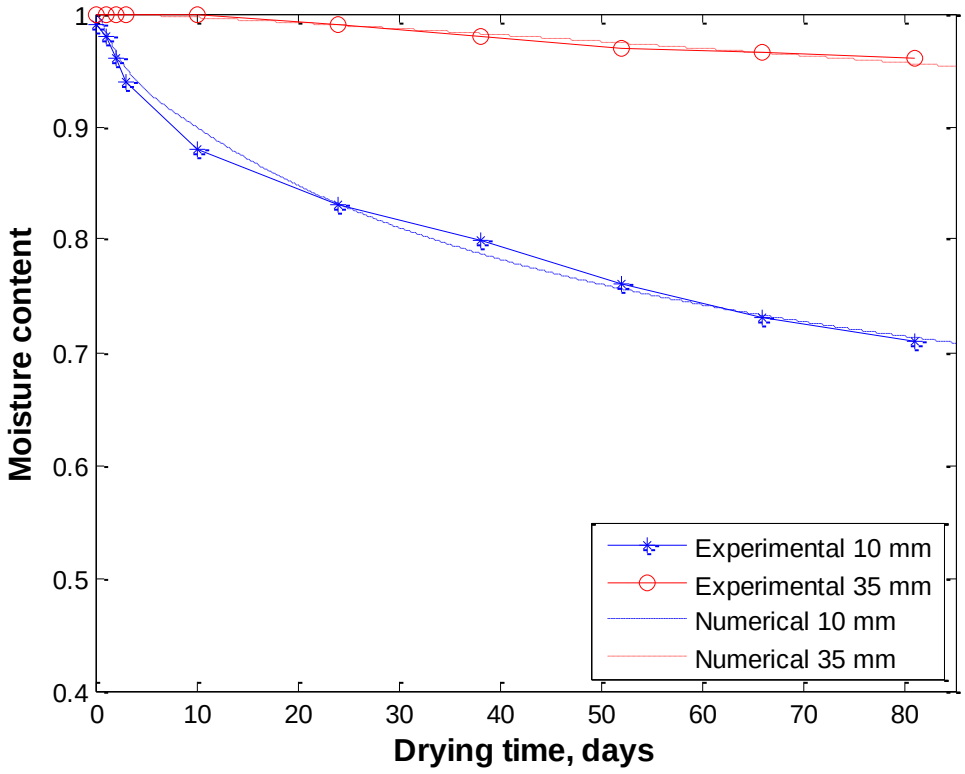

(a) Plain CC mix

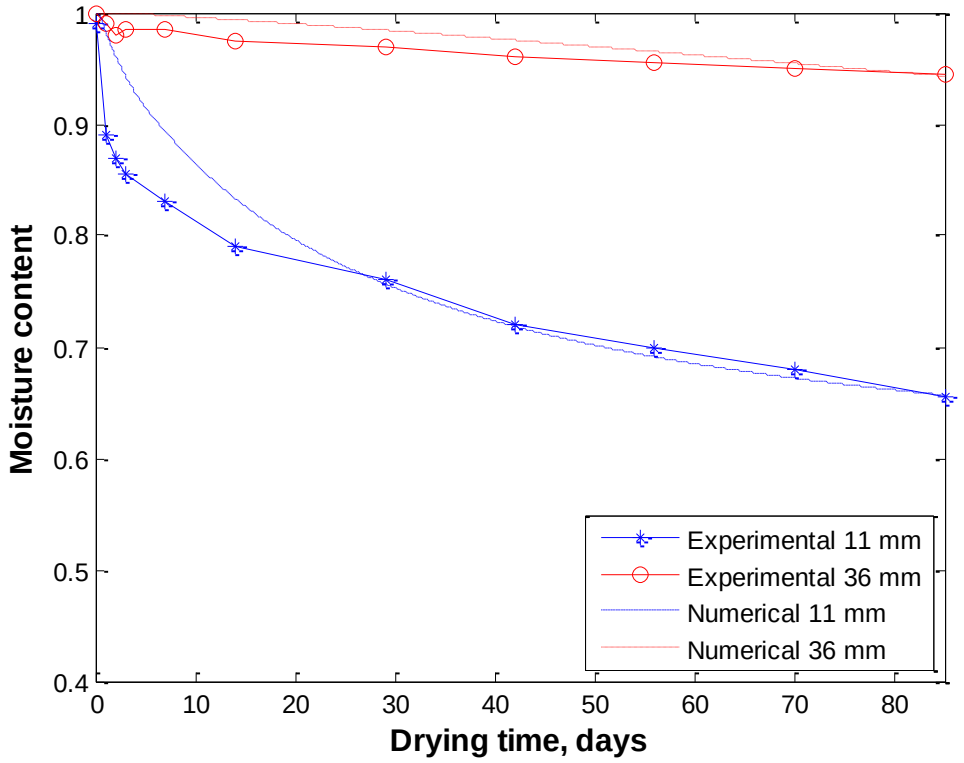

(b) Plain RCC mix

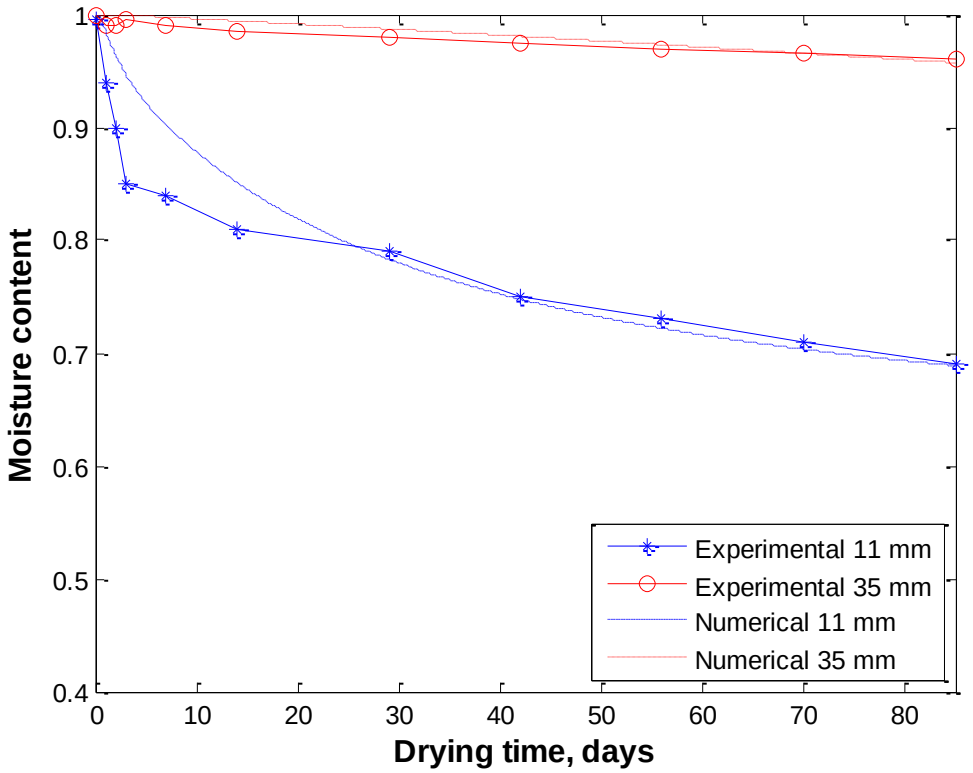

(c) SFR-CC mix

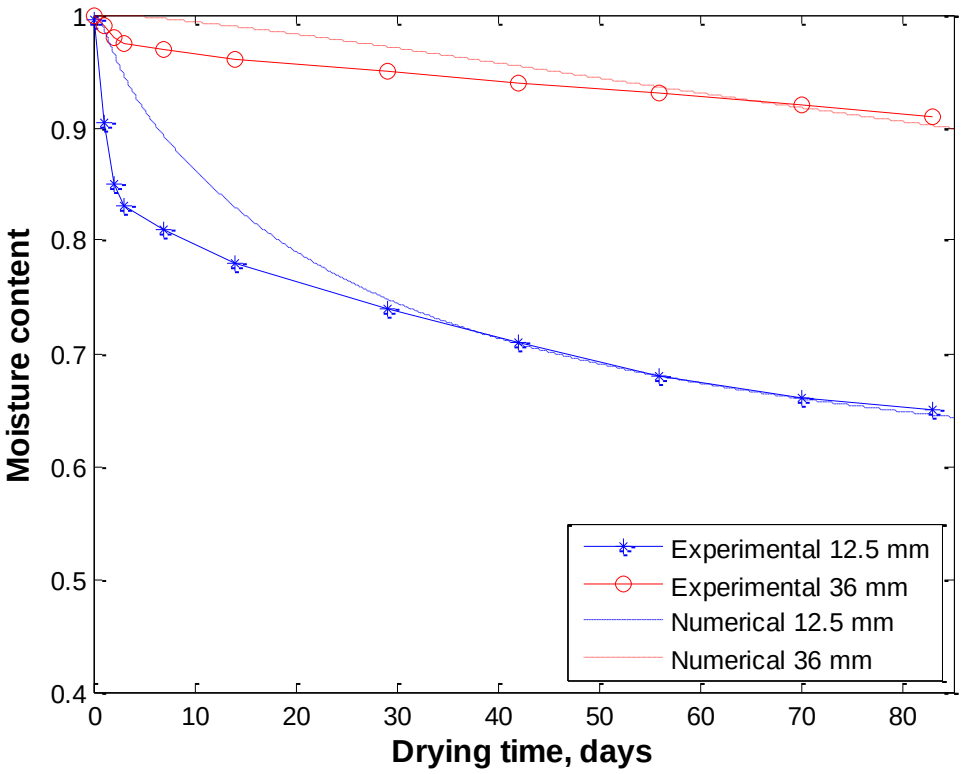

(d) SFR-RCC mix

Figure 4.11: Numerical moisture profiles compared with the experimental results simulated using finite difference method: (a) Plain CC mix; (b) Plain RCC mix; c) SFR-CC mix; (d) SFR-RCC mix

4.13 Third simulation with Kim and Lee (1999)

An experimental investigation has performed with three different types of concrete for a specimen having dimension of 10 cm × 10 cm × 20 cm drying one side at cross-section of 10 cm × 10 cm and total depth of 20 cm and rest of the surfaces are sealed with paraffin wax against moisture movement. Relative humidity measured at three different depths of concrete 3 cm, 7 cm and 12 cm using humidity probe inserted into the concrete prism (Kim and Lee 1999).

Figure 4.12 represents the relationship between moisture diffusivity and moisture content was extracted using Equation 4.5 from CEB-FIP (1990) and which is been used to simulate the experimental results shown in Figure 4.13 and 4.14. There are three types of concrete having different water-cement ratios with two different moist curing conditions are 3 and 28 days respectively.

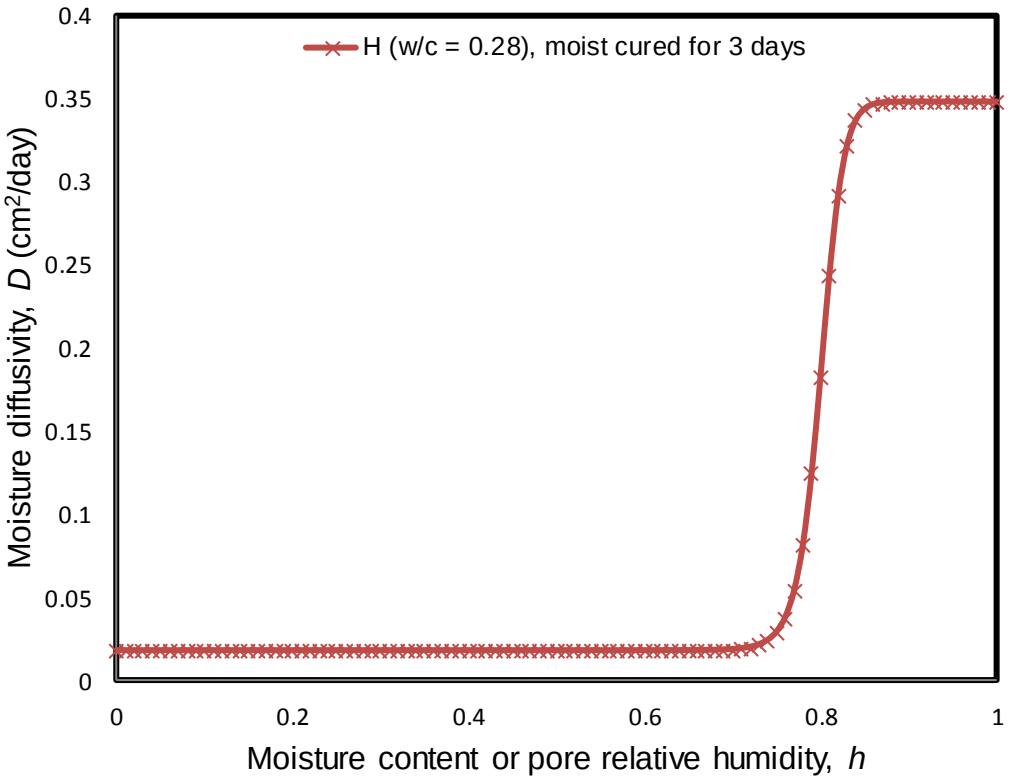

(a) H (w/c = 0.28) drying commence after 3 days moist cured

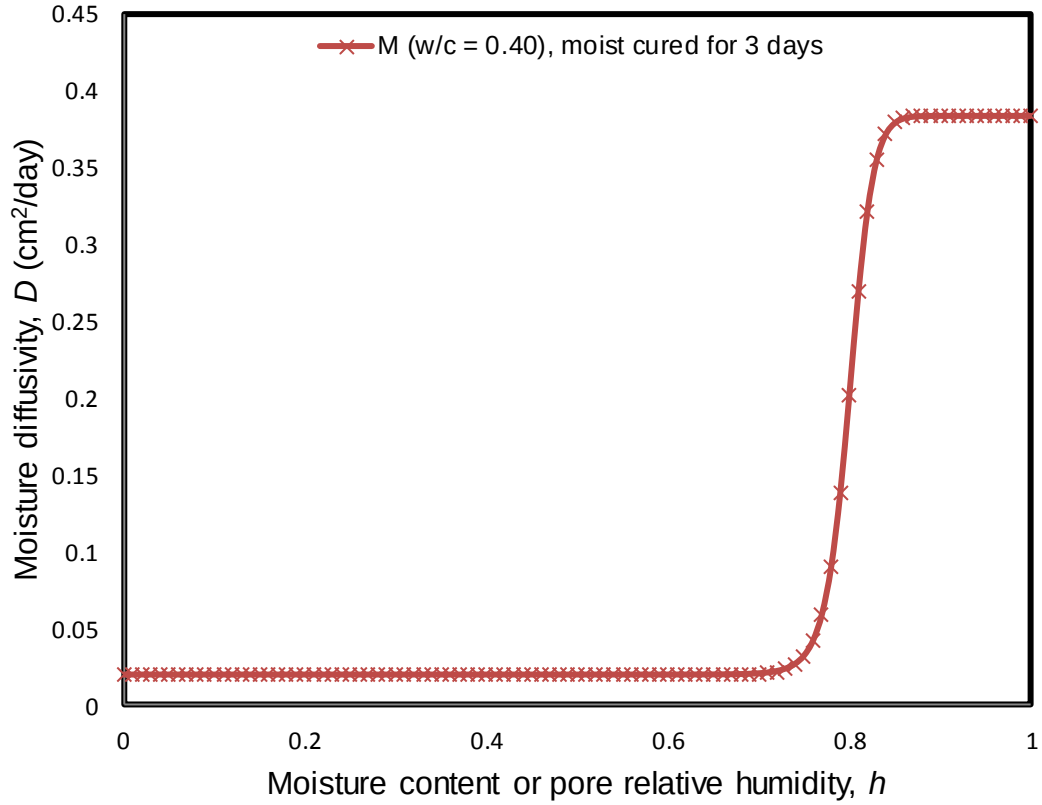

(b) M (w/c = 0.40) drying commence after 3 days moist cured

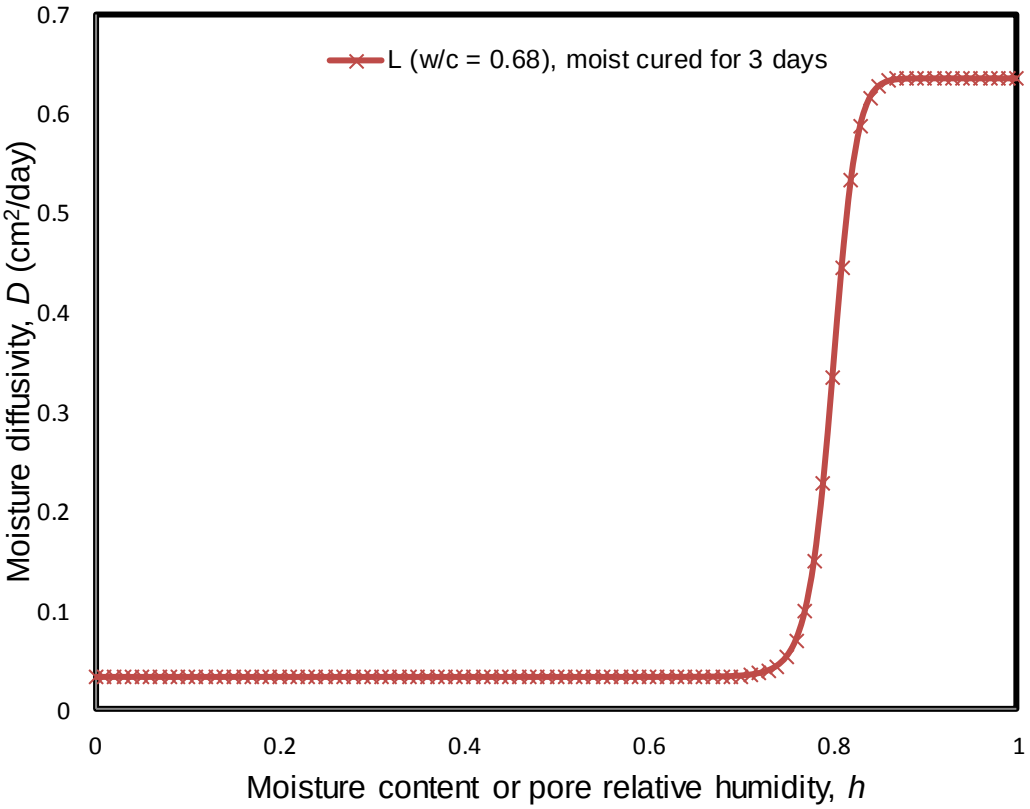

(c) L (w/c = 0.68) drying commence after 3 days moist cured

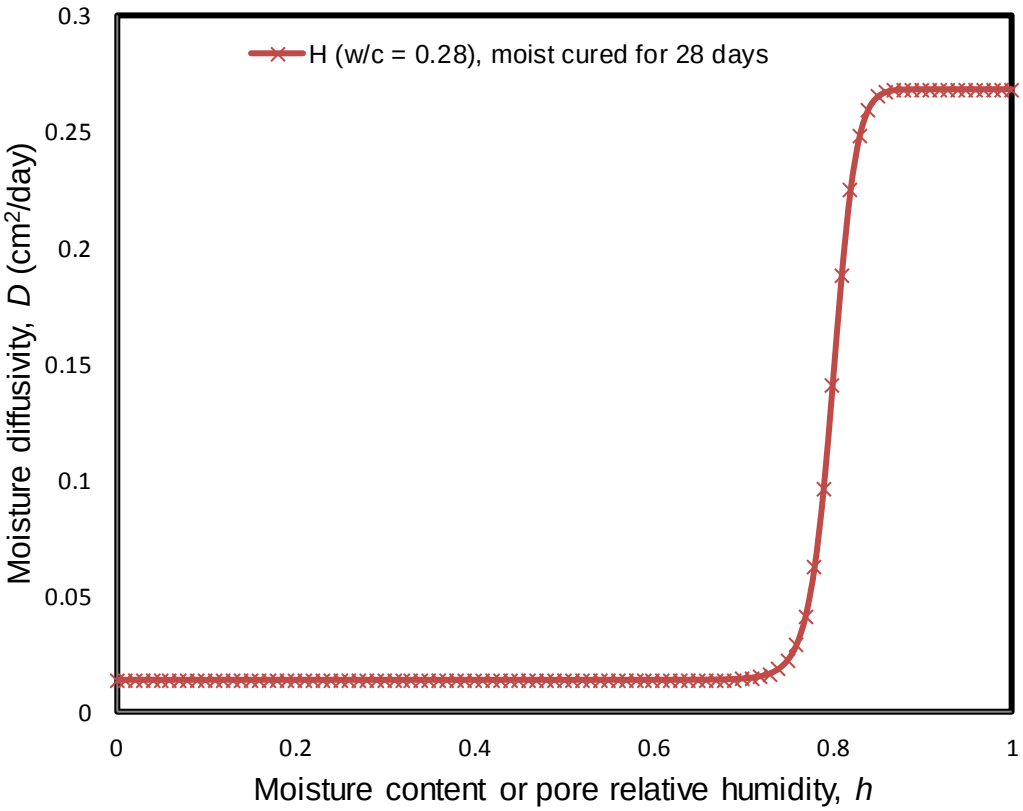

(d) H (w/c = 0.28) drying commence after 28 days moist cured

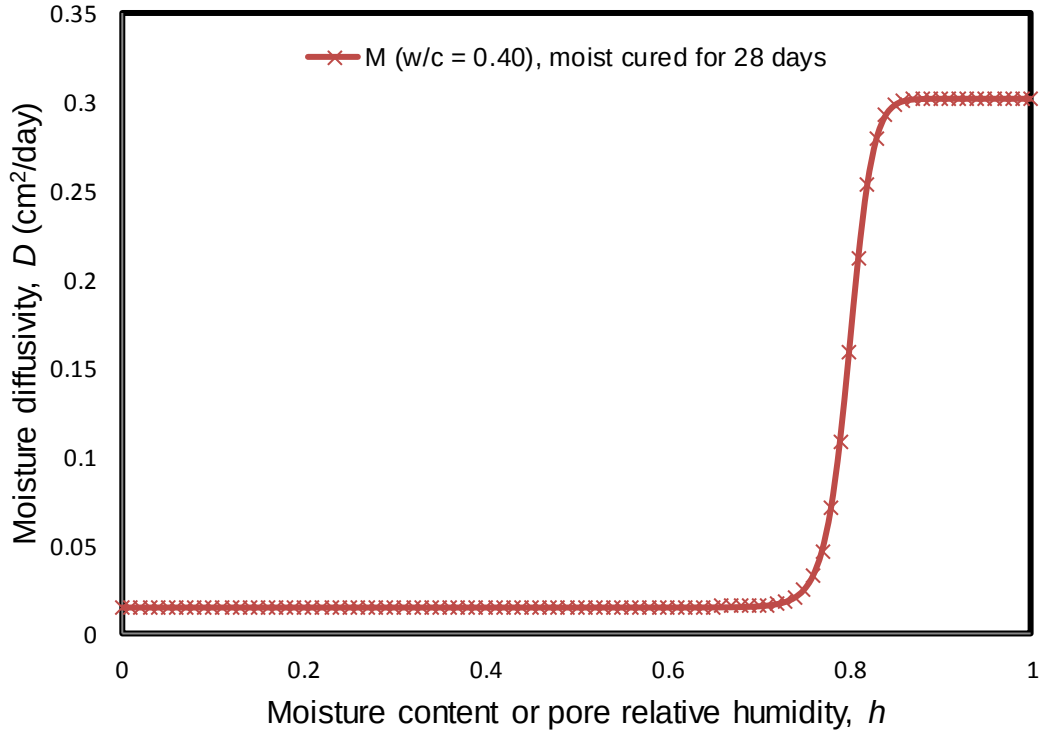

(e) M (w/c = 0.40) drying commence after 28 days moist cured

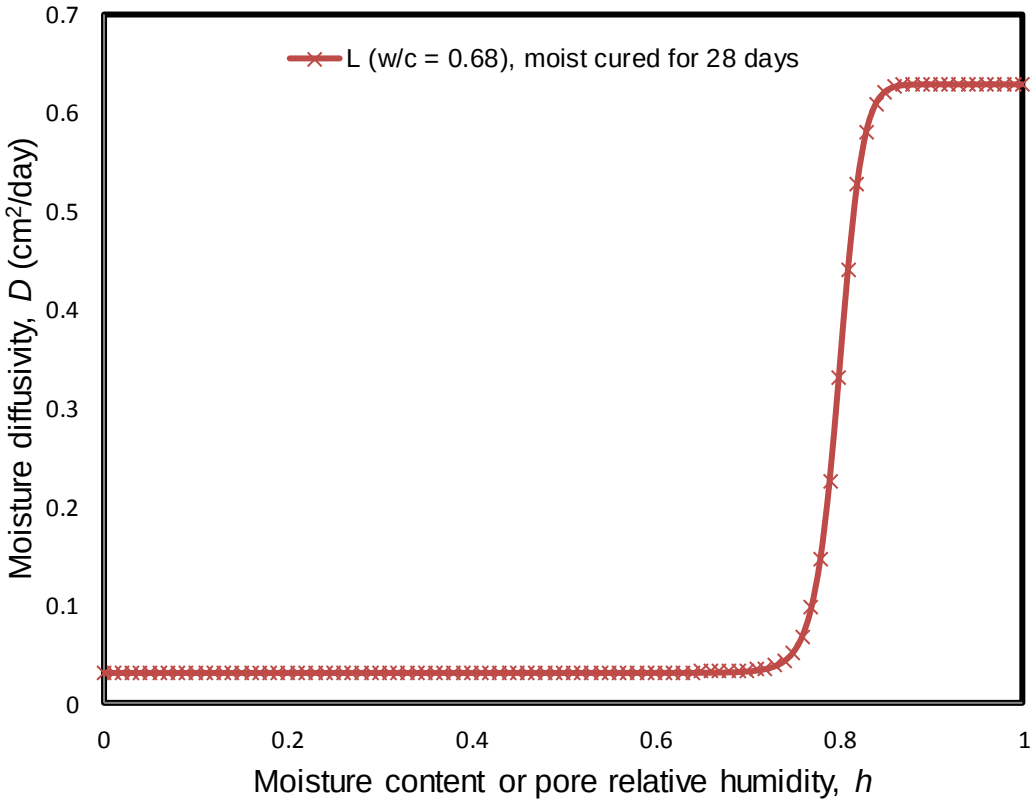

(f) L (w/c = 0.68) drying commence after 28 days moist cured

Figure 4.12: Relationship between moisture diffusivity and moisture content for three different types of concrete a) H (w/c = 0.28) b) M (w/c = 0.40) c) L (w/c = 0.68) with moist cured for 3 days and d) H (w/c = 0.28) e) M (w/c = 0.40) f) L (w/c = 0.68) with moist cured for 28 days

Figure 4.13 and 4.14 shows the numerical simulation of relative humidity measured at three different locations inside the concrete prism at 3 cm, 7 cm and 12 cm from the drying surface. These curves are best fitted to the experimental results considering the maximum moisture diffusion coefficient expressed through the Figure 4.12 for different concrete mixes with two different moist curing conditions at 3 days and 28 days.

These best fit curves are achieved by changing the moisture diffusivity and surface factors which shows in good accuracy of predicted relative humidity with comparison of experimentally measured relative humidity inside the concrete specimen while drying. It can be appeared that the moisture diffusion model developed in this study can well predict the moisture or humidity diffusion in these different types of concrete specimens in 3 days moist cured exposed to the ambient air at early ages as well as in 28 days moist cured concrete.

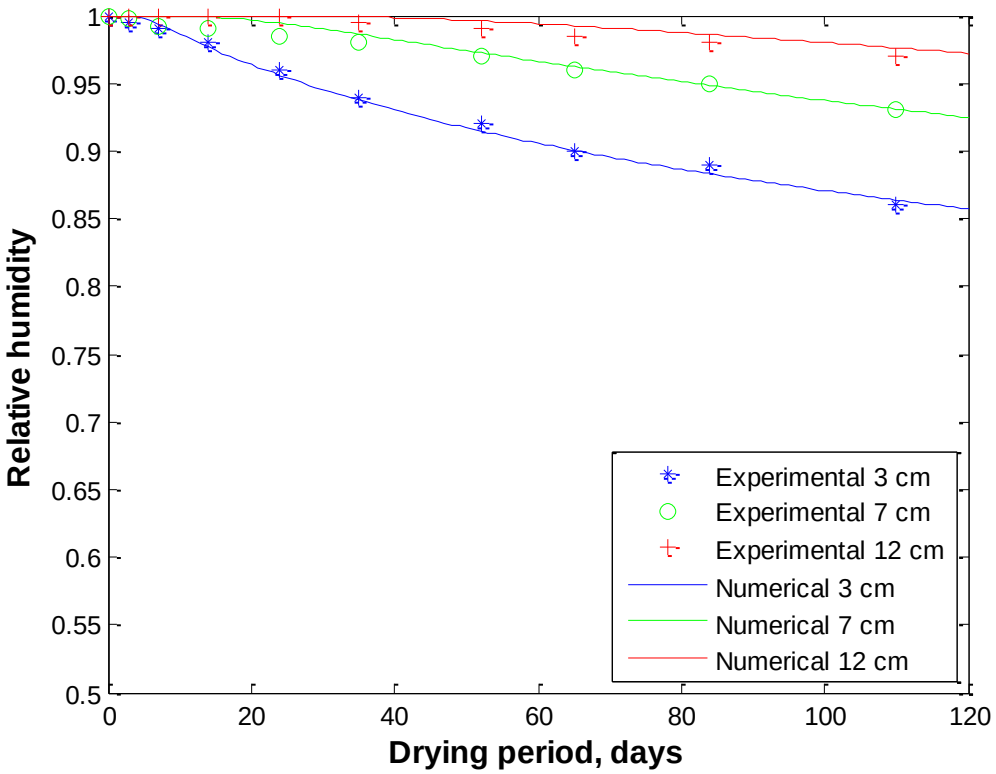

(a) H (w/c = 0.28), moist cured for 3 days

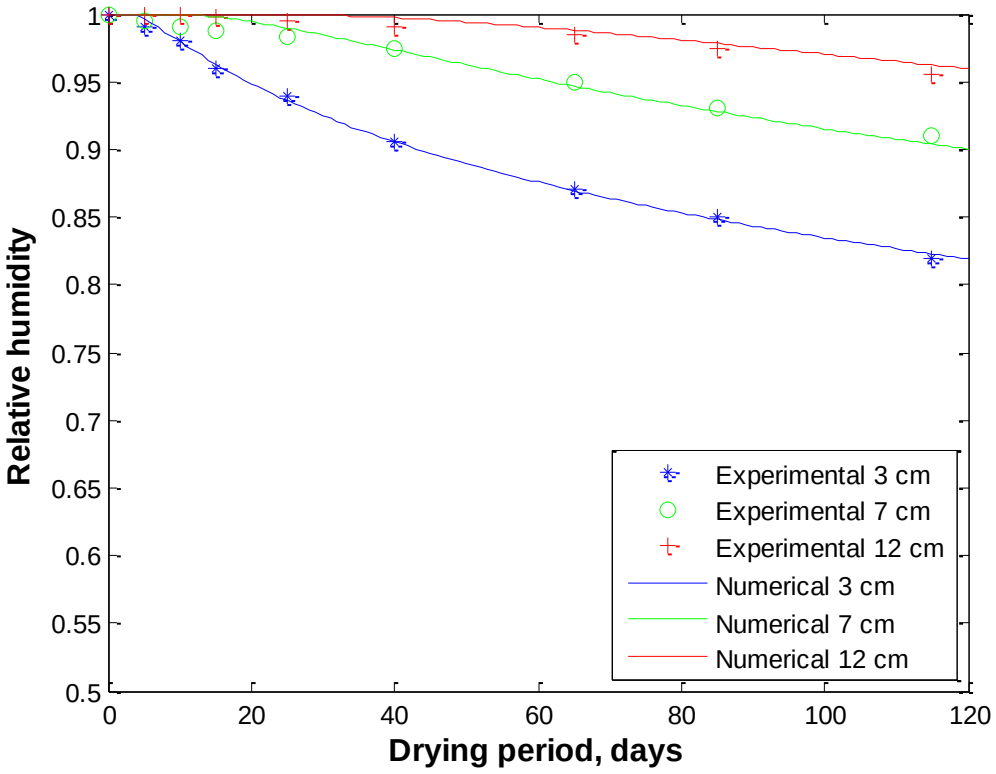

(b) M (w/c = 0.40), moist cured for 3 days

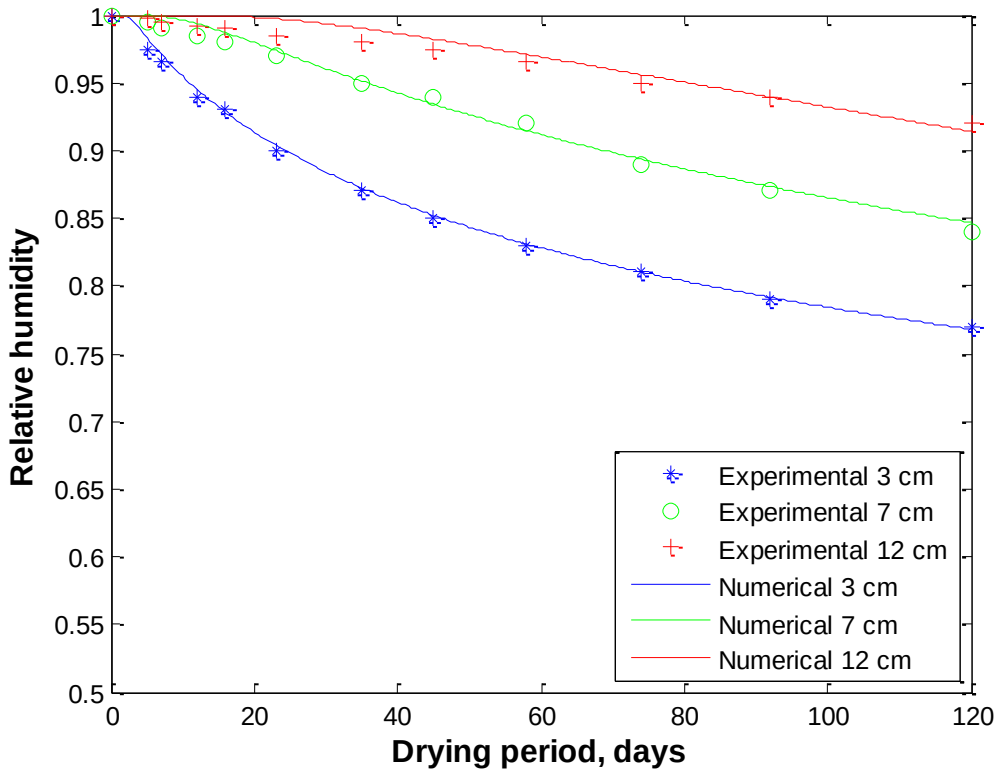

(c) L (w/c = 0.68), moist cured for 3 days

Figure 4.13: Numerical simulation of experimental results for three different types of concrete after moist cured for 3 days a) H (w/c = 0.28) b) M (w/c = 0.40) and c) L (w/c = 0.68)

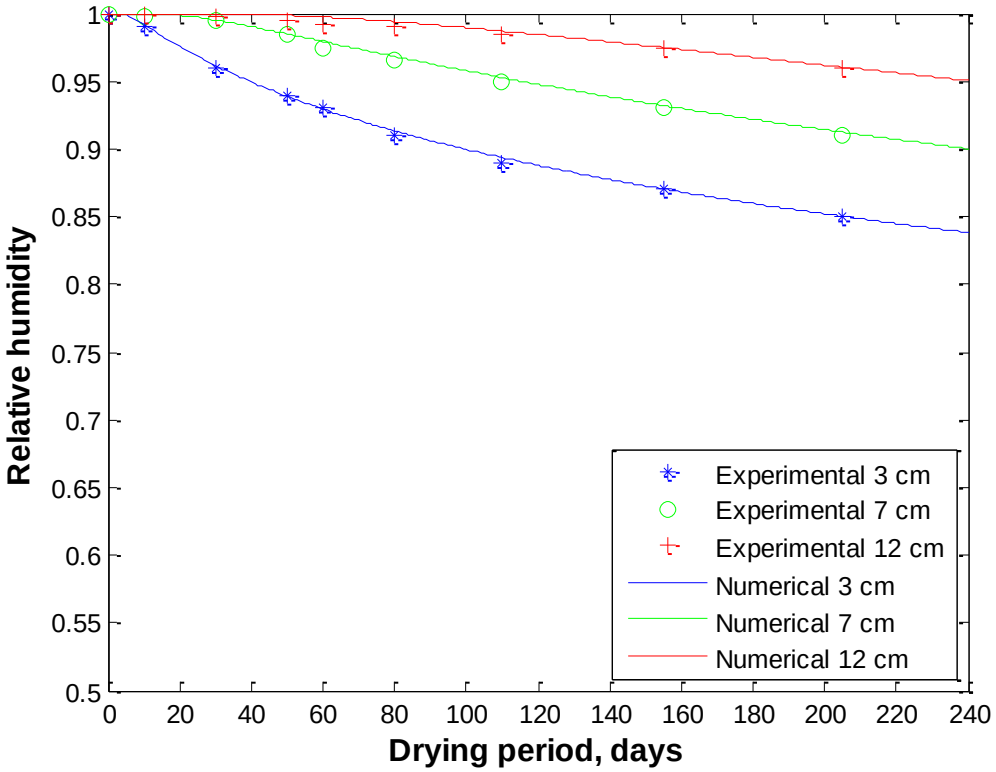

(a) H (w/c = 0.28), moist cured for 28 days

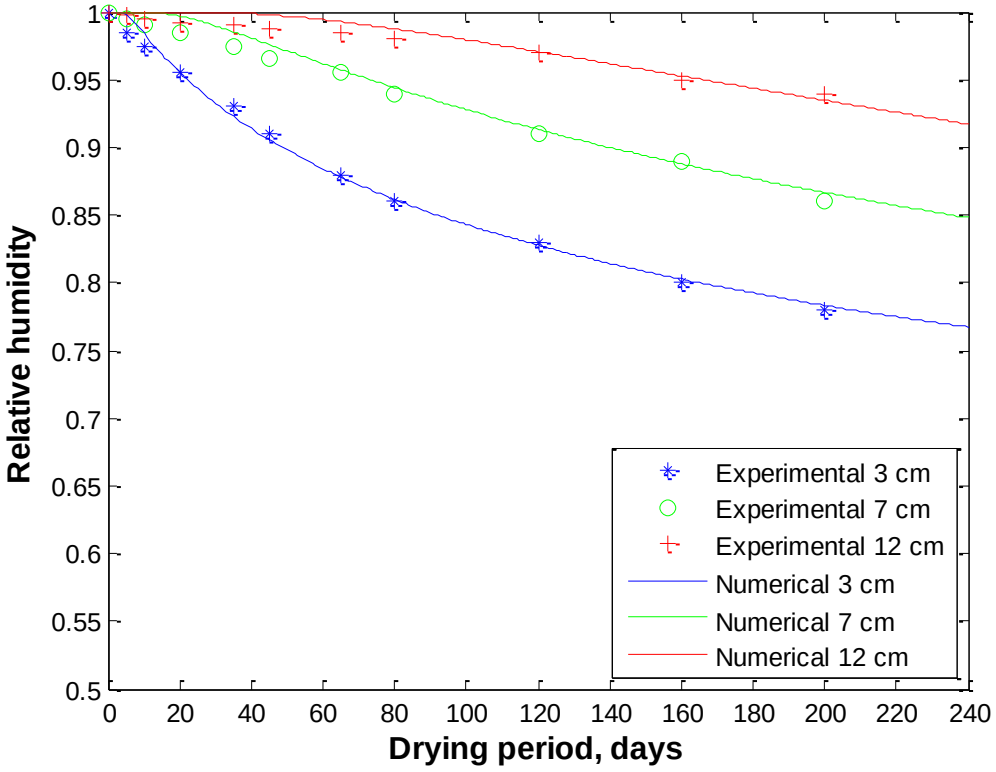

(b) M (w/c = 0.40), moist cured for 28 days

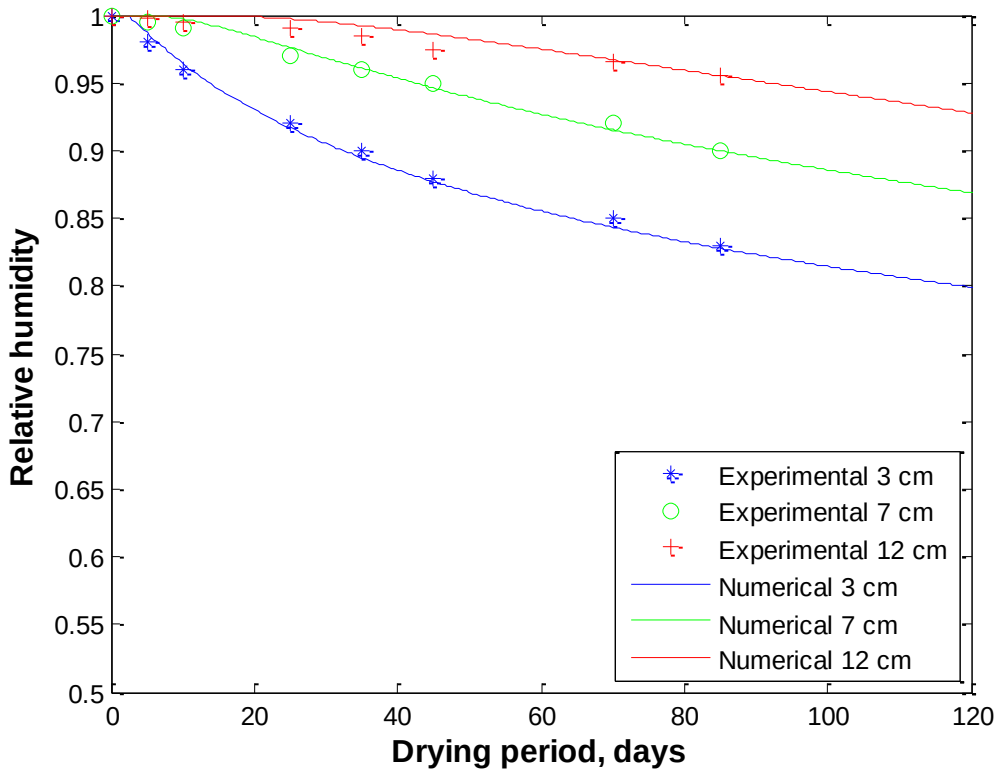

(c) L (w/c = 0.68), moist cured for 28 days

Figure 4.14: Numerical simulation of experimental results for three different types of concrete after moist cured for 28 days a) H (w/c = 0.28) b) M (w/c = 0.40) and c) L (w/c = 0.68)

Chapter 5 Proposed Experimental Work

5.1 Introduction

This chapter proposes a new experimental test setup which can better quantify the variation in shrinkage strain along the width and depth of a cross section and can allow for variation in surface permeability. Current shrinkage test methodologies have some limitations that is all surfaces are exposed and they are small scale which leads to a uniformity of shrinkage strain and which is not present in full size beams. Importantly the approach considers the influence of member size in terms of the volume over exposed surface area ratio (V/S) of the member. Experimental tests are proposed to be performed to measure the long term (> 1 year) shrinkage strain and to obtain all material properties required to simulate concrete shrinkage via moisture diffusion modelling as proposed in Chapter 4.

5.2 Purpose of tests

The proposed test regime will provide experimentally the non-linear variation in shrinkage strain along depth of the prism for one and two direction diffusion processes. It also provides the non-linear shrinkage strain variations through depth as well as width of the prism for three and four direction diffusion processes. Importantly, in the proposed experiments no internal strain gauges are employed as the presence of internal instrumentation restrains shrinkage and influences the measured results. Hence in the proposed setup measurement of shrinkage strain is based on the use of DEMEC gauges to quantify the deformation of the prism at the concrete surface. These readings can then be

correlated with the results of a moisture diffusion analysis as outlined in Chapter 4 in order to quantify the variation in shrinkage strain throughout the width and depth of the specimen.

5.3 Sizes of specimen

To variation in moisture diffusion and hence shrinkage with specimen size, it is proposed that for a given concrete under consideration, tests be performed on specimen of size ranging from 75 mm ×75 mm × 1200 mm to 300 mm × 800 mm × 1200 mm as in Figure 5.1 to Figure 5.6. In these tests the ends of the prism are to be sealed such that the prisms represent a beam segment extracted from the central region of a beam span. When considering a three directional diffusion process represent a T beam as in Figure 5.3 to 5.4 only in addition to the beam ends all but the bottom surface will be exposed, while for a two direction diffusion process representing a slab, the top and bottom surfaces will be exposed whereas bottom surface will be exposed only for one direction. Details specimen sizes are provided in Table 5.1. In Table 5.1, specimen having V/S ratios of 75 (bolded) will be casted in paired form to compare the shrinkage strain variations among themselves.

Table 5.1: Specimen size details with V/S ratios for one up to four direction diffusion processes

Specimen size (mm)	One direction (V/S)	Two direction (V/S)	Three direction (V/S)	Four direction (V/S)
75×75×1200	**75**	37.50	25	18.75
150×150×1200	150	**75**	50	37.50
150×300×1200	300	150	**75**	50
200×600×1200	600	300	120	**75**
300×800×1200	800	400	171.43	109.09

5.4 Testing for material properties

In addition to the shrinkage tests outlined above, it is suggested that additional tests are required to measure the compressive and tensile strength of concrete at various ages of 3, 7, 14, 28, 56, 90, 180 and 365 days curing periods. Details are given in the table 5.2 below:

Table 5.2: Test details for material properties

Test name	Specimen sizes (mm)	Number of specimens
Compressive strength test	100 × 200	24
Cylinder split test	100 × 200	24
Flexural strength test	100 × 100 × 350	24

5.5 Standard shrinkage test

Standard shrinkage test of specimens are crucial to be performed as they are done with a smaller sizes of concrete prismatic specimens compare to the real sizes of RC members and all the surfaces are exposed to the environment which are not the case as it happens always in practice. Therefore, standard shrinkage test of 6 prisms with specimen sizes of 75 mm ×75 mm × 280 mm will also be carried out to simulate with proposed experimental test results.

5.6 Instrumentation in details

Detailed instrumentation processes are shown in Figure 5.1 to Figure 5.6 below for four different diffusion processes. Hence Figure 5.1 and 5.2 depict the arrangement of demec gauge points through the depth of the prism to measure the shrinkage strain along its depth and total deformation of the prismatic specimens for one and two direction moisture

diffusion processes. Figure 5.3 and 5.5 shown the demec gauge points arrangement for measuring the shrinkage strain at three different points of the prism along its depth for three and four direction moisture diffusion processes respectively. In Figure 5.4 and 5.6, it can be seen that the arrangement of demec gauge points to measure the shrinkage strain along the width at three different locations of the prism for three and four diffusion moisture diffusion processes respectively.

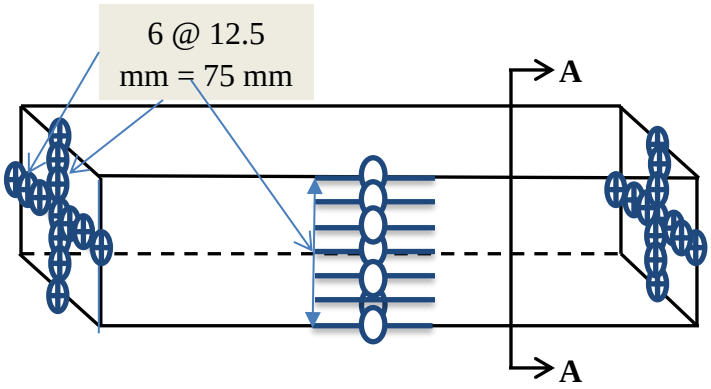

75×75×1200 mm

Section A-A
75×75 mm

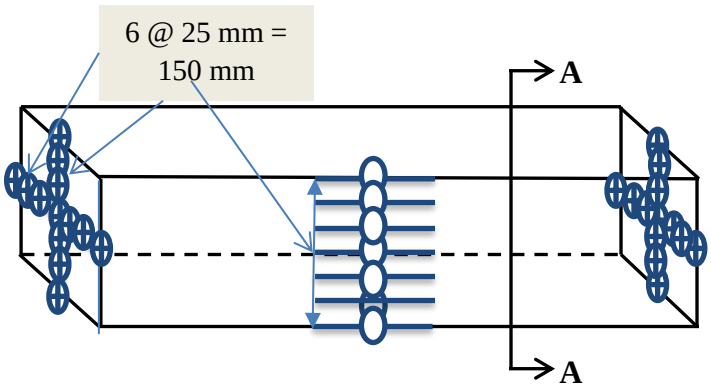

150×150×1200 mm

Section A-A
150×150 mm

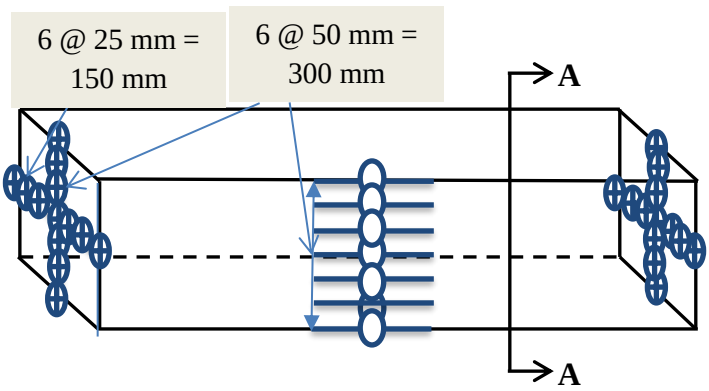

150×300×1200 mm

Section A-A
150×300 mm

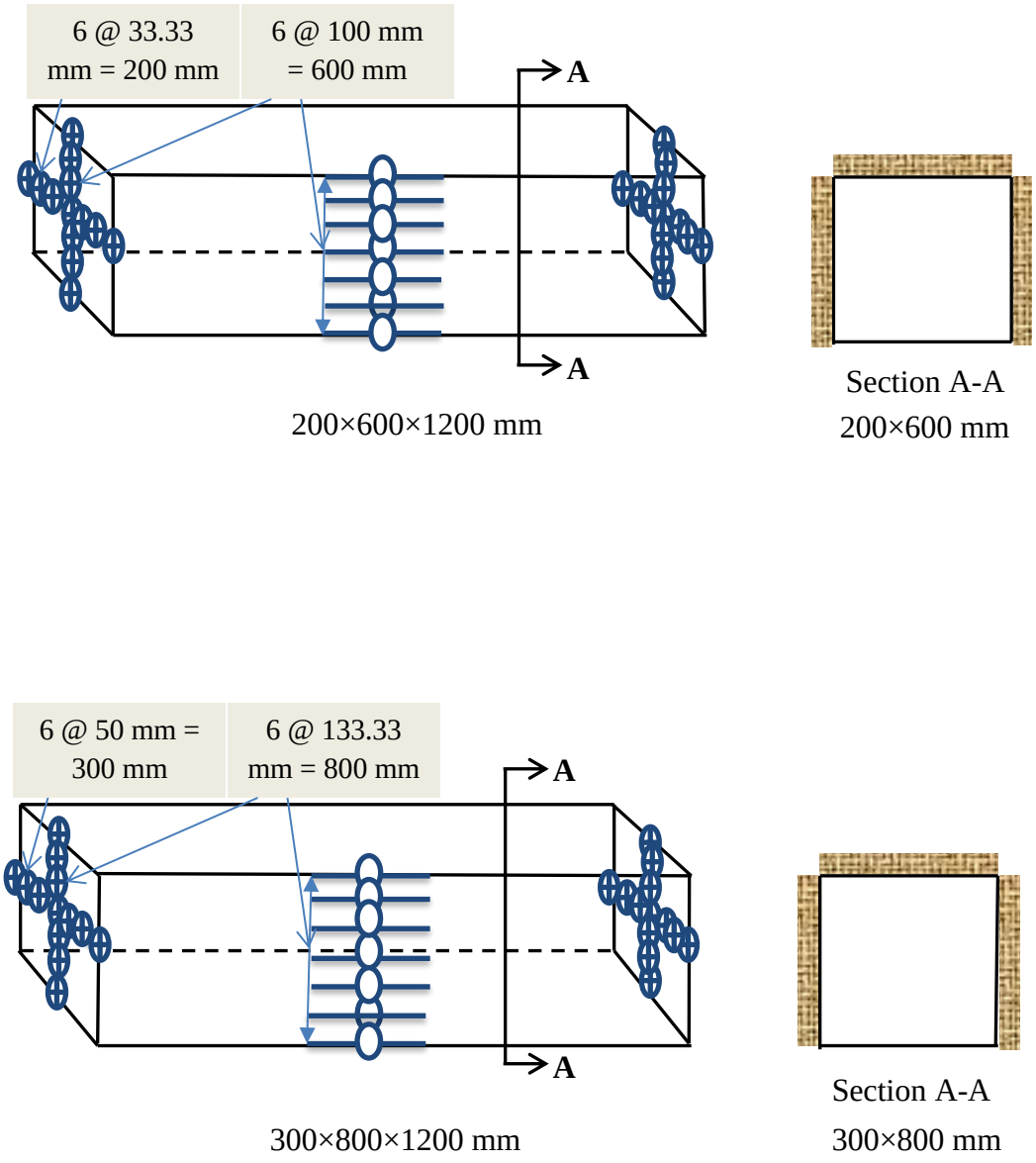

Figure 5.1: Arrangements of demec gauge points along the depth at front (shown only) and rear surfaces and at both ends through the depth as well as width of the prism for measurements of shrinkage strains and total deformations of the prisms in one direction moisture diffusion process

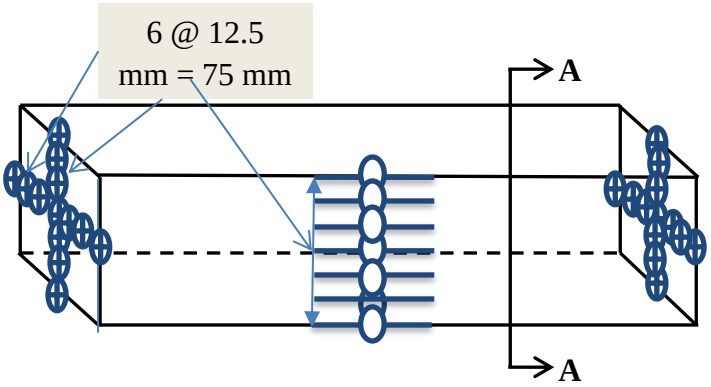

75×75×1200 mm

Section A-A
75×75 mm

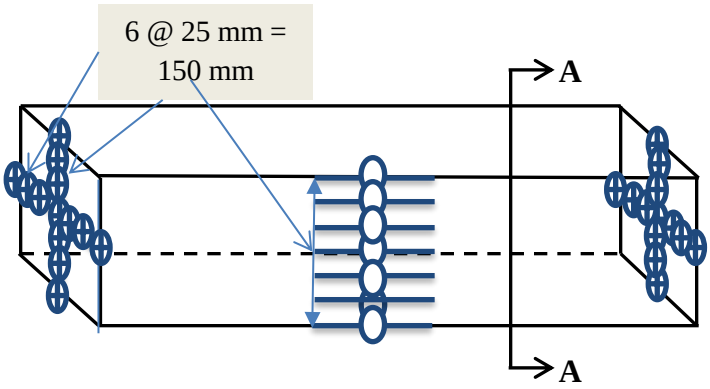

150×150×1200 mm

Section A-A
150×150 mm

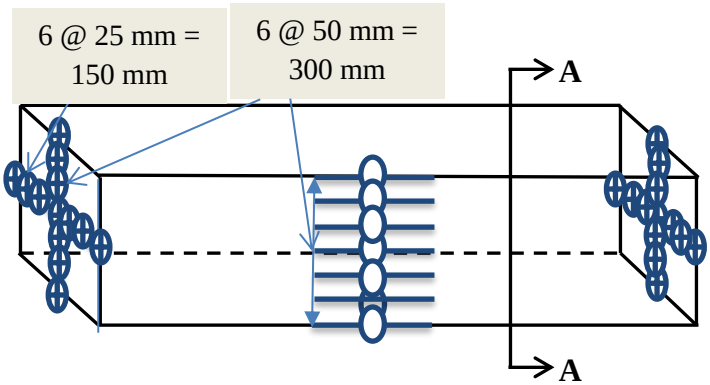

150×300×1200 mm

Section A-A
150×300 mm

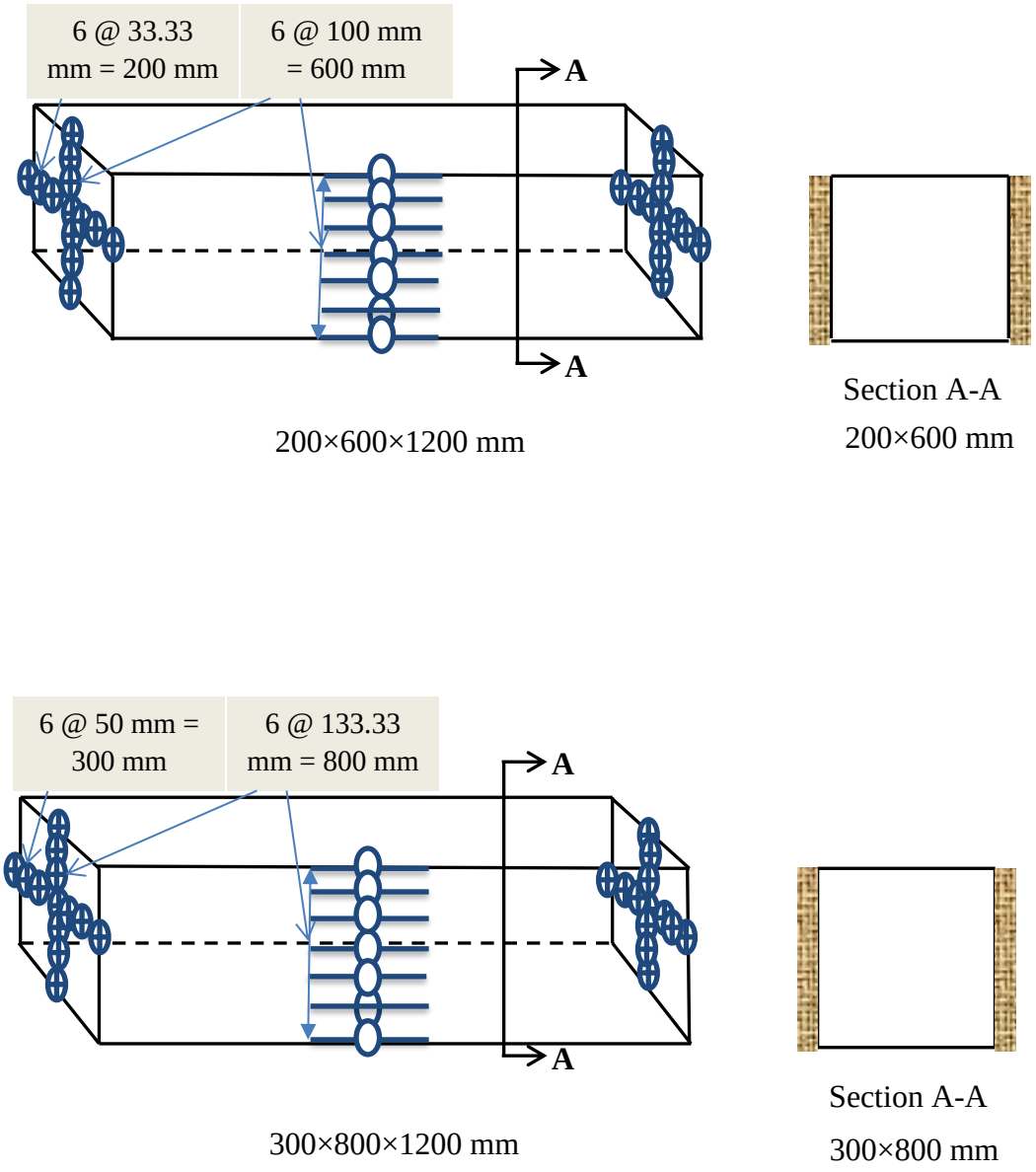

Figure 5.2: Arrangements of demec gauge points along the depth at front (shown only) and rear surfaces of the prisms and at both ends through the depth as well as width of the prisms for measurements of shrinkage strains and total deformations of the prisms in two direction moisture diffusion processes

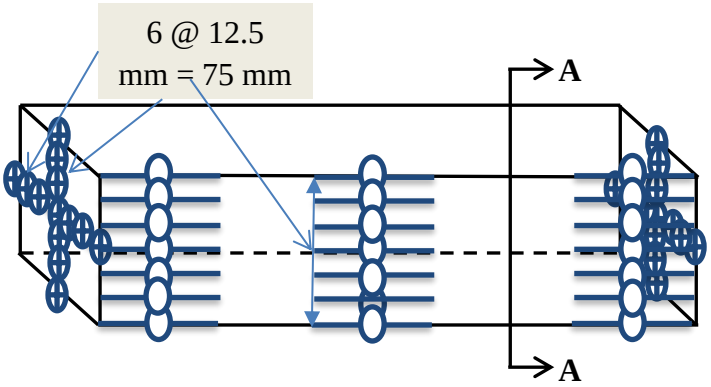

75×75×1200 mm

Section A-A
75×75 mm

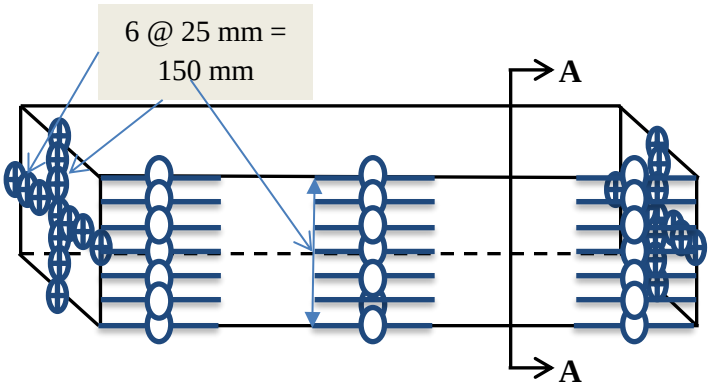

150×150×1200 mm

Section A-A
150×150 mm

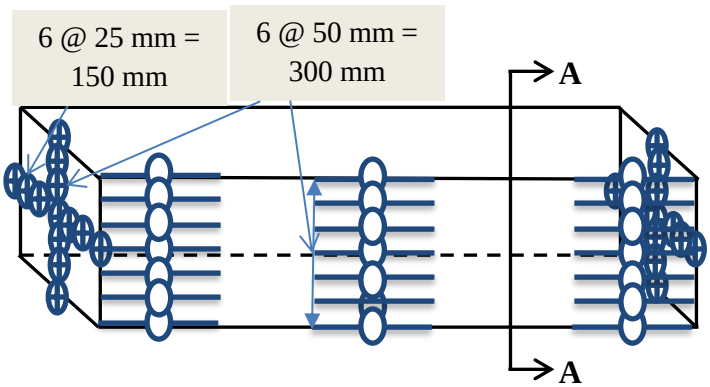

150×300×1200 mm

Section A-A
150×300 mm

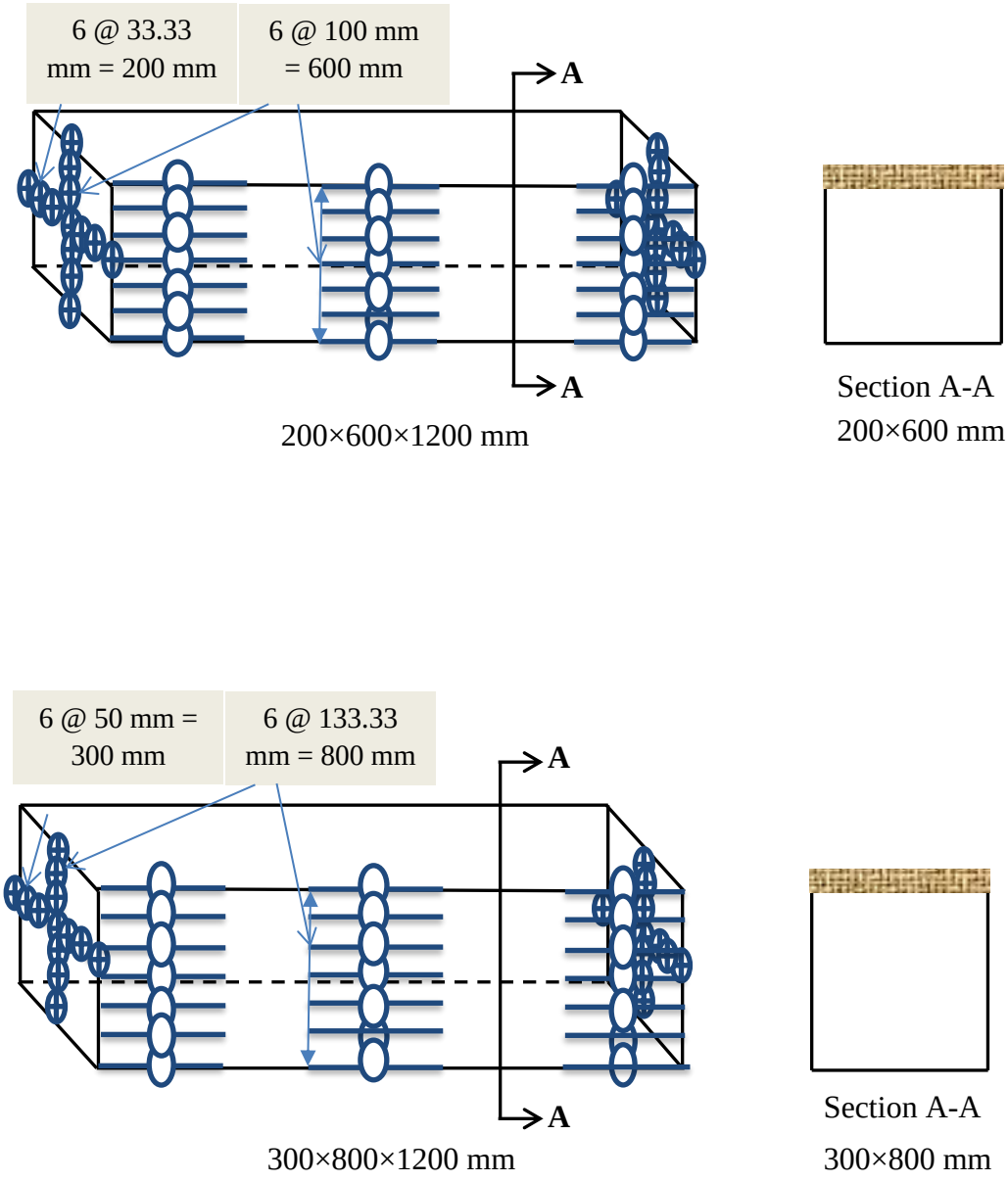

Figure 5.3: Arrangements of demec gauge points along the depth at front (shown only) and rear surfaces of the prisms and at both ends through the depth as well as width of the prisms for measurements of shrinkage strains along its depth and total deformations of the prisms in three direction moisture diffusion processes

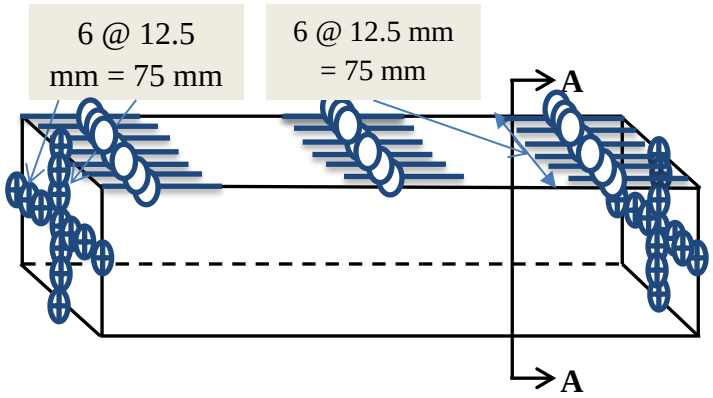

75×75×1200 mm

Section A-A
75×75 mm

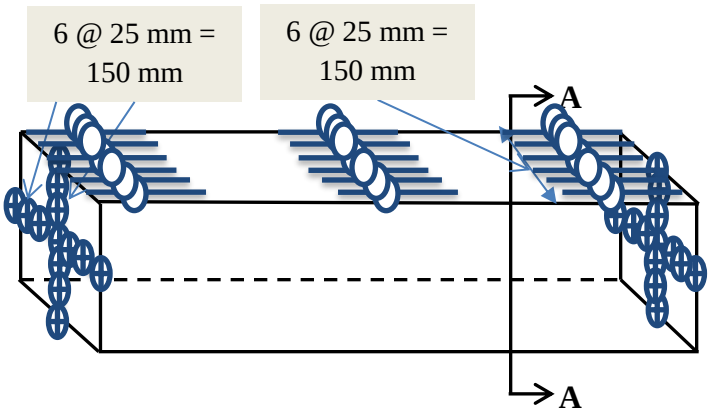

150×150×1200 mm

Section A-A
150×150 mm

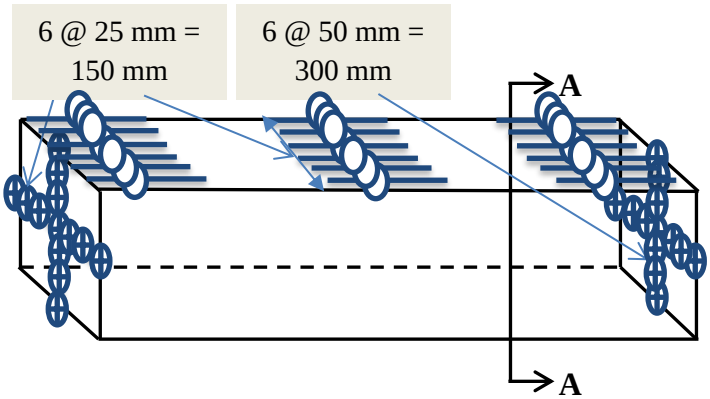

150×300×1200 mm

Section A-A
150×300 mm

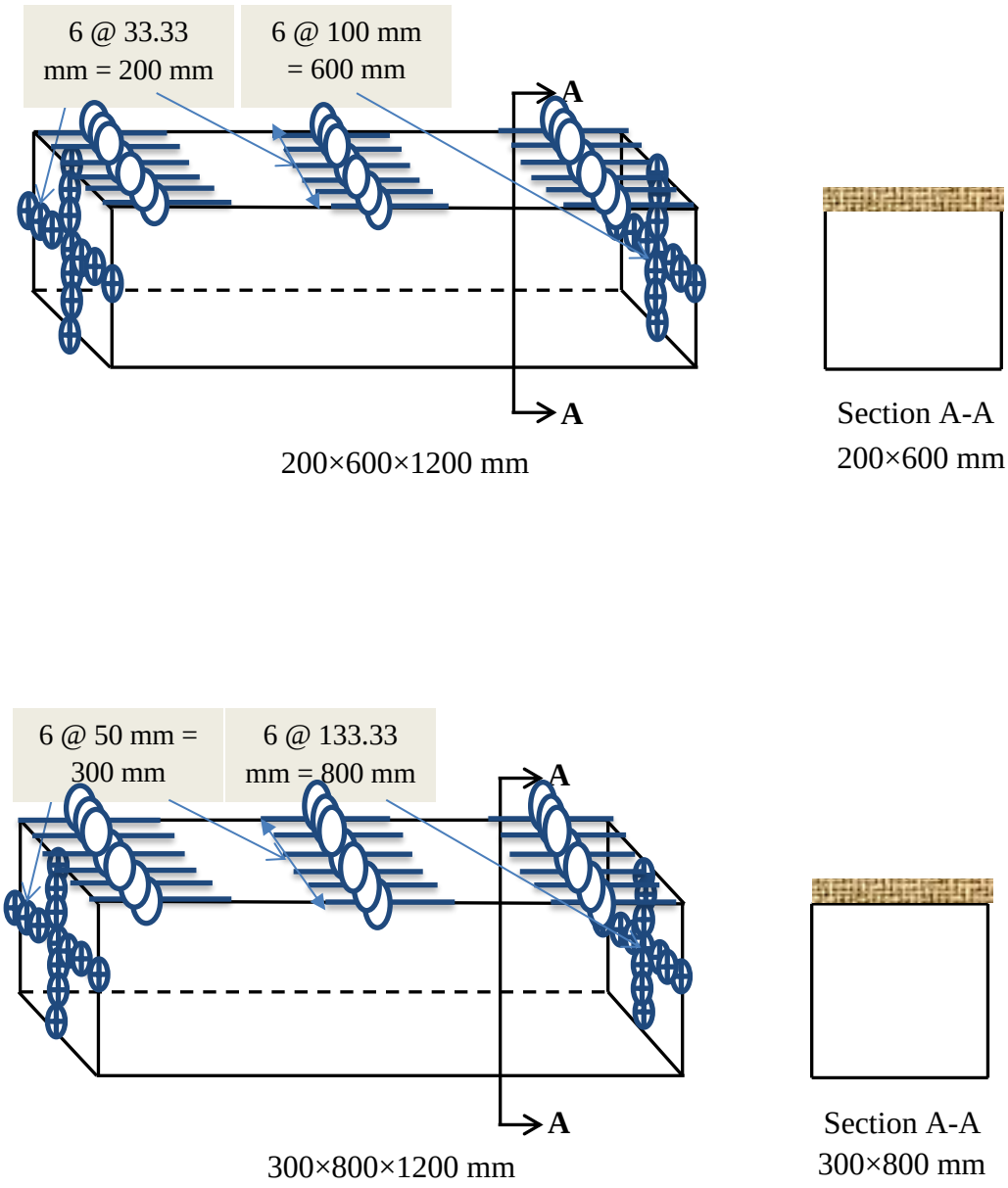

Figure 5.4: Arrangements of demec gauge points along the width at top (shown only) and bottom surfaces of the prisms and at both ends through the depth as well as width of the prisms for measurements of shrinkage strains along its width and total deformations of the prisms in three direction moisture diffusion processes

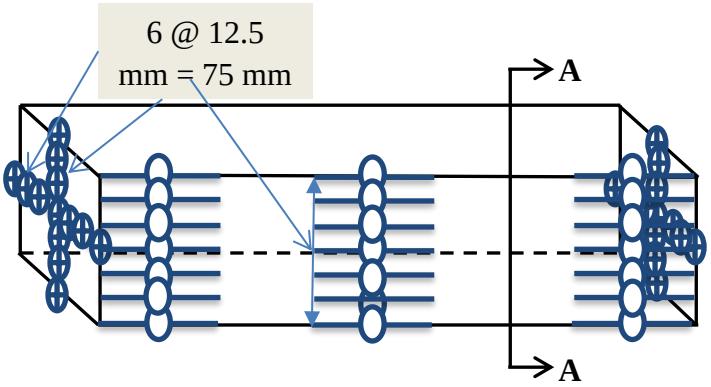

75×75×1200 mm

Section A-A
75×75 mm

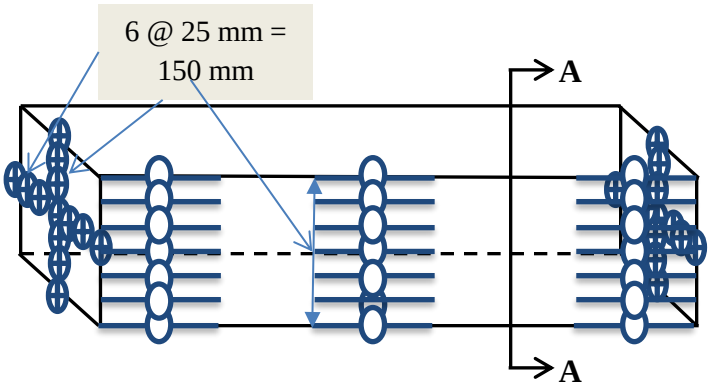

150×150×1200 mm

Section A-A
150×150 mm

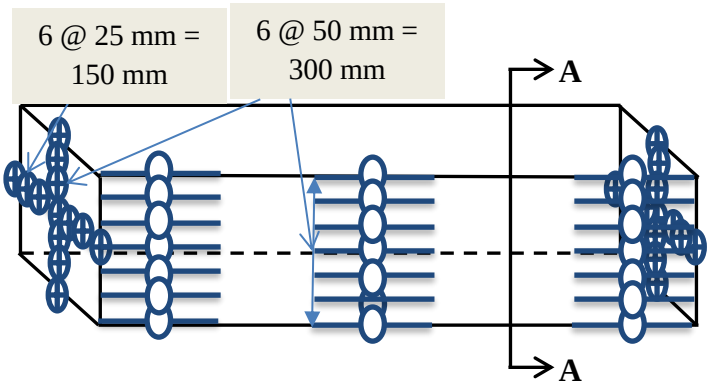

150×300×1200 mm

Section A-A
150×300 mm

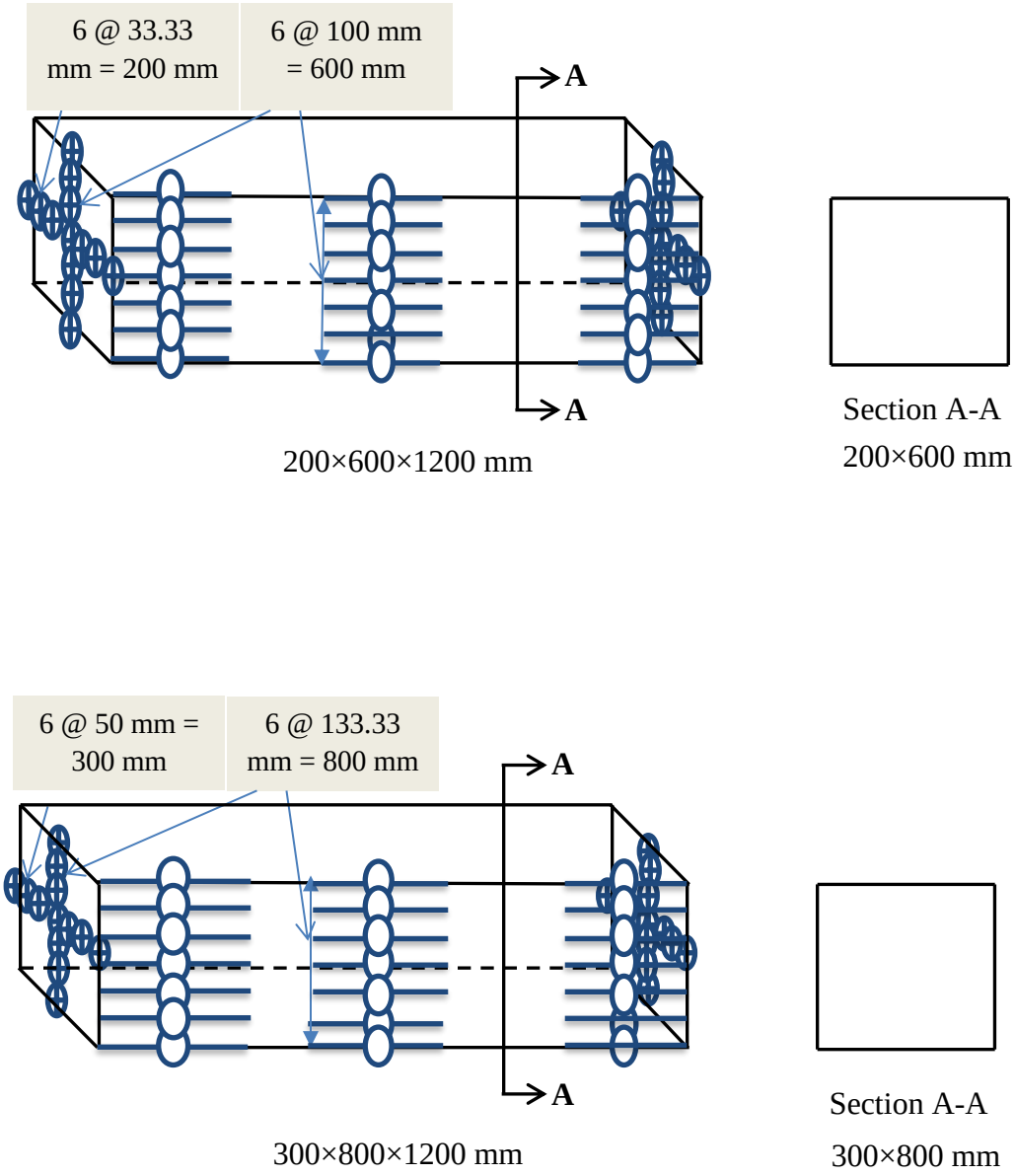

Figure 5.5: Arrangements of demec gauge points along the depth at front (shown only) and rear surfaces of the prisms and at both ends through the depth as well as width of the prisms for measurements of shrinkage strains along its depth and total deformations of the prisms in four direction moisture diffusion processes

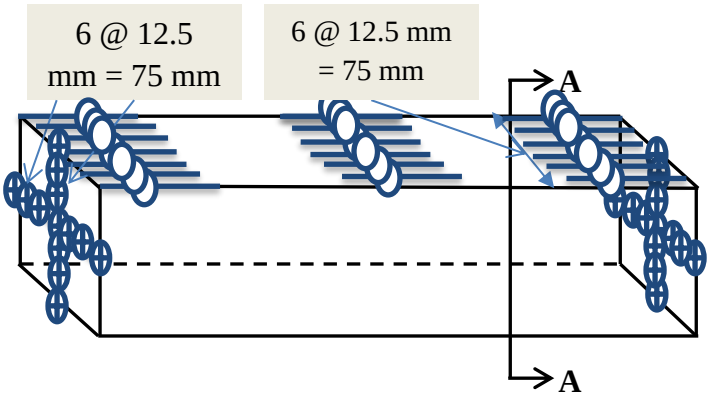

75×75×1200 mm

Section A-A
75×75 mm

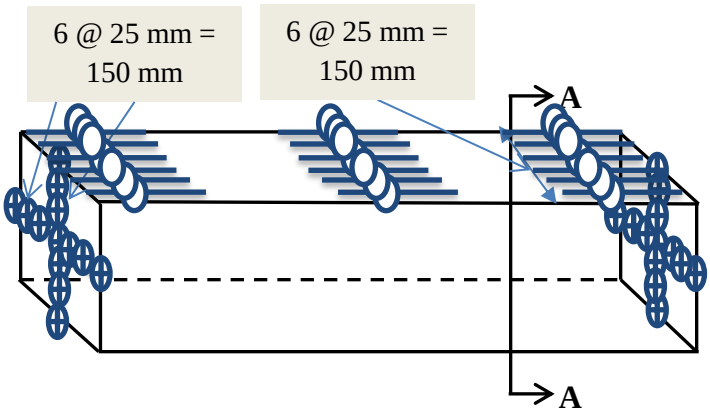

150×150×1200 mm

Section A-A
150×150 mm

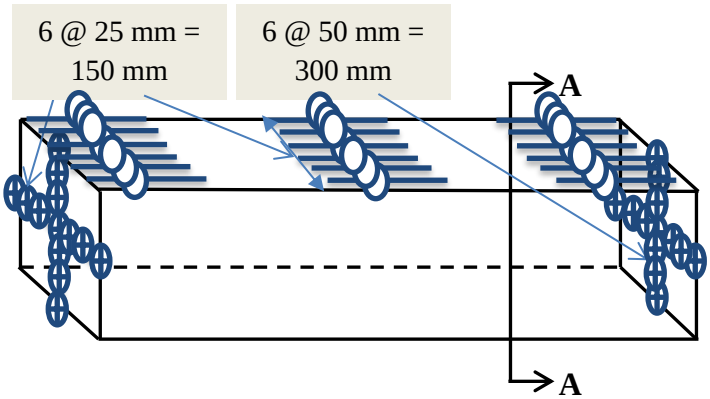

150×300×1200 mm

Section A-A
150×300 mm

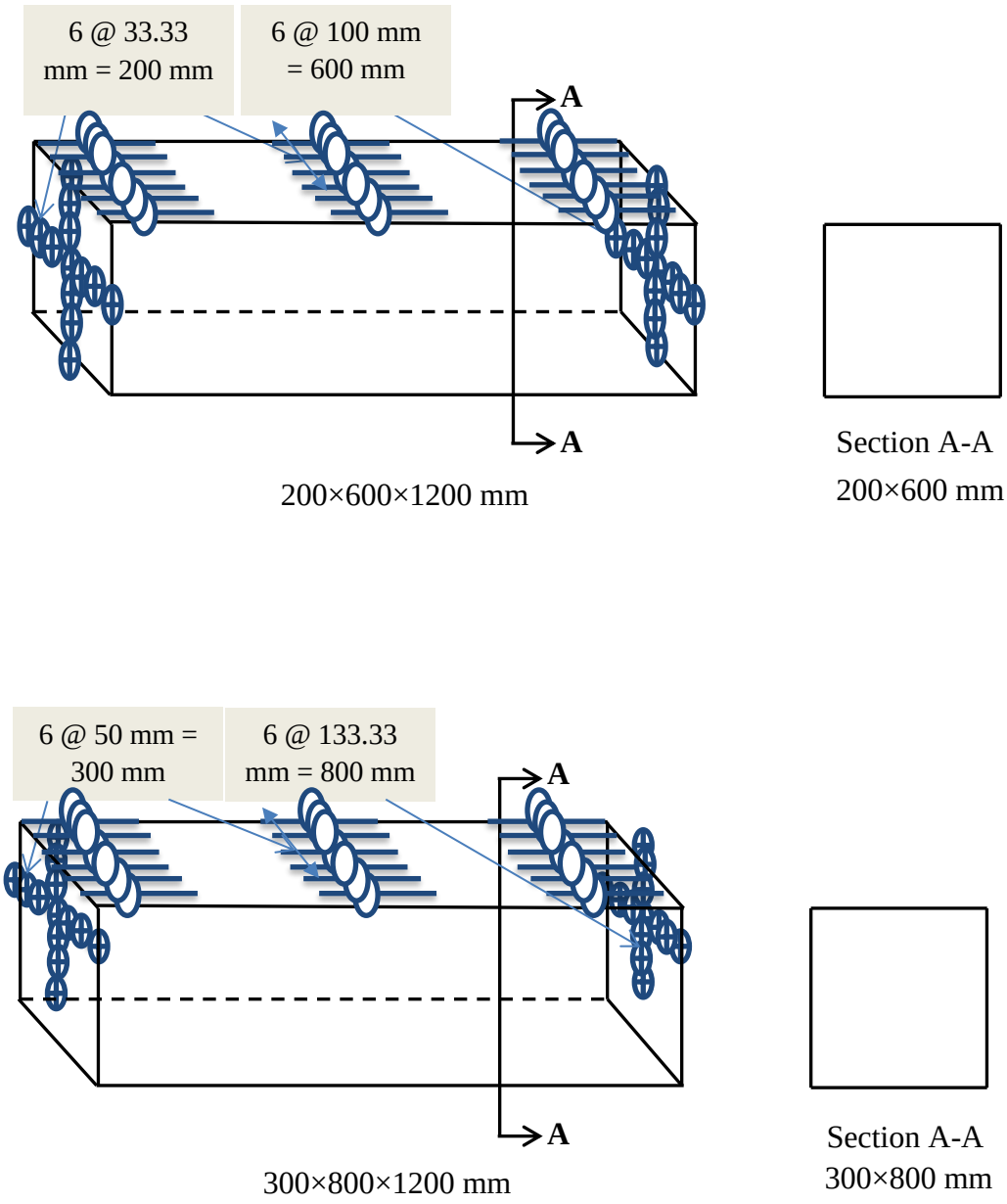

Figure 5.6: Arrangements of demec gauge points along the width at top (shown only) and bottom surfaces of the prisms and at both ends through the depth as well as width of the prisms for measurements of shrinkage strains along its width and total deformations of the prisms in four direction moisture diffusion processes

5.7 Concluding remarks

Current test methodology of shrinkage has major limitations and which are outlined below:

1) Specimen sizes are very small (75 mm ×75 mm × 280 mm according to AS 1012.8.4:2015) compare to the real sizes of RC members which provide uniformity of shrinkage strains and that does not happen in practice and all these issues are also reported in ACI 209R-92 (1992).
2) It also considers the specimens are exposed in all surfaces which are not always present in practice.

The proposed test setup will provide the better estimations of shrinkage strain for various sizes of concrete prism specimens according to its volume over exposed surface area ratios (V/S). It also benefits the size variations starting from 75 mm ×75 mm × 1200 mm to 300 mm × 800 mm ×1200 mm and measurement of shrinkage strains in terms of one up to four different exposed surface conditions to correlate with real sizes in appropriate exposed condition of RC members. However non-linear shrinkage strains will be achieved from these experimental test results that normally happens in practice and could be utilised for long term analysis of RC members.

Chapter 6 Long term Beam Deflection using Segmental Approach

6.1 Introduction

This chapter deals with the development of a sophisticated numerical segmental approach to quantify the long term deflection of RC beams. Prior to flexural cracking, the deflection of an RC beam can be derived from strain based approaches, such as the use of flexural rigidities or moment-curvature, and it is fairly straightforward to incorporate constant values of shrinkage (Visintin, Oehlers et al. 2013). This approach can be used to predict the formation of an initial flexural crack, however once the initial flexural crack occurs then the behaviour is governed by tension-stiffening as this partial-interaction behaviour controls the crack spacing and crack widths that have a major effect on the deflection (Oehlers, Mohamed Ali et al. 2011, Visintin, Oehlers et al. 2012, Visintin, Oehlers et al. 2013).

Previous research has allowed for the incorporation of a constant shrinkage strain into a partial interaction analysis, that is an analysis where the longitudinal shrinkage strain that is constant along both the depth and width of the member (Visintin, Oehlers et al. 2013). While the assumption of a constant shrinkage strain is convenient for numerical analysis, tests have shown that the shrinkage strain does vary along the depth and width of the member (Terrill, Richardson et al. 1986, Mu and Forth 2009, Gilbert, Bradford et al. 2012). The main purpose of this study is therefore to develop a numerical procedure that allows for non-linear shrinkage strains which normally happens in practice and also to determine whether a constant shrinkage strain is an adequate design simplification for the non-constant shrinkage strains that can occur in practice.

A partial-interaction segmental numerical model is first described. It is then shown how this model can be adapted to allow for variations in the shrinkage strain along the depth and width of the member. A standard diffusion analysis (Kim and Lee 1998, Kim and Lee 1999, Kang, Kim et al. 2011) described in Chapter 4 is then used to quantify the variations in the shrinkage strains within beams for known diffusion coefficients. It is also shown in Chapter 4 how these diffusion coefficients (Bažant and Najjar 1971, CEB-FIP 1990) can be achieved from CEB FIP model code 1990 using concrete material properties. The analyses are then used to simulate test specimens of six RC beams under sustained load up to 400 days tested by Gilbert and Nejadi (2004) and the predicted results provided good correlation with experimental test results.

6.2 Partial interaction segmental analysis

The partial interaction (PI) moment rotation (M/θ) segmental analysis (Oehlers, Mohamed Ali et al. 2011, Visintin, Oehlers et al. 2012, Visintin, Oehlers et al. 2013) of a segment of a beam is illustrated in Figure 6.1a on a segment of the crack spacing $S_{cr} = 2L_{def}$ and which is extracted from a beam having total length of L >> d (depth of beam) or b (width of beam) such that Euler-Bernoulli beam theory applies.

For analysis a constant moment of M_{seg} is applied to the beam which causes the ends of the segment in Figure 6.1a rotate θ from A-A to B-B at each crack faces. The segment is symmetrical along C-C and symmetrically assigned moment of M_{seg} and thereby both ends rotate θ such that by symmetry only half of the segment needs to be considered only for analysis as in Figure 6.2a.

Let us now consider the segmental analysis to be performed prior to flexural cracking of the beam under the application of constant sustained load/ moment of M_{seg}.

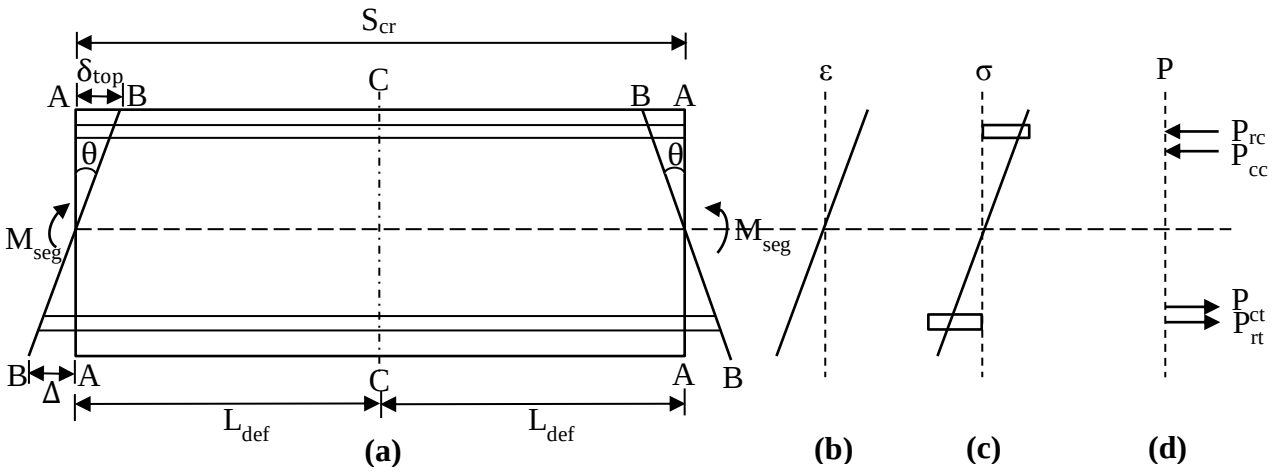

Figure 6.1: A standard multi-crack segmental analysis

6.3 Prior to cracking segmental analysis

The left half portion of the segment shown in Figure 6.2a and Figure 6.3a below depict the separation of RC beams with concrete and reinforcement element respectively prior to cracking for segmental analysis been performed. Left half segment length of L_{def} in Figure 6.2a rotate from A-A to B-B with an amount of rotation θ which causes deformation of δ_{top} at top fibre of the concrete by inducing a constant moment of M_{seg}. This deformation profile can be converted to a strain profile as shown in Figure 6.2b by dividing the δ_{top} with deformation length of L_{def} and these are real strains which can be measured by attaching strain gauges on the member body. By achieving the strain distribution in the segment, the stress profile shown in Figure 6.2c can also be determined using any conventional material stress-strain relationship as because these are real strains and eventually can be determined internal forces as displayed in Figure 6.2d of the member. After determining all the internal forces, the top deformation of the concrete fibre δ_{top} can be varied for a fixed rotation value of θ which adjusts the neutral axis depth until equilibrium of internal forces is achieved. The same procedure as described above need

to be applied to Figure 6.3a to achieve the strain, stress and force profile as shown in Figure 6.3b, Figure 6.3c and Figure 6.3d respectively bearing in mind to keep exactly the same top deformation of the concrete fibre δ_{top} for a fixed rotation of θ in both cases.

By achieving the equilibrium of internal forces that is the sum of forces in both Figure 6.2d and 6.3d sum to zero and it provides a single point in Figure 6.4a moment rotation (M/θ) curve and the procedure is repeated by increasing rotations until concrete strain reaches to its flexural tensile cracking strain and the crack tip reaches the tensile reinforcement which leads to be plotted the moment rotation curve up to the uncracked portion. This crack can be initiated anywhere along the beam and where the moment exceeds the cracking moment of the beam element. After achieving the uncracked portion of moment rotation (M/θ) curve as shown in Figure 6.4a, this iteration process is repeated with increasing rotations until reaches the serviceability limit.

The moment rotation (M/θ) relationship in Figure 6.4a can be converted into the traditional moment curvature (M/χ) relationship by dividing with deformation length L_{def} as shown in Figure 6.4b and both of them are identical for uncracked segments but for cracked element moment rotation (M/θ) allows the partial interaction (PI) tension stiffening mechanism for calculating the forces at the tensile reinforcement whereas conventional moment curvature (M/χ) relationship uses full interaction (FI) in between reinforcement and surrounding concrete. Hence, the moment rotation (M/θ) approach shown in Figure 6.4a converted to moment curvature (M/χ)

as shown in Figure 6.4b and the secant stiffness's of the moment curvature (M/χ) are EI as displayed in Figure 6.4c. Hence integrating the curvatures in the beam from Figure 6.4b gives the deflections.

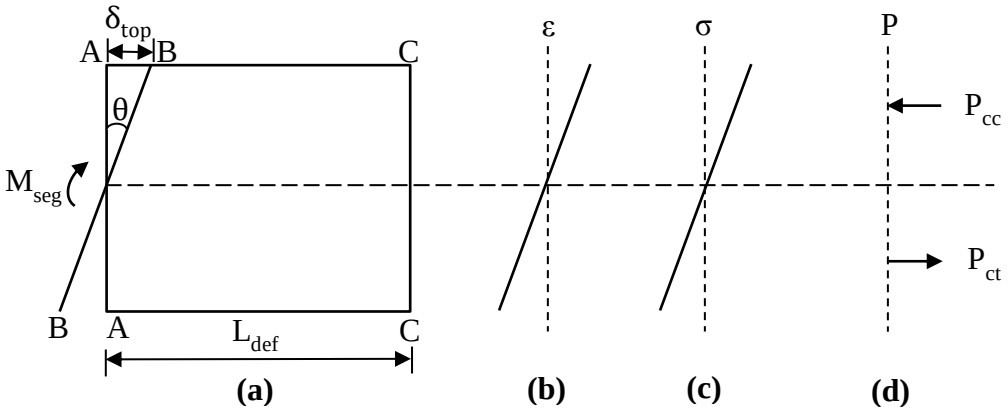

Figure 6.2: Separating elements of RC beam (Concrete element)

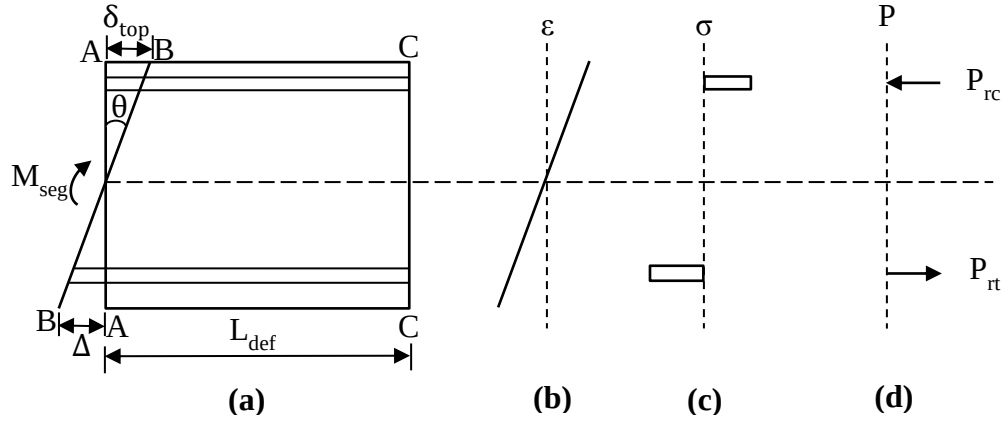

Figure 6.3: Separating elements of RC beam (Reinforcement element)

6.4 Accommodation of cracking in the segmental approach

Let us now considering the crack tip is just above the tension reinforcement and when M_{seg} exceeds the cracking moment (M_{cr}) and that follows the cross-section of left hand segment of Figure 6.1a for single concrete element and which is strain based moment curvature (M/χ) approach that is full interaction (FI) in between reinforcement and

concrete. If when the crack tip goes above, tension stiffening takes over and is shown in Figure 6.5a for multi concrete element. At this stage, partial interaction theory must be used to describe the behaviour of the tensile reinforcement and the crack formation as because the load developed in the reinforcement bar is now dependent on the slip of the bar, Δ at the crack face which in turn depends on the bond slip (τ/δ) properties between the reinforcing bars and the concrete surrounding it (Muhamad, Ali et al. 2011, Visintin, Oehlers et al. 2012, Visintin, Oehlers et al. 2013, Visintin, Oehlers et al. 2013). The partial interaction load slip behaviour can be determined through the well-established numerical technique (Haskett, Oehlers et al. 2008, Oehlers, Mohamed Ali et al. 2011) and will be described in the next section of this chapter. This analysis procedure as described above can be readily expanded for multi-concrete element by slicing the member into n number of slices shown here up to four slices along its width and which can be seen in Figure 6.5a represents the multi-concrete element after tension stiffening mechanism is named as partial interaction (PI) moment rotation (M/θ) approach will be discussed briefly in the next section of this chapter.

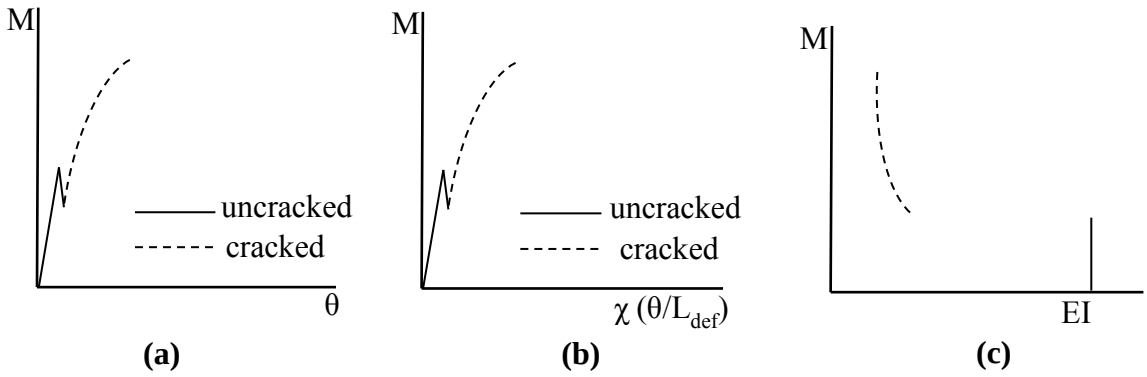

Figure 6.4: Flexural properties (M/θ, M/χ and M/EI)

6.5 Partial interaction tension stiffening model

The segment shown in Figure 6.5b is required to allow for partial interaction tension stiffening (Visintin, Oehlers et al. 2013, Knight, Visintin et al. 2015) and in this case, the length of the segment $2L_{def}$ is equal to the flexural crack spacing S_{cr}. Furthermore, it is common practice to allow for tension stiffening through the use of axially loaded RC prisms (Knight, Visintin et al. 2013) as shown where the depth of the prism $2d_{rt}$ is twice the cover to the tension reinforcing bar from the tension face. The mean shrinkage strain within each prism ε_{shn} in Figure 6.5a is determined from the results of a diffusion analysis discussed in Chapter 4 that is the mean shrinkage within the depth $2d_{rt}$.

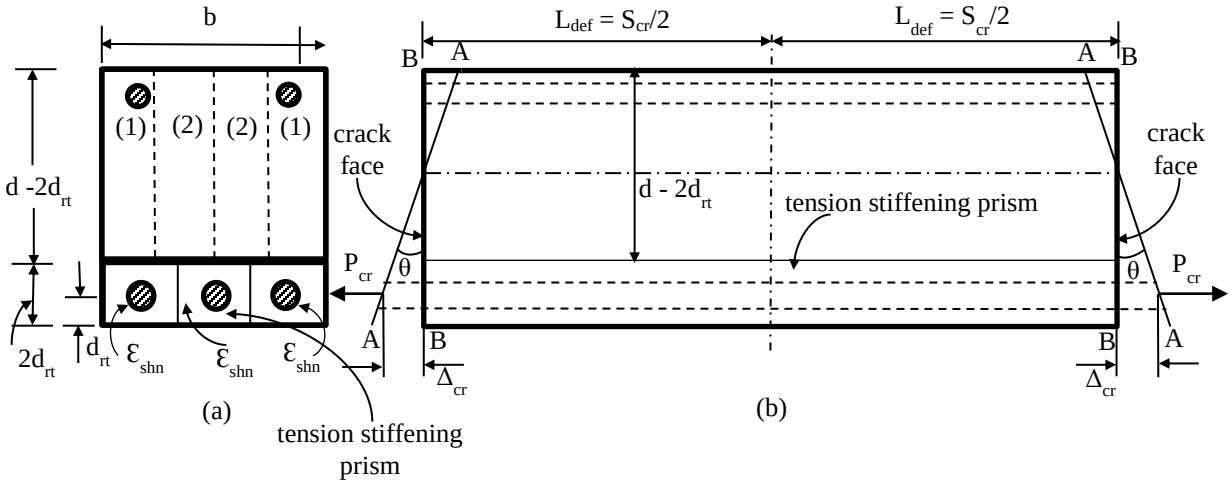

Figure 6.5: Cracked segmental analysis

Consider the tension stiffening prism in the segment in Figure 6.5b, half the length of which L_{def} is shown by itself in Figure 6.6b and the prism is divided into x segments of a very short length L_s that is $L_s << L_{def}$,to understand the mechanics behind the tension stiffening model. The cross section is shown in Figure 6.6a where the perimeter length of the interface between the reinforcement and adjacent concrete is L_{per} and the bond-slip

properties (τ_b-δ_b), that is the relationship between the interface bond shear stress τ_b and interface bond slip δ_b, control the behaviour across this interface of area $L_{per}L_s$. For an example, if the bond stress between the reinforcement and adjacent concrete is τ_b such that the slip is δ_b, then the bond force B over the segment length is $\tau_b L_{per} L_s$ and the bond stiffness is τ_b/δ_b.

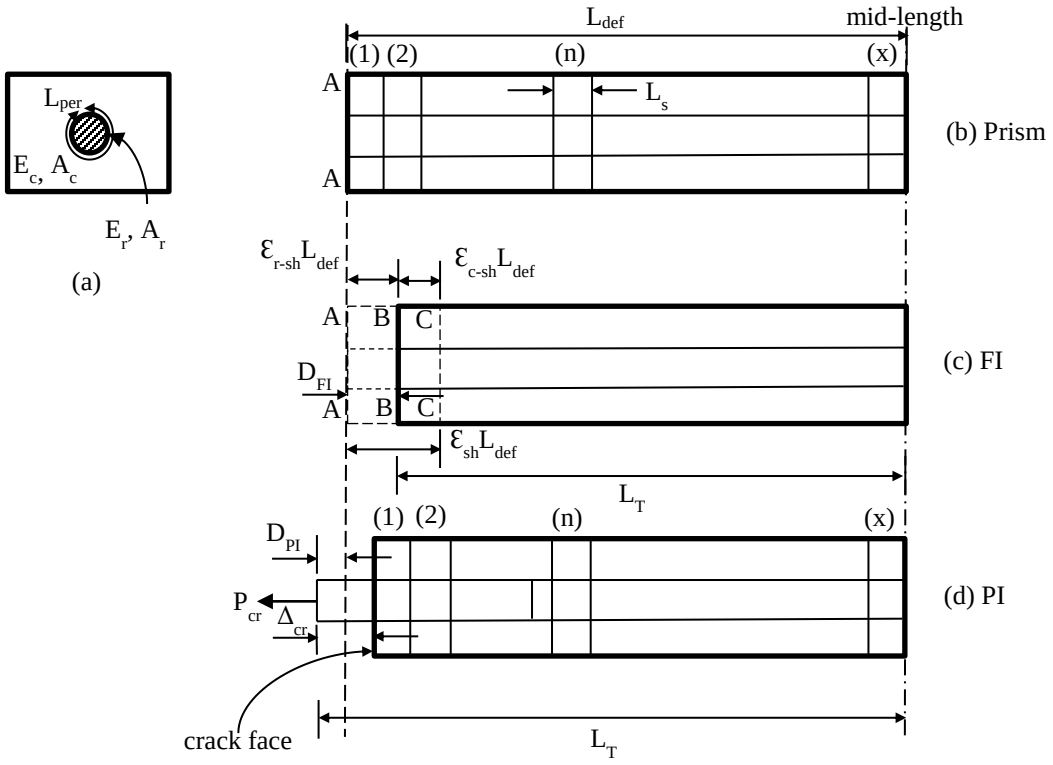

Figure 6.6: Tension stiffening prism

First consider the FI case where the bond stiffness τ_b/δ_b is infinite which is shown in Figure 6.6c and in which the concrete shrinkage strain is ε_{sh}. If there were no bond, that is no restraint from the reinforcement, then the concrete face which was originally at A-A in Figure 6.6b would shrink by $\varepsilon_{sh}L_{def}$, that is slip relative to the reinforcement $\varepsilon_{sh}L_{def}$, to C-C in Figure 6.6c as shown. However, an infinite bond stiffness prevents interface slip such that the concrete and reinforcement face B-B lies between the unstressed face of the

reinforcement A-A and the unstressed face of the concrete C-C. Applying equilibrium and compatibility (Visintin, Oehlers et al. 2013), it can be shown that the residual compressive strain in the reinforcement due to shrinkage is given by

$$\varepsilon_{r-sh} = \frac{\varepsilon_{sh}}{1+\frac{E_r A_r}{E_c A_c}} \qquad \text{Equation 6.1}$$

where: E_rA_r is the axial rigidity of the reinforcement; E_cA_c the axial rigidity of the concrete prism; the shrinkage strain is taken as positive; and tensile strains are also taken as positive. From compatibility in Figure 6.6c, it can be shown (Visintin, Oehlers et al. 2013) that the residual tensile strain in the concrete due to shrinkage is

$$\varepsilon_{c-sh} = \varepsilon_{sh} - \varepsilon_{r-sh} \qquad \text{Equation 6.2}$$

Furthermore, the displacement of the reinforcement face relative to its original position whilst there is FI as shown in Figure 6.6c is given by

$$D_{FI} = L_T - L_{def} = \varepsilon_{r-sh} L_{def} \qquad \text{Equation 6.3}$$

in which D_{FI} is negative when in contraction.

Now consider the effect of PI that is slip between the reinforcement and concrete as illustrated in Figure 6.6d. The n^{th} segment in Figure 6.6b which is also shown in Figure 6.6d is displaying now in Figure 6.7. At the position of the n^{th} segment, the reinforcement force and concrete force to the left of the segment is P_n and C_n respectively, the slip relative to the concrete is Δ_n and the bond force due to this slip Δ_n is B_n. The parameters P_n, C_n and Δ_n depend on the behaviour of the whole prism and will be determined later. As the chosen segment length L_s is very small compared with L_{def}, the mean strains will

be dealt with. The force in the reinforcement to the left P_n reduces due to the bond to P_n-B_n. Hence the mean strain in the reinforcement ε_{rn} is due to the average of the forces P_n and P_n-B_n. Similarly the mean strain in the concrete ε_{cn} is due to the mean of the forces C_n and C_n+B_n.

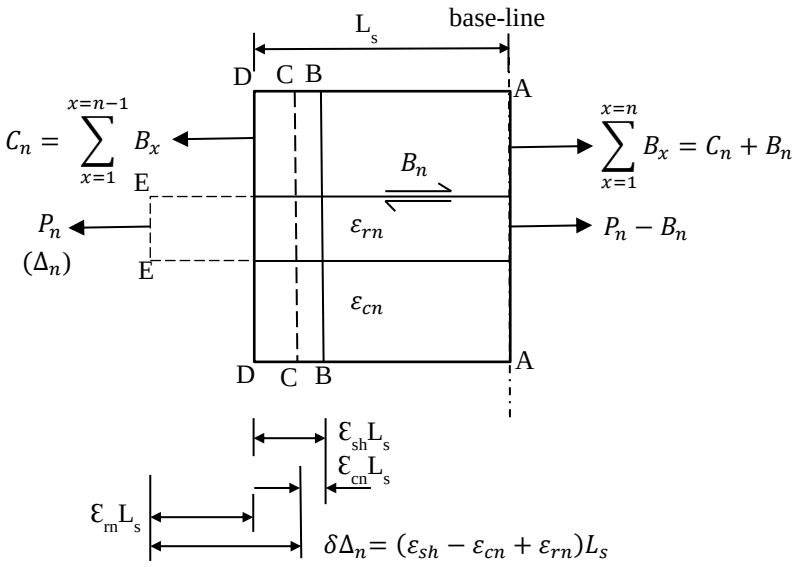

Figure 6.7: Local deformation of n^{th} segment in prism

The concrete shrinkage strain causes the concrete face to displace $\varepsilon_{sh}L_s$ from D-D to B-B as shown in Figure 6.7. The stress in the concrete ε_{cn} increases this by $\varepsilon_{cn}L_s$ as shown to C-C. Similarly the strain in the reinforcement ε_{rn} increases it by $\varepsilon_{rn}L_s$ to E-E as shown. Hence the increase in the slip in the n^{th} segment is given by the following in which the term in brackets is often referred to as the slip strain dΔ/dx.

$$\delta\Delta_n = (\varepsilon_{sh} - \varepsilon_{cn} + \varepsilon_{rn})L_s \qquad \text{Equation 6.4}$$

The application of the analysis depicted in Figure 6.7 to the first two segments in Figure 6.6d are shown in Figure 6.8. The initial crack is to the left of Segment 1, hence the force

in the concrete on the left hand side C is zero. Let the force in the reinforcement at the crack be P_{cr} and the slip Δ_{cr} such that the width of the crack w is $2\Delta_{cr}$. From Δ_{cr} and the bond-slip properties τ_b-δ_b can be derived the bond force B_1 as shown in the equations below. Hence the forces on the right of the prism and consequently the material strains ε_{c1} and ε_{r1}, also in the equations below. Finally the slip-strain $d\Delta_1/dx$, and increase in slip of Segment 1 that is $\delta\Delta_1$. The forces on the left hand side of Segment 2 are those already derived on the right hand side of Segment 1. The analysis then follows the same steps as for Segment 1 which are listed below Segment 2 and so on with further segments.

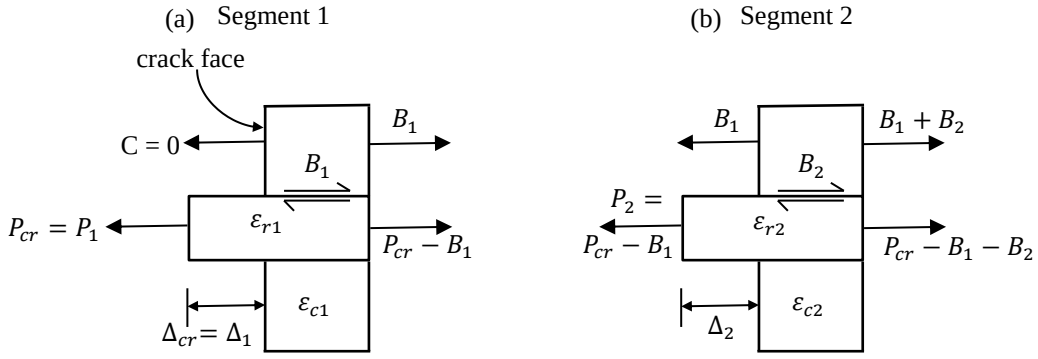

$$\tau_{b1} = fn(\Delta_1)$$

$$B_1 = \tau_{b1} L_{per} L_s$$

$$\varepsilon_{c1} = \frac{0 + B_1}{2A_c E_c}$$

$$\varepsilon_{r1} = \frac{2P_{cr} - B_1}{2A_r E_r}$$

$$d\Delta_1/dx = \varepsilon_{sh} - \varepsilon_{c1} + \varepsilon_{r1}$$

$$\delta\Delta_1 = (d\Delta_1/dx)\, L_s$$

$$\Delta_2 = \Delta_1 + \delta\Delta_1$$
$$= \Delta_{cr} + (\varepsilon_{sh} - \varepsilon_{c1} + \varepsilon_{r1})\, L_s$$

$$\tau_{b2} = fn(\Delta_2)$$

$$B_2 = \tau_{b2} L_{per} L_s$$

$$\varepsilon_{c2} = \frac{2B_1 + B_2}{2A_c E_c}$$

$$\varepsilon_{r2} = \frac{2P_{cr} - 2B_1 - B_2}{2A_r E_r}$$

$$\delta\Delta_2 = (\varepsilon_{sh} - \varepsilon_{c2} + \varepsilon_{r2})\, L_s$$

Figure 6.8: Tension stiffening analysis

An iterative shooting method is used to find a solution. The first case to consider is when only the initial crack has occurred from the analysis of the uncracked segment in Figure

6.3. Hence there is only one crack on the left hand side of the prism in Figure 6.6d. For a given force P_1 in Figure 6.8a, an estimated slip Δ_1 is chosen. At each segment, the slip Δ_n and the slip-strain $d\Delta_1/dx$ are derived. It is a question of finding the x_{th} element where FI occurs which in this case is that the slip is zero and the slip-strain is $\varepsilon_{r\text{-}sh}$-$\varepsilon_{c\text{-}sh}$, which can be derived from Equations 6.1 and 6.2, is also zero. The estimate Δ_1 is varied until this occurs. Once this boundary condition is achieved the position of the x_{th} segment is the first primary crack spacing $S_{cr\text{-}pr}$. When the concrete strain in this x^{th} segment ε_{cx} reaches the concrete strain capacity ε_{ct}, the reinforcement force to cause primary cracks $P_{cr\text{-}pr}$.

Having formed primary cracks at known spacings $S_{cr\text{-}pr}$, this is used in a tension stiffening analysis in which L_{def} in Figure 6.6 is equal to $S_{cr\text{-}pr}/2$ to determine the tension stiffening behaviour between primary cracks. The analysis depicted in Figure 6.6 still applies except that the boundary condition is no longer that for FI but instead that at mid-length, that is $S_{cr\text{-}pr}/2$ from the crack faces, the slip is zero. This analysis gives the relationship between P_{cr} and Δ_{cr} in Figure 6.6d, that is the crack opening stiffness P_{cr}/Δ_{cr} required for the segmental analysis. Furthermore it gives the reinforcement force to cause secondary cracks $P_{cr\text{-}sec}$ that is when ε_c is equal to ε_{ct} should they occur and if so an analysis with a prism length of $S_{cr\text{-}pr}/4$ gives the behaviour in regions where there are secondary cracks.

It can be seen in Figure 6.7 and Equation 6.4, that the shrinkage strain ε_{sh} causes a more rapid build up of slip and therefore bond force, so that shrinkage will reduce the crack spacings and also the reinforcement force to cause cracking.

6.6 Partial-interaction segmental model

After flexural cracking from the segmental analysis in Figure 6.3, the properties of the beam within the cracked regions are determined from a segmental analysis of a segment between two adjacent cracks as shown in Figure 6.5.

Starting with primary cracks, the length of the segment in Figure 6.5 is $S_{cr\text{-}pr}$ which is obtained from the above tension stiffening analysis and which allows for the effects of shrinkage. Euler-Bernoulli deformations A-A are applied. Within the tension stiffening region of depth $2d_{rt}$, the force in the tensile reinforcement P_{cr} is now determined from Δ_{rt} that is from the crack opening stiffness P_{rt}-Δ_{rt} also previously obtained from the tension stiffening analysis and which also allows for shrinkage within the tension stiffening region. For the region of depth d-$2d_{rt}$ above the tension stiffening analysis, the segmental analysis follows that depicted in Figure 6.1 except that flexural cracking of the concrete can occur at ε_{ct} that is the progression of a flexural crack tip can continue. When the force in the reinforcement is $P_{cr\text{-}pr}$ that was obtained from the above tension stiffening analysis, this gives the moment to cause primary cracks $M_{cr\text{-}pr}$. Hence the moment to cause primary cracks is the lesser of $M_{cr\text{-}pr}$ and $M_{cr\text{-}in}$ (Visintin, Oehlers et al. 2013) as both can occur in a FI region. When the force in the reinforcement in Figure 6.5 reaches $P_{cr\text{-}sec}$, this gives the moment to cause secondary cracks $M_{cr\text{-}sec}$ should they occur. Hence in regions of the beam where $M_{cr\text{-}sec}$ is exceeded both primary and secondary cracks occur where the crack spacing is now $S_{cr\text{-}pr}/2$.

The analysis in Figure 6.5 can be used to derive the M/θ at serviceability loads in members with non-linear shrinkage strains not only along the depth of the beam d but also along the width of the beam b. Dividing the rotations by L_{def} gives the equivalent M/χ; this is

not an approximation in mechanics terms but in mechanics terms an exact solution that directly copes with variations in shrinkage. The equivalent M/χ can then be used in the analysis of a loaded beam to determine its deflection and can cope with any shape of beam, any cross-section properties, any environmental conditions and any surface conditions.

6.7 Constant longitudinal shrinkage along depth and width

The M/θ approach can be applied to the cracked section in Figure 6.9a after having defined the tension stiffening behaviour using partial interaction theory (PI) with incorporation of shrinkage strain as stated above. L_{def} in this Figure 6.9a will be equal to half of the crack spacing ($S_{cr\text{-}p}/2$) in regions where primary cracks take place and in regions where secondary cracks occur will be equal to $S_{cr\text{-}p}/4$. Figures 6.9 and 6.10 below represent the concrete and reinforcement element separately from left half portion of Figure 6.1a where a constant shrinkage strain ε_{sh} is been applied to the segment along both depth and width of the member and that causes a reduction of length of concrete with an amount of $\varepsilon_{sh}L_{def}$ from A-A to A´-A´ in concrete element and this shortening in length would not induce a stress. Hence any deformation would take place away from A´-A´ induces a stress in the concrete and therefore, A´-A´ becomes the baseline for the concrete to induce stresses in concrete element for any further deformation from A´-A´. Hence also from Figure 6.10a, it can be seen that there is no contraction of reinforcement due to an applied constant shrinkage strain ε_{sh} and so the baseline of reinforcement remain unchanged at A-A. Hence there will be two neutral axis depth one for concrete and another one for reinforcement due to have two base line with the effect of shrinkage strain ε_{sh}.

Let us now consider a moment M_{seg} is been applied to the segment and sustained for some period of time, t to cause a total rotation of θ with the combined effect of shrinkage ε_{sh}

and applied moment M_{seg}. This rotation θ induces a deformation δ_{top} from A-A to B-B and the same analysis outlined above for the case of without shrinkage is now been applied with shrinkage. Hence the neutral axis of concrete in Figure 6.9a lies in between the intersection of new base line of concrete A´-A´ and B-B and for the reinforcement the neutral axis is in between the intersection of A-A and B-B as shown in Figure 6.10a measured from top or bottom fibre of member.

However, in this case the rotation θ can be varied until the resulting moment M_{seg} is been achieved and hence the longitudinal equilibrium in both Figures 6.9d and 6.10d should be at zero whilst the rotational equilibrium requires a moment of M_{seg}. An alternative approach would be to fix the rotation θ and varying the top deformation δ_{top} until there was longitudinal equilibrium of forces in Figures 6.9d and 6.10d and after that the moment could be taken for that imposed or fixed rotation θ. The analysis is exactly similar to the Figures 6.2a and 6.3a until the concrete is uncracked but when the crack tip reaches above the tension reinforcement partial interaction theory would be applied at the tension stiffening zone to determine the load developed at the reinforcing bar P_{rt} in Figure 6.3d based on the total length of the reinforcement L_T and where L_T in Figure 6.6a can be determined from simple geometry and also explained in the previous section of this chapter. Hence, the analysis in Figure 6.9a and 6.10a can be applied for increasing rotations θ to determine the moment rotation relationship in Figure 6.4a with the effect of constant longitudinal shrinkage strain along depth and width of the member.

The moment rotation M/θ relationship with the incorporation of constant longitudinal shrinkage strain along the member achieved from the analysis can be converted to an equivalent moment curvature M/χ relationship by dividing by the deformation length L_{def}

as shown in Figure 6.4b and these results can be used to derive the variation of equivalent flexural rigidity EI_{equ} of the member with moment as represented in Figure 6.4c. Moreover, the variation of these equivalent flexural rigidities (EI_{equ}) that are been derived from partial interaction PI moment rotation M/θ approach are different from those that are achieved from a standard full interaction FI moment curvature M/χ analysis as because the M/θ approach uses PI theory which incorporates the shrinkage effect to allow for crack formation and widening when crack occurs and eventually it can represent a mechanics based solution to describe the behaviour of cracked concrete which also includes the time effects.

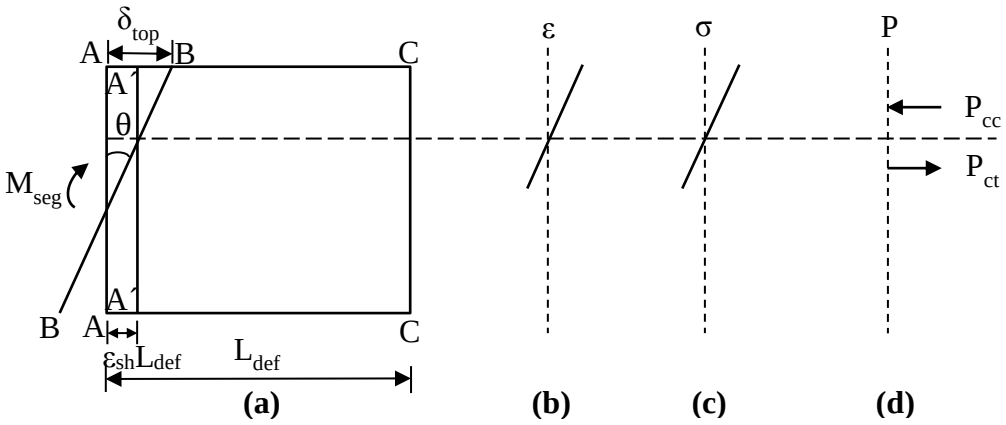

Figure 6.9: Linear shrinkage strain over width and depth (Concrete element)

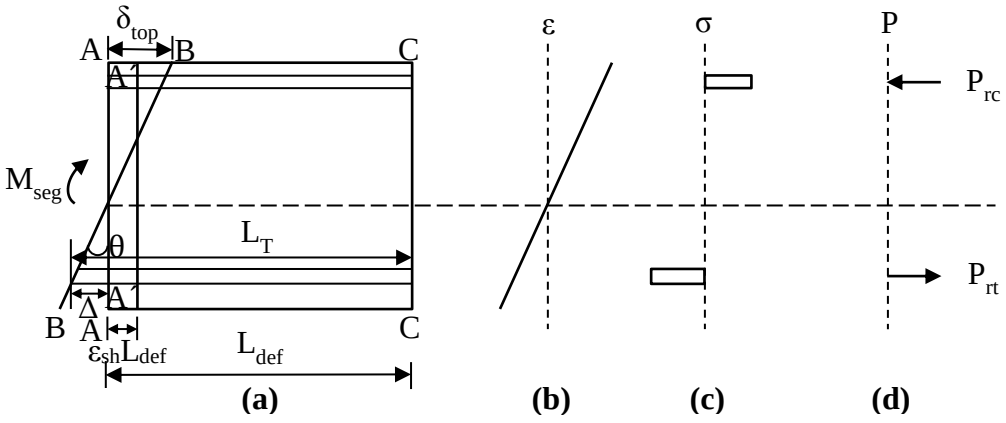

Figure 6.10: Linear shrinkage strain over width and depth (Reinforcement element)

6.8 Variation in longitudinal shrinkage strain along depth

Let us now consider a non-constant shrinkage profile along the depth of the member is been employed and which shown in Figure 6.11a for concrete element and in Figure 6.12a for reinforcement element for cracked member specimens. According to Gilbert's experimental investigation for the composite slab (Gilbert, Bradford et al. 2012) it can be found that shrinkage strain is not constant along the depth of the member, it does vary along the depth and shows nonlinear and non-uniform shape as shown in Figure 6.11a to Figure 6.15a. Furthermore, numerical diffusion model also can predict the nonlinear shrinkage strain profile along the depth and width of the member which is been used in this report for analysis.

As it can be seen from the Figure 6.11a, due to a non-uniform shrinkage strain concrete baseline moved from A-A to A´-A´ with an amount of $\varepsilon_{sh}L_{def}$ where L_{def} is the half of the crack spacing but the reinforcement baseline remains stationary at A-A shown in Figure 6.12a. Hence, for concrete any deformation away from new baseline A´-A´ will induce a stain dividing by length of deformation L_{def} will produce a stress in the concrete and for reinforcement any movement occurs from A-A will cause a strain to stress in the reinforcement bars and so therefore, two strain profiles exist with the application of shrinkage strain in the member one for concrete as shown in Figure 6.11b and another one for reinforcement as shown in Figure 6.12b. Therefore, two neutral axis exist in the analysis one for concrete element (intersection in between A´-A´ and B-B) and other one for reinforcement element (intersection in between A-A and B-B) which can be seen in Figure 6.11a and 6.12a respectively.

An iterative approach would be used for performing the sophisticated segmental analysis by fixing the rotation θ and varying the top deformation δ_{top} until there was longitudinal equilibrium in both Figures 6.11d and 6.12d after which the moment could be taken for that fixed or imposed rotation θ. Therefore, by repeating the analysis for increasing rotations moment rotation relationship shown in Figure 6.4a will be established bearing in mind to apply the partial interaction theory as soon as the crack tip just crosses the tensile reinforcement bars to calculate the load developed at the reinforcement bars P_{rt} as shown in Figure 6.12d. Hence therefore, M/θ can be converted to equivalent M/χ relation as shown in Figure 6.4b by dividing by the deformation length L_{def} and hence can be achieved the M/EI as shown in Figure 6.4c and finally be able to quantify the deflection of a member.

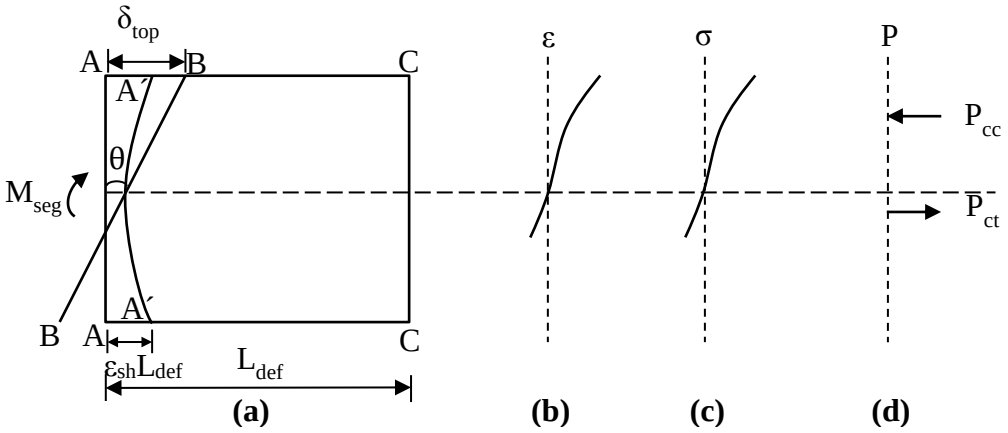

Figure 6.11: Non-linear shrinkage strain over depth (Concrete element)

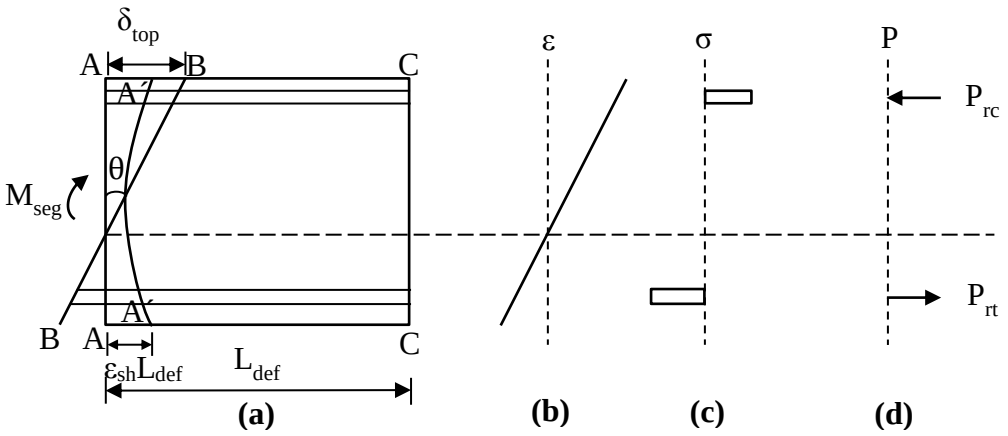

Figure 6.12: Non-linear shrinkage strain over depth (Reinforcement element)

6.9 Variation in longitudinal shrinkage strain along depth and width

Let us now consider the non-constant shrinkage strain were applied along the depth and width of the member as shown in Figure 6.13a to Figure 6.15a. This segmental analysis will also be continued by breaking down into components along the width of the member shown in Figure 6.5a, bearing in mind with applying same rotation and depth of neutral axis to all of the components. The concrete member is sliced up to four components along the width of the specimen having identical shrinkage profile for slices width of b1 and b2 due to symmetry so therefore only half of the member analysis could be performed and is been displayed in Figure 6.13a and 6.14a.

Similar procedure has been discussed earlier for the segmental M/θ approach would be applied for this case, by fixing the rotation θ, guessing the top deformation δ_{top} initially then varying δ_{top} until longitudinal equilibrium is been achieved that is sum up all the forces in Figures 6.13d, 6.14d and 6.15d to zero and after that moment could be taken for that particular imposed or fixed rotation θ. Therefore, by repeating the analysis for increasing rotations, the moment rotation M/θ relationship is established for both cracked

and uncracked conditions but when the concrete is cracked and the crack tip reaches above the tension reinforcement, partial interaction theory is been used to determine the forces developed in the reinforcement bars P_{rt} as shown in Figure 6.15d.

Moreover, it should also be noted that in order to allow for creep a reduced elastic modulus must be used where the magnitude of this reduction can be determined by using any convenient method at the time of calculating stress in the concrete.

Hence the M/θ approach can be converted to an equivalent standard M/χ approach by dividing the deformation length L_{def} and the results according to Figure 6.4b can be used to determine the variation of flexural rigidity EI_{equ} with moment along the member. Both M/θ and M/χ approaches are identical up to uncracked portion so therefore EI_{equ} is similar value of $EI_{uncracked}$ but after cracked it is not the same as because M/θ approach uses partial interaction theory which includes the effect of nonlinear shrinkage strains to allow for crack formation and widening and hence provide a mechanics based solution to explain the behaviour of cracked concrete members including time effects due to shrinkage and creep.

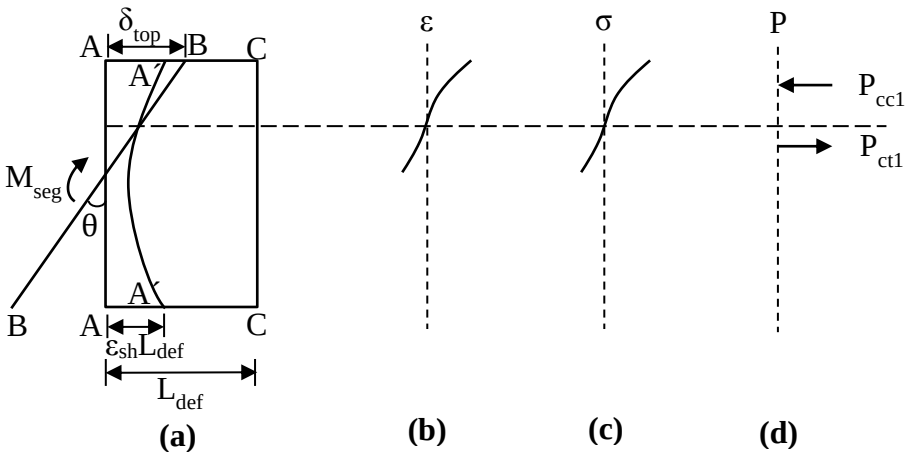

Figure 6.13: Non-linear shrinkage strain over width and depth (Concrete element 2b1)

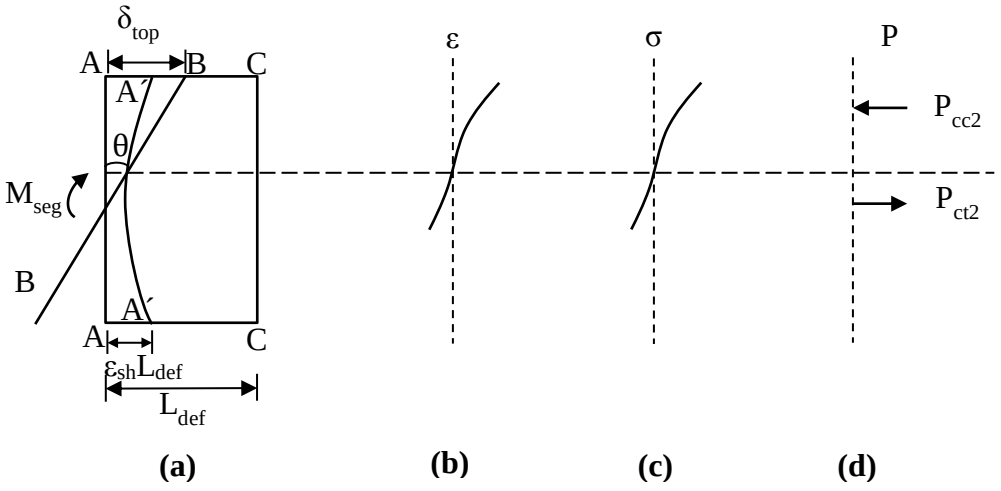

Figure 6.14: Non-linear shrinkage strain over width and depth (Concrete element 2b2)

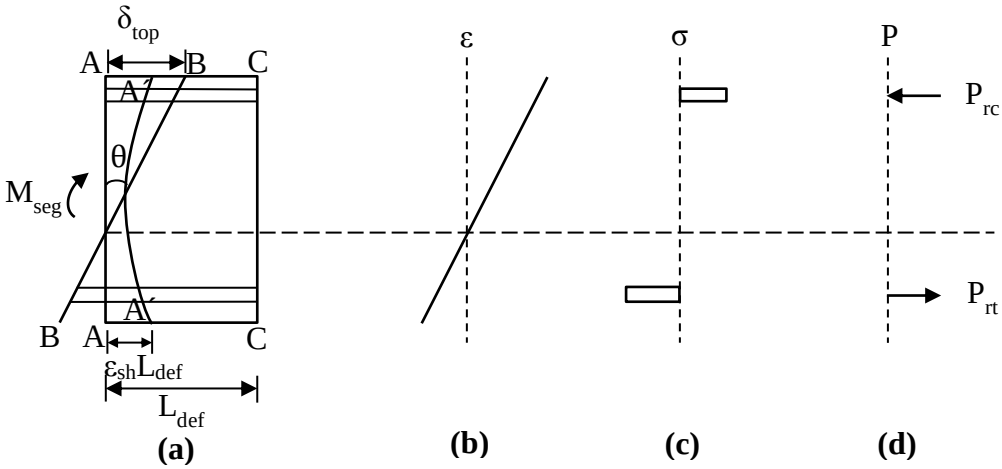

Figure 6.15: Non-linear shrinkage strain over width and depth (Reinforcement element)

6.10 Parametric study

Some material properties need to be defined to apply the moment rotation M/θ segmental analysis and these are not the critical component of the segmental approach and that is why any material models can provide better results could be replaced. The following material models have been used in the parametric study to illuminate the time dependent

behaviour of cracked reinforced concrete members where the effect of both shrinkage and creep need to be considered simultaneously but for this study only shrinkage effect has taken into account. Hence at later stage to simulate with experimental test results (Gilbert and Nejadi 2004), both shrinkage and creep effect have been considered to quantify the deflection of RC beams under sustained loading conditions for a period of 394 days.

The elastic modulus of concrete in a time *t* after first loading at time t_0 at any point can be defined as $E_c(t, t_0)$ and using effective modulus method can be written as

$$E_C(t, t_0) = \frac{E_c(t, t_0)}{1 + \varphi(t, t_0)} \qquad \text{Equation 6.5}$$

Where t_0 is the time at initial loading and φ is the creep coefficient of concrete at time *t* after initial loading at time t_0. According to Gilbert and Ranzi (2011), the change in elastic modulus in concrete due to creep would be applied to both in compression and tension zone of concrete at the segmental analysis for time dependent deformations of the RC members.

A linear elastic stress-strain relationship has been assumed for concrete in tension and for concrete in compression the following parabolic stress distribution by Popovics (1973)

$$\sigma = f_c \frac{\left(\frac{\varepsilon}{\varepsilon_{pk}}\right) r}{r - 1 + \left(\frac{\varepsilon}{\varepsilon_{pk}}\right)^r} \qquad \text{Equation 6.6}$$

Where ε is the concrete strain to cause a stress r is a factor that controls the ductility of the concrete and it is given by $[E_c/ (E_c - f_c/\varepsilon_{pk})]$. ε_{pk} is the strain corresponds to the peak stress, f_c and that has been taken as defined by Chen, Visintin et al. (2013)

$$\varepsilon_{pk} = 4.76 \times 10^{-6} f_c + 2.13 \times 10^{-3} \qquad \text{Equation 6.7}$$

Where f_c is in MPa and the peak strain ε_{pk} must need to be increased according to the reduction of elastic modulus due to creep as defined by Equation 6.5.

Let us investigate the analysis of a simply supported beam B1a having depth = 340 mm, width = 250mm and length = 3500 mm reinforced with 2 No. 16 mm bars with 48 mm cover tested by Gilbert and Nejadi (2004) under sustained loaded with 2 point loading of 18.6 kN for a period of 394 days. The partial interaction PI moment rotation M/θ approach have been used to determine the variations in moment curvature M/χ and moment equivalent flexural rigidities M/EI_{equ} for this beam B1a with consideration of nonlinear shrinkage profile as shown in Chapter 4 of this thesis. Due to the application of sustained point loading, the distribution of moments in the beam can be calculated and hence from the M/EI_{equ} relationship variation in flexural rigidities EI also known. The variation in curvature χ can also be determined by dividing moment M with flexural rigidities EI and then these variations in curvature can be integrated to achieve the member deflection at some point in time and the analysis can be repeated with a new M/EI_{equ} relationship at various points in time. These section properties described above will now be used to analyse the beam B1a by dividing the section along its width into 10, 4 and single slices to show the influence of slices on member deflection with accounting the effect of shrinkage over time. It can be found in Figure 6.16, deflection of the beam increases over time in which 10 slices and 4 slices shown negligible variations in member deflections over time whereas single slice provides the higher estimation with almost constant values after 28 days of loading. Therefore 4 slices would be appropriate consideration for the analysis need to be performed to simulate with experimentally tested six beams by Gilbert and Nejadi (2004) under sustained loading for a period of 394 days.

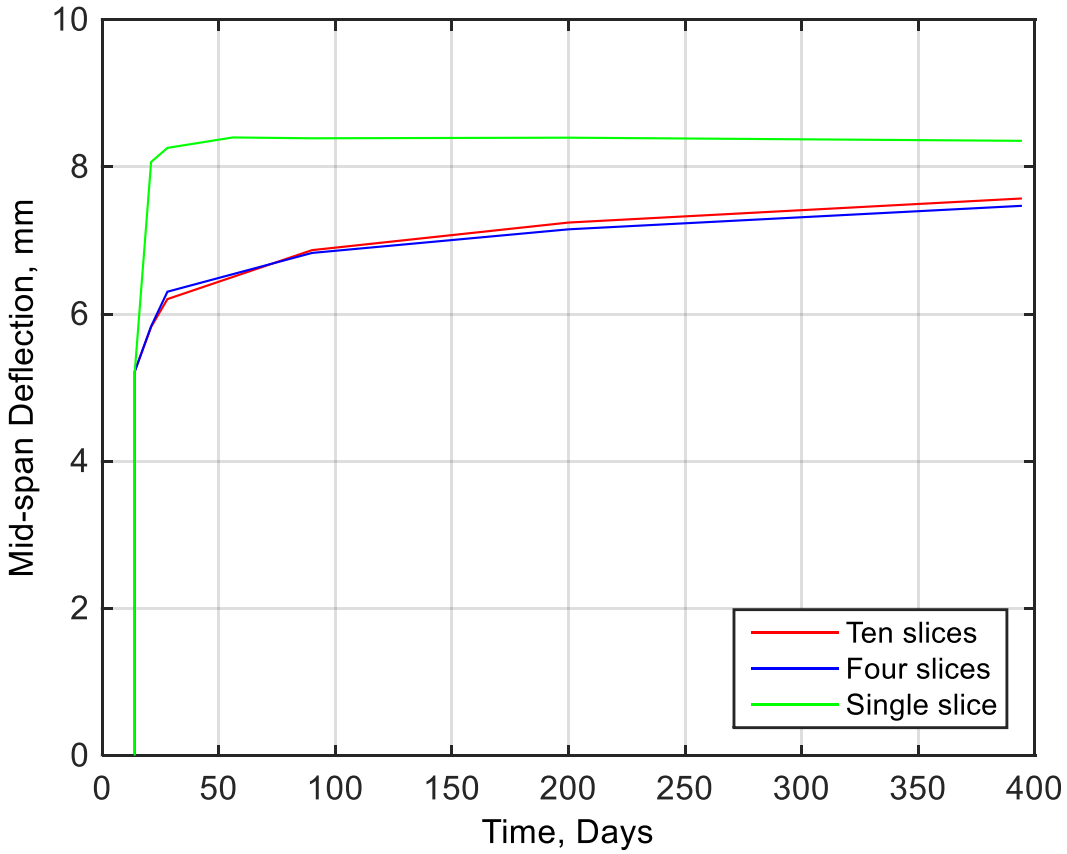

Figure 6.16: Influence of slice number along the width of beam on member deflection

6.11 Application to test specimens

These methods have been applied to a series of six beams tested by Gilbert and Nejadi (2004) in order to validate the partial interaction PI moment rotation M/θ segmental approach on quantifying the deflection of RC beams. There were six simply supported beams having span of 3500 mm with a fixed width of 250 mm and depth varying from 325 to 340 mm under two points at third span point sustained loading conditions varying from 11.8 to 27.0 kN and reinforced with 2 No. 16 to 3 No. 16 mm diameter bars been tested for a period of 394 days. Beams B1a and B1b with having reinforcement of 2 No. 16 mm diameter bars with clear cover of 48 mm, beams B2a and B2b with having

reinforcement of 2 No. 16 mm diameter bars with clear cover of 33 mm and beams B3a and B3b with having reinforcement of 3 No. 16 mm diameter bars with clear cover of 33 mm. All beam specimens were subjected to two concentrated loads located at third span point at an age of 14 days. Beam B1a and B2a were loaded with two point loads of 18.6 kN, Beams B1b and B2b were loaded with two point loads of 11.8 kN, Beam b3a sustained loaded with 27.0 kN and Beam B3b was loaded with 15.2 kN located at third point of the span of the beam. Concrete strength was increased to 24.8 MPa at 28 days after been loaded having strength of 18.3 MPa at an age of 14 days. Creep coefficient was determined periodically through test over the testing period by Gilbert and Nejadi (2004) and concrete strength calculations over time been performed using CEB-FIP (’90) model code. Non-linear shrinkage strain profile shown in Chapter 4 also been determined numerically for each specimen by using finite difference method from diffusion model and that already discussed at earlier stages.

The partial interaction PI moment rotation M/θ approach was used to determine the variations in moment curvature M/χ and moment flexural rigidity M/EI as shown in Figure 6.4 for each of the beam specimens which is then used to quantify the deflections of the experimentally tested six beams. The predicted beam deflections have been simulated with experimental test results and which are represented in Figure 6.17 for beams B1a to B3b. Generally, it can be found that the partial interaction PI moment rotation M/θ segmental approach is able to predict the beams deflections over time reasonably well. Beams B1b, B2b and B3b have shown close agreement with the experimental test results whereas beams B1a, B2a and B3a given some variations in a range below 15% with recorded and predicted results. These could be due to the variations in loading conditions with same cross section of beams in which primary crack spacing considered in the analysis may be

reduced due to its higher loading conditions compare to others. Therefore, it may mean that the stiffness of the cross section reduces as the reduction of primary crack spacing which in turn can provide higher deflections over time.

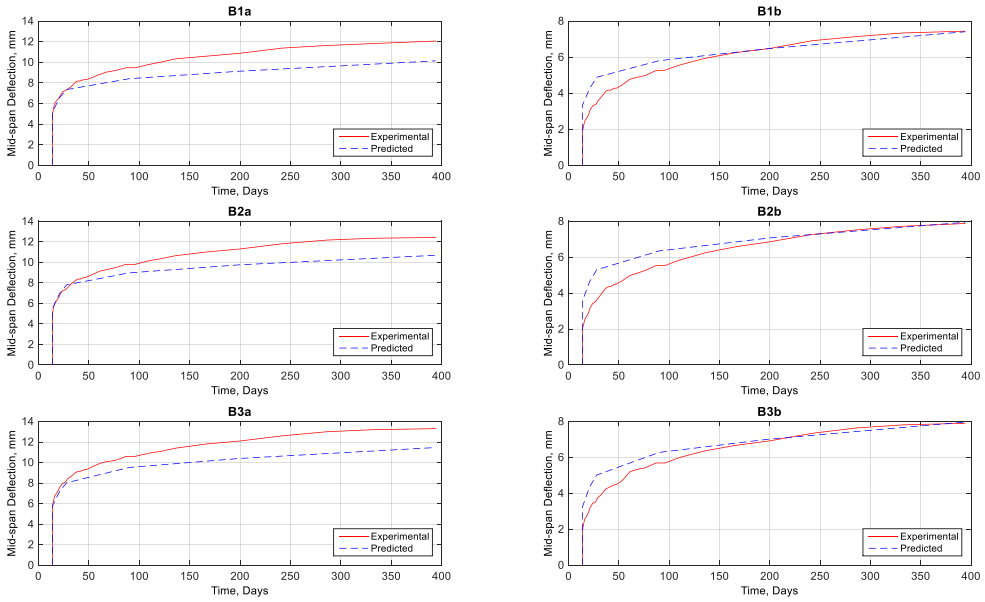

Figure 6.17: Predicted deflection of six beams tested by Gilbert and Nejadi (2004)

In order to show the influence of exposed surfaces on member deflection, the partial interaction PI moment rotation M/θ has also been applied to three way and one way flow in a beam as shown in Chapter 4, to predict the deflections of the beams over time. According to Figure 6.18, it can be found that member deflection is reduced significantly over time as the minimization of exposed surfaces due to the effect of shrinkage strain profile and which is decreasing over time in effect of reduced exposed surface areas.

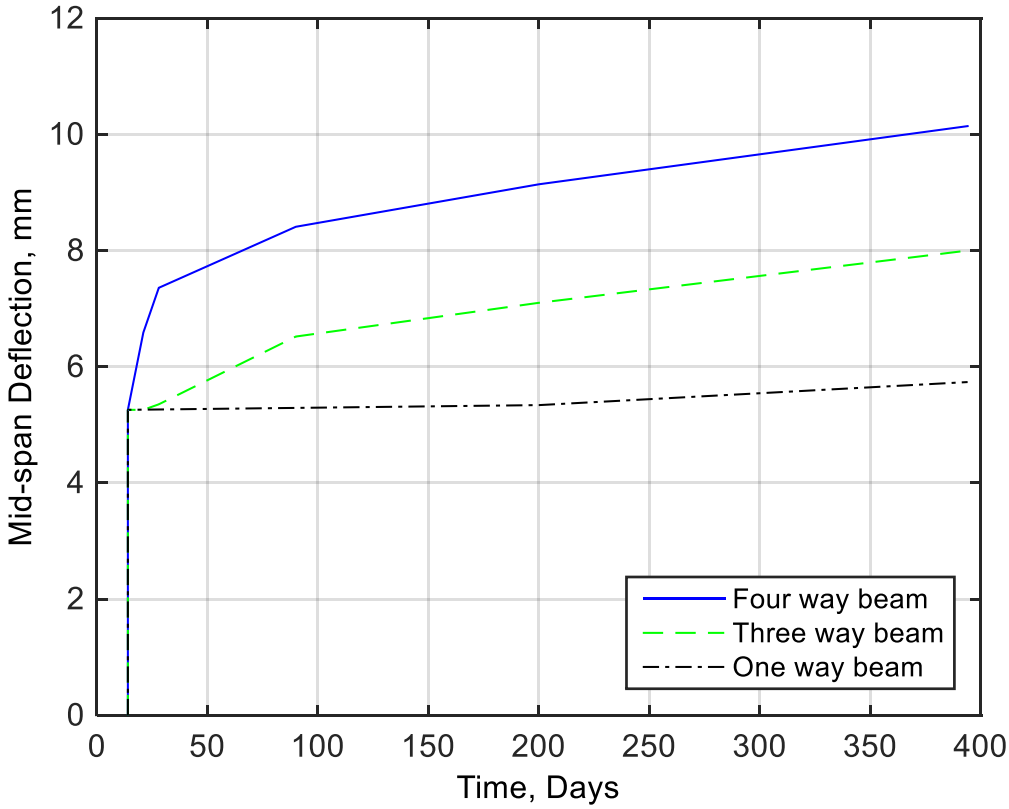

Figure 6.18: Influence of exposed surfaces on member deflection

Chapter 7 Conclusions and Recommendations

The research presented in this thesis covers the development of a complete numerical procedure to quantify the long term deflection of RC members. Significantly, the proposed model simulates the observed non-linear shrinkage strain distribution by considering diffusion of moisture throughout the cross section. Moreover the approach directly simulates the partial interaction mechanism, which is responsible for the formation and widening of cracks as well as tension stiffening and which in this thesis is shown to be highly dependent upon concrete shrinkage.

The major outcomes of this research are:

i) the development of a moisture diffusion model to predict the non-linear variation in shrinkage strain throughout a reinforced concrete

ii) the proposal of a new form of long term experiment to measure the non-linear shrinkage profile within a concrete block.

iii) the development of a sophisticated numerical partial interaction segmental approach to predict the long term serviceability deflection of RC members.

Based on the development of the models above several specific conclusions can be drawn:

1) Current design code approaches suggest a uniform shrinkage profile for RC members determined through small scale test on prismatic specimens with all surfaces are exposed to the environment. Based on moisture diffusion modelling this has been shown to be inappropriate for a full size RC beams in which the shrinkage profile is highly non-linear.
2) To address the issues in # 1) above a test methodology for predicting the non-linear shrinkage strain distribution has been developed. Importantly this approach can

allow for concrete with different exposed surfaces and different member sizes in terms of volume over exposed surface areas (V/S) of the member.

3) It has been found that moisture diffusion model predicts well the non-linear shrinkage variations in a full size RC members and where it shows the non-linear variations along both its width and depth of the member for four way and three way flow in a beam. It has been shown that shrinkage strains are symmetrical about mid-depth and are of maximum at top and bottom sections of the beam for four way flow condition. In three way flow condition, the shrinkage strain has the greatest variation and is maximum at the bottom of the beam and in the remaining region the shrinkage strain can be considered to be uniform.
4) It has been observed that existing models for predicting long term deflection of RC members are based on the constant shrinkage strain profile. These do not simulate the non-linear shrinkage distribution observed in practice. This is significant as it has been shown that the non-linearity of the shrinkage strain has a significant influence on member deflection. It has also been shown that the greatest variation in shrinkage occurs in the region where tensile reinforcement is located. It is therefore suggested that the consideration of non-linear shrinkage may be particularly important in the design of pre-stressed concrete members where shrinkage leads to a loss of prestress.
5) The wider variations of deflection of a RC beam have been observed due to the effect of exposed surface conditions and it shows reduction in deflections over time with respect to the minimized surface exposers.

Although a lot of research has been conducted on the shrinkage behaviour of concrete; further research is required to better understand the effect of shrinkage on material and member level in other types of concrete as well. Based on the development of numerical procedure allowing the non-linear shrinkage strains for quantifying the long term serviceability deflection of RC members, the following recommendations for future research can be suggested:

1) The moisture diffusion model developed in this thesis can be used to reanalyse all existing shrinkage test data in order to develop a material model for describing the non-linear distribution of shrinkage strain.
2) A simplified hand calculation procedure should be developed from the model in # 1) as well as a simplified material model for the 'best' constant shrinkage strain in members.
3) A series of experiments should be undertaken using the proposed work to further understand the influence of size effect in RC members.
4) The developed segmental model should be extended to allow for prestressed concrete members where an accurate understanding of shrinkage strain is required. According to Knight, Visintin et al. 2013 and Knight, Visintin et al. 2015, this can be done by changing the partial interaction tension stiffening model.
5) The developed moisture diffusion model may be extended to various types of new concretes such as Ultra high performance, Self-consolidating and Geopolymer concrete members to extract the shrinkage variations and then segmental model can be applied to quantify the long term deflections of RC members.

References

AASHTO (2010). LRFD Bridge Design Specifications, 5th Edition. Washington D. C.: American Association of State Highway and Transportation Officials.

ACI209R-92 (1992). Prediction of Creep, Shrinkage and Temperature Effects in Concrete Structures. USA, American Concrete Institute**:** 47.

ACI209R-92 (1997). Prediction of Creep, Shrinkage and Temperature Effects in Concrete Structures. USA, American Concrete Institute**:** 47.

ACI Committee 209 (1982). Prediction of creep, shrinkage and temperature effects in concrete structures. Farmington Hills, Michigan: American Concrete Institute

Akita, H., T. Fujiwara and Y. Ozaka (1997). "A practical procedure for the analysis of moisture transfer within concrete due to drying." Magazine of Concrete Research **49**(179): 129-137.

Al-Saleh, S. A. (2014). "Comparison of theoretical and experimental shrinkage in concrete." Construction and Building Materials **72**: 326-332.

Al-Saleh, S. A. and R. Z. Al-Zaid (2006). "Effects of drying conditions, admixtures and specimen size on shrinkage strains." Cement and concrete research **36**(10): 1985-1991.

Almudaiheem, J. A. and W. Hansen (1987). "Effect of specimen size and shape on drying shrinkage of concrete." ACI MATERIALS JOURNAL **84**(2).

American Concrete Institute (2008). Building code requirements for structural concrete, ACI 318-08. Detroit, USA, American Concrete Institute.

Asad, M. (1995). "Computational Modelling of shrinkage in repaired concrete." Civil Engineering.

Asad, M., M. Baluch and A. AI-Gadhib (1997). "Drying shrinkage stresses in concrete patch repair systems." Magazine of Concrete Research **49**(181): 283-293.

AS 1012.8.4 (2015). Methods of testing concrete; Method 8.4: Method for making and curing concrete - Drying shrinkage specimens prepared in the field or in the laboratory. Sydney (Australia). Australian Standard.

Bazant, Z. P., Baweja S (1995). "Creep and shrinkage prediction model for analysis and design of concrete structures – Model B3". Materials and Structures **28**: 357–365.

Bazant, Z. and G. Li (2008). Database on concrete creep and shrinkage. Infrastructure Technology Institute (ITI), Northwestern University. Evanston, IL,USA.

Bažant, Z. and L. Najjar (1971). "Drying of concrete as a nonlinear diffusion problem." Cement and Concrete Research **1**(5): 461-473.

Bazant, Z. P. and L. J. Najjar (1972). "Nonlinear water diffusion in nonsaturated concrete." Materials and Structures **5**(1): 3-20.

Bazant, Z. P. and B. H. Oh (1984). "Deformation of progressively cracking reinforced concrete beams." Computer-Aided Design **16**(6): 338-338.

Bazant, Z. P., S. Sener and J.-K. Kim (1987). "Effect of cracking on drying permeability and diffusivity of concrete." ACI Materials Journal **84**(5).

Bažant, Z. P. and X. Yunping (1994). "Drying creep of concrete: constitutive model and new experiments separating its mechanisms." Materials and structures **27**(1): 3-14.

Bissonnette, B. t., P. Pierre and M. Pigeon (1999). "Influence of key parameters on drying shrinkage of cementitious materials." Cement and Concrete Research **29**(10): 1655-1662.

CEB-FIP (1990). CEB-FIP model code 1990: design code, Telford.

Chen, Y., P. Visintin, D. Oehlers and U. Alengaram (2013). "Size-Dependent Stress-Strain Model for Unconfined Concrete." Journal of Structural Engineering **140**(4): 04013088.

Faber, O. (1928). Plastic Yield, Shrinkage, and Other Problems of Concrete, and their Effect on Design. Minutes of the Proceedings, Thomas Telford.

Fantilli, A. P., D. Ferretti, I. Iori and P. Vallini (1998). "Flexural deformability of reinforced concrete beams." Journal of Structural Engineering **124**(9): 1041-1049.

fib Bulletin 65. (2012) "Model code 2010 Vol 1 & 2", International Federation for Structural Concrete Lausanne Switzerland.

Gardner, N. J., Lockman M. J (2001). "Design provisions for drying shrinkage and creep of normal-strength concrete." ACI Materials Journal **98**:159–167.

Gilbert, R. and S. Nejadi (2004). "An experimental study of flexural cracking in reinforced concrete members under sustained loads, UNICIV Report No." R-435, School of Civil and Environmental Engineering, University of New South Wales, Sydney, Australia.

Gilbert, R. I. (1988). Time effects in concrete structures. Amsterdam, The Netherlands, Elsevier Science Publishers B.V.

Gilbert, R. I. (1999). "Deflection calculation for reinforced concrete structures—why we sometimes get it wrong." Structural Journal **96**(6): 1027-1032.

Gilbert, R. I., M. A. Bradford, A. Gholamhoseini and Z. T. Chang (2012). "Effects of shrinkage on the long-term stresses and deformations of composite concrete slabs." Engineering Structures **40**: 9-19.

Gilbert, R. I. and G. Ranzi (2011). Time-dependent behaviour of concrete structures. UK, Spon Press.

Granger, L., J.-M. Torrenti and P. Acker (1997). "Thoughts about drying shrinkage: experimental results and quantification of structural drying creep." Materials and Structures **30**(10): 588-598.

Gravina, R. J. (2002). "Non-linear overload behaviour and ductility of reinforced concrete flexural members containing 500MPa grade steel reinforcement/by Rebecca Jane Gravina."

Gravina, R. J. and S. T. Smith (2008). "Flexural behaviour of indeterminate concrete beams reinforced with FRP bars." Engineering Structures **30**(9): 2370-2380.

Gravina, R. J. and R. Warner (2003). "Local deformation model for reinforced concrete members in flexure." Australian Journal of structural engineering **5**(1): 29-36.

Gribniak, V. (2009). Shrinkage influence on tension-stiffening of concrete structures. PhD, Vilniaus Gedimino technikos universitetas.

Gribniak, V., G. Kaklauskas and D. Bacinskas (2008). "Shrinkage in reinforced concrete structures: A computational aspect." Journal of Civil Engineering and Management **14**(1): 49-60.

Hansen, T. C. and A. H. Mattock (1966). Influence of Size and Shape of Member on the Shrinkage and Creep of Concrete. ACI Journal Proceedings, ACI.

Haskett, M., D. J. Oehlers and M. M. Ali (2008). "Local and global bond characteristics of steel reinforcing bars." Engineering Structures **30**(2): 376-383.

He, W. (2013). Creep and Shrinkage of High Performance Concrete, and Prediction of Long-Term Camber of Prestressed Bridge Girders. Masters, Iowa State University.

Holt, E. and M. Leivo (2004). "Cracking risks associated with early age shrinkage." Cement and Concrete Composites **26**(5): 521-530.

Huo, X. S.-O (2001). "Creep, shrinkage and modulus of elasticity of high performance concrete." ACI Materials Journal **98**(6), 440-449.

Jafarifar, N. (2012). Shrinkage Behaviour of Steel-Fibre-Reinforced-Concrete. PhD, The University of Sheffield.

Jayasinghe, T. (2011). Prediction of time-dependent deformations in post-tensioned concrete suspended beams and slabs in tall buildings. PhD, RMIT University Australia.

Jun, Z., H. Dongwei and C. Haoyu (2010). "Experimental and theoretical studies on autogenous shrinkage of concrete at early ages." Journal of Materials in Civil Engineering **23**(3): 312-320.

Kang, S. T., J. S. Kim, Y. Lee, Y. D. Park and J. K. Kim (2011). "Moisture Diffusivity of Early Age Concrete Considering Temperature and Porosity." KSCE Journal of Civil Engineering **16**(1): 179-188.

Kim, J. K. and C. S. Lee (1998). "Prediction of differential drying shrinkage in concrete." Cement and Concrete Research **28**(7): 985-994.

Kim, J. K. and C. S. Lee (1999). "Moisture diffusion of concrete considering self-desiccation at early ages." Cement and Concrete Research **29**: 1921-1927.

Knight, D., P. Visintin, D. Oehlers and M. Jumaat (2013). "Incorporating residual strains in the flexural rigidity of RC members with varying degrees of prestress and cracking." Advances in Structural Engineering **16**(10): 1701-1718.

Knight, D., P. Visintin and D. J. Oehlers (2015). "Displacement-based simulation of time-dependent behaviour of RC beams with prestressed FRP or steel tendons." Structural Concrete **16**(3): 406-417.

Lam, J. P. (2002). Evaluation of concrete shrinkage and creep prediction models. Masters, San Jose State University.

Lewis, R. W., B. A. Schrefler and N. Abd Rahman (1998). "A finite element analysis of multiphase immiscible flow in deforming porous media for subsurface systems." Communications in numerical methods in engineering **14**(2): 135-149.

Mu, R. and J. Forth (2009). "Modelling shrinkage of concrete from moisture lost using moisture diffusion theory." Magazine of Concrete Research **61**(7): 491-497.

Mu, R. and J. P. Forth (2009). "Moisture shrinkage of concrete from moisture lost using moisture diffusion theory." Magazine of Concrete Research **61**(7): 491-497.

Muhamad, R., M. M. Ali, D. Oehlers and A. H. Sheikh (2011). "Load-slip relationship of tension reinforcement in reinforced concrete members." Engineering Structures **33**(4): 1098-1106.

Oehlers, D. J., I. Liu and R. Seracino (2005). "The Gradual Formation of Hinges Throughout Reinforced Concrete Beams#." Mechanics based design of structures and machines **33**(3-4): 373-398.

Oehlers, D. J., M. Mohamed Ali, M. Haskett, W. Lucas, R. Muhamad and P. Visintin (2011). "FRP-Reinforced concrete beams: unified approach based on IC theory." Journal of Composites for Construction **15**(3): 293-303.

Ong, K. C. G., L. R. Chandra and K. M. Lay (2010). "Early-Age Shrinkage Strains Versus Depth of Low Water-Cement Ratio Mortar Prisms." ACI Matetrials Journal **107**(3): 213-221.

Pickett, G. (1946). "Shrinkage stresses in concrete." Journal of the American Concrete Institute **17**(3): 165-203.

Popovics, S. (1973). "A numerical approach to the complete stress-strain curve of concrete." Cement and concrete research **3**(5): 583-599.

Powers, T. C. and T. L. Brownyard (1946). Studies of the physical properties of hardened Portland cement paste. ACI Journal Proceedings, ACI.

Prasada Rao, A., R. Jayaraman, V. Vimalanandam and S. S. Babu (1994). "Predicting creep and shrinkage effects in cracked concrete elements." Journal of Structural Engineering **120**(9): 2784-2792.

Pulmano, V. A. and Y. S. Shin (1987). "Simplified finite-element analysis of deflections of reinforced concrete beams." Structural Journal **84**(4): 342-348.
Sakata, K. (1982). "A Study on moisture diffusion in drying and drying shrinkage of concrete " Cement and Concrete Research **13**: 216-224.

Sakata, K (1993). "Prediction of concrete creep and shrinkage of concrete." In: 5th international RILEM Symposium, Barcelona, Spain.

Sakata, K. and T. Shimomura (2004). "Recent progress in research on and code evaluation of concrete creep and shrinkage in Japan." Journal of Advanced Concrete Technology **2**(2): 133-140.

Silliman, K. R. and C. M. Newtson (2006). Effect of misting rate on concrete shrinkage. HPC: Build Fast, Build to Last. The 2006 Concrete Bridge Conference.

StandardsAustralia (2009). Australian Standard for Concrete Structures. AS3600-2009. Sydney (Australia): Standards Australia. Sydney, AS 3600-2009.

Suwito, A., A. Ababneh, Y. Xi and K. William (2006). "The coupling effect of drying shrinkage and moisture diffusion in concrete." Computers and Concrete **3**(2/3): 103-122.

Terrill, J., M. Richardson and A. Selby (1986). "Non-linear moisture profiles and shrinkage in concrete members." Magazine of Concrete Research **38**(137): 220-225.

Visintin, P., D. Oehlers and M. Haskett (2013). "Partial-interaction time dependent behaviour of reinforced concrete beams." Engineering Structures **49**: 408-420.

Visintin, P., D. Oehlers, R. Muhamad and C. Wu (2013). "Partial-interaction short term serviceability deflection of RC beams." Engineering Structures **56**: 993-1006.

Visintin, P., D. Oehlers, C. Wu and M. Haskett (2012). "A mechanics solution for hinges in RC beams with multiple cracks." Engineering Structures **36**: 61-69.

Walker, D., M. Leonard, A. Metcalfe and M. Lambert (2009). Engineering Modelling and Analysis, Taylor and Francis.

Zhang, J., H. Dongwei and S. Wei (2010). "Experimental study on the relationship between shrinkage and interior humidity of concrete at early age." Magazine of Concrete Research **62**(3): 191-199.

Zhang, J., D. Hou and Y. Gao (2012). "Integrative studies on autogenous and drying shrinkages of concrete at early-age." Advances in Structural Engineering **15**(7): 1041-1052.

Zhang, J., D. Hou, Y. Gao and S. Wei (2011). "Determination of Moisture Diffusion Coefficient of Concrete at Early Age from Interior Humidity Measurements." Drying Technology **29**(6): 689-696.

Zhang, J., D. Hou and Y. Han (2012). "Micromechanical modeling on autogenous and drying shrinkages of concrete." Construction and Building Materials **29**: 230-240.

Zhang, J., K. Qi and Y. Huang (2009). "Calculation of moisture distribution in early-age concrete." Journal of engineering mechanics **135**(8): 871-880.